Faculty of Engineering, Built Environment and Information Technology

THE EFFECT OF LARGE VALUES OF RELATIVE SURFACE ROUGHNESS ON HEAT TRANSFER AND PRESSURE DROP CHARACTERISTICS IN THE LAMINAR, TRANSITIONAL, QUASI-TURBULENT AND TURBULENT FLOW REGIMES

---

by

FAIYAAD MAHOMED

A dissertation submitted in partial fulfilment of the requirements for the degree of

MASTER OF ENGINEERING (MECHANICAL ENGINEERING)

In the

DEPARTMENT OF MECHANICAL AND AERONAUTICAL ENGINEERING

UNIVERSITY OF PRETORIA

Supervisor: Dr. M. Everts

June 2023

Abstract

Title: The effect of large values of relative surface roughness on heat transfer and pressure drop characteristics in the laminar, transitional, quasi-turbulent, and turbulent flow regimes

Supervisor: Dr. M. Everts

Department: Mechanical and Aeronautical Engineering

University: University of Pretoria

Degree: Master of Engineering (Mechanical Engineering)

Numerous studies experimentally investigated the heat transfer and pressure drop characteristics of laminar, transitional, quasi-turbulent, and turbulent flow through smooth tubes, however, studies that investigate the effect of surface roughness on the heat transfer and pressure drop characteristics in macrotubes are sparse. This study experimentally investigated the effect of large values of relative surface roughness on the heat transfer and pressure drop characteristics using simultaneously measured heat transfer and pressure drop data. Experiments were conducted using a horizontal circular tube with a base inner diameter of 5 mm, a length of 4 m, and a square-edged inlet. The constricted diameter was used for the rough tubes. One smooth and two rough tubes, with relative roughnesses of 0.04 and 0.11, were tested at different constant heat fluxes between Reynolds numbers of 100 and 8 500. Water was used as the test fluid and the Prandtl number varied between 3 and 7. The smooth tube was used for validation purposes, as well as a reference to compare the rough tube results. The heat transfer and pressure drop results were plotted and discussed using the average Nusselt numbers, friction factors, and Reynolds numbers. Contrary to the trend in the Moody Chart, a significant increase in friction factors with increasing surface roughness was observed in the laminar flow regime. Free convection effects of both Nusselt numbers and friction factors were suppressed by the velocity of the fluid caused by the large roughness elements, even so at low Reynolds numbers. It was found that for a rough tube with a relative roughness of 0.04 at a constant heat flux of 3 kW/m^2, the transitional flow regime occurred at a Reynolds number of 560, and the quasi-turbulent flow regime at a Reynolds number of 760. For a tube with relative roughness of 0.11, the critical Reynolds number was below 390 and the quasi-turbulent flow regime occurred as early as at a Reynolds number of 490. In general, for both the friction factors and Nusselt numbers as functions of Reynolds number, there was a clear upward and leftward shift with increasing surface roughness across the different flow regimes in comparison to a smooth tube. The transitional flow regime for friction factors and Nusselt numbers were narrower and had a differing profile in comparison to smooth tubes. The relative roughnesses of both rough tubes were in the saturating region and the influence of heat flux and thus the Grashof number had little effect on the critical Reynolds number. The quasi-turbulent and turbulent flow regimes occurred at lower Reynolds number for increasing roughness. Trends of the friction factors and Colburn *j*-factors were similar in all the flow regimes for the smooth and rough tubes and the boundaries between the flow regimes were the same for both the pressure drop and heat transfer results. When comparing the relationship between heat transfer and pressure drop, it was found that an increase in surface roughness favoured heat transfer in the quasi-turbulent flow regime. This is useful for rough tubes as the quasi-turbulent flow regime onsets early with regards to the Reynolds number in tubes with large roughnesses.

In the name of Allah, the most gracious the most merciful

Acknowledgements

I would like to acknowledge the following people for their assistance and support:

- Dr. Marilize Everts for her supervision, extensive knowledge, valuable insights, and resources.
- Prof Josua Meyer for his supervision provided until August 2021.
- Dr. Ruxana Jina for language editing and moral support.
- Mr. Danie Gouws, Mr. Koos Mthombeni, and Mr. Chris Govender for their technical knowledge and assistance.
- Mr. Pascal Robbertse and Mr. Blayne Spitholt for their guidance on software and instrumentation.
- Mr. Ismail Mahomed and Mrs. Anisa Jina for their moral support and patience throughout this long journey.
- My family and friends for their upliftment and motivating words during difficult times.
- Finally, the NRF and the University of Pretoria for their funding and extension of resources.

Table of Contents

List of Figures

List of Tables

Nomenclature

A	Area	m^2
C_p	Constant pressure specific heat	J/kg.K
D	Inner diameter of smooth tube	m
D_r	Inner diameter of rough tube	m
D_o	Outer diameter	m
EB	Energy balance	%
g	Gravitational acceleration	m/s^2
h	Heat transfer coefficient	$W/m^2.K$
I	Current	A
k	Thermal conductivity	W/m.K
L	Total length	m
Lh	Hydrodynamic entrance length	m
Lt	Thermal entrance length	m
M	Measurement value	
$\dot{m}$	Mass flow rate	kg/s
m	Constant Used in Correlations	
n	Constant Used in Correlations	
ΔP	Pressure drop	kPa
$\dot{q}$	Heat flux	W/m^2
$\dot{Q}$	Heat transfer rate	W
R	Thermal resistance	°C/W
R_{total}	Total thermal resistance	°C/W
Ra	Mean roughness height	m
Rq	Root mean square	m
Rz	Mean roughness depth	m
T	Temperature	°C
V	Velocity or voltage	m/s or V
x	Distance from inlet	m
X_s	Sampling Length	m
Z_p	Peak Height	m
Z_t	Valley to Peak Height	m
Z_p	Valley Height	m

Dimensionless Parameters

C_f	Skin Friction Coefficient
f	Friction Factor
Gr	Grashof Number
Gz	Graetz Number
j	Colburn *j*-Factor
Nu	Nusselt Number
Pr	Prandtl Number
Re	Reynolds Number
St	Stanton Number
λ	Buoyancy Parameter

Greek letters

α	Thermal Diffusivity	m^2/s
ε	Roughness Height	m
δ	Fouling Layer Thickness	m
δ_o	Limiting Fouling Layer Thickness	m
ρ	Density	kg/m^3
μ	Dynamic Viscosity	kg/m.s
τ	Surface Shear Stress	N/m^2

Subscripts

b	Bottom/Bulk
c	Cross section
cf	Constricted flow
cor	Correlation
cr	Critical
exp	Experimental
h	Heated
i	Inlet
i,g	Inner glue layer
l	Laminar
o	Outlet/Asymptotic
o,g	Outer glue layer
p	Pressure
qt	Quasi-turbulent
s	Surface
t	Time/Top/Turbulent
w	Water

1. Introduction

1.1. Background

Heat exchangers play vital roles in numerous industries and aid cycles by rejecting or consuming heat, thereby maintaining the heat transfer between fluids in a process. Improving the efficiency of industrial processes directly depends on improving the effectiveness of heat transfer equipment, for example, heat exchangers. In improving the effectiveness of heat exchangers, less energy is consumed in an application for the same heat transfer performance, which decreases operational costs.

Single-phase flow through tubes can be classified into four flow regimes [2]: laminar, transitional, quasi-turbulent, and turbulent. In practice, engineers are advised to design heat exchangers to operate within the laminar and turbulent flow regimes due to limited design information outside of these two flow regimes. Engineers design for high heat transfer rates and low pressure drops, as optimized heat transfer is excellent for improved efficiency, while the required pumping power (and thus operational running costs) can be minimized by reducing the pressure drops. The laminar flow regime has low pressure drops and low heat transfer rates compared to the turbulent flow regime, which has high heat transfer rates and high pressure drops. For some cases, the optimum operating range would be in or close to the transitional flow regime because the heat transfer rate is better than in the laminar flow regime, and the pressure drop is smaller compared to that in the turbulent flow regime. Furthermore, heat exchangers that were not designed to operate in the transitional flow regime, might, later on, operate in this flow regime due to scaling and corrosion that changes the flow characteristics, or due to additional equipment and possible changes concerning the operating conditions [3].

Due to their importance in our everyday lives, fluid flow characteristics were knowingly investigated from as early as 1883 [4]. The initial research was primarily focused on the laminar and turbulent flow regimes, while studies on the transitional flow region began in the 1990s. The initial research on transitional flow focussed on the effect of inlet geometries on the isothermal and diabatic friction factors, and heat transfer coefficients using a constant heat flux boundary condition and ethylene glycol-water mixtures with Prandtl numbers between 40 and 160 [5-18] as well as using a constant surface temperature boundary condition and water with Prandtl numbers of approximately 7 [3,19-22]. Overall, it was concluded that the onset of the transitional flow regime was delayed for smoother inlet geometries, as well as increasing heat fluxes. An increase in heat flux also increased the friction factors and heat transfer coefficients in the laminar and transitional flow regimes but had a negligible effect on the turbulent flow regime. Thereafter, a series of studies were conducted investigating the effect of enhanced tubes [21,22], mixed convection [2,23], developing flow [24-27], flow regime boundaries [28], nanofluids [29-31], multiple tubes [32], twisted tape inserts [33-35], annuli [36,37], inclination angles [23,38], and forced convection [39] on transitional flow. These studies, however, were all limited to transitional flow through smooth tubes, except for the studies conducted using enhanced tubes [21,22] and the recent study that investigated tubes with low values of relative surface roughness [40].

Enhanced tubes have been proven effective in enhancing heat transfer and thus increase efficiency by creating turbulence and flow rotation along the axial direction of the tube [16,21,22]. Older literature termed some of these studies on enhanced tubes as artificial roughness. However, enhanced tubes differ from ‘natural roughness’ [41], for example - gluing sand grains, electroplating, corrosion, and scaling, primarily because of their differing shape, size, randomness, asymmetry, and nonuniformity. Fluid flow properties are highly dependent

on the surface roughness type. According to Webb [42], flow lines would follow the shape of the element and only reattach a distance six to eight times the height of the element. Therefore, fluid flow characteristics may differ between rough tubes and enhanced tubes and must be studied separately [40,42,43].

The effects of surface roughness on heat transfer and pressure drop in the transitional flow regime for a macrotube have still not been investigated fully. The relative surface roughness is a "ratio of the mean height of surface roughness inside the tube to the inner tube diameter" [44]. Unfortunately, a functional form showing the dependence of pressure drop on fluid flow cannot be produced through theoretical analysis for rough tubes. Because of varying shapes and sizes, the flow characteristics would differ. This dependence was shown through an experimental analysis where artificially rough surfaces were produced and then tested. From as early as 1858, Darcy [45] conducted pressure drop experiments using different roughnesses and tube materials and concluded that the flow in tubes depended on the surface roughness, slope, and tube diameter. In 1993, Nikuradse conducted experiments of this nature by gluing sand particles of known size to the inside surface of copper tubes [44]. In 1939, Colebrook combined transitional and turbulent data for smooth and rough tubes into an implicit relation known as the Colebrook equation [46]. After verifying Colebrook's relation, Rose presented a graphical plot of friction factor against the Reynolds number [47]. He also produced a table showing commercial tubes' roughness and a laminar flow relation. Thereafter, the Moody chart, which is used to this day, was produced [45]. Researchers are continuously trying to improve the accuracy of friction factor correlations.

Many investigations were done on the effects of surface roughness on pressure drop but were limited on heat transfer. The few studies that have been conducted focused on micro- and minitubes [16,48-59]. Dipprey and Sabersky [60] studied three rough (relative roughnesses of 0.0024–0.049) tubes and one smooth tube in the turbulent flow regime. An improvement factor of 2 to 3 in Stanton number (ratio of heat transfer to fluid over the thermal capacity of that fluid) was achieved by using rough tubes instead of smooth tubes. For the roughness ratios and Prandtl numbers used, plots of the coefficients of heat transfer as a function of Reynolds number and coefficients of heat transfer divided by friction factor as a function of Reynolds number, have maximum values in or near the transitional or quasi-turbulent flow regimes. This is an interesting discovery as heat transfer coefficients to pressure drop ratios for rough tubes can possibly be optimized by operating in these flow regimes. However, this observation was not found at high Prandtl numbers in the transitional regime [60]. This can mainly be attributed to the different flow characteristics in this regime. There is very little information that exists that defines the effects of surface roughness on heat transfer close to and in the transitional flow regime for macrotubes.

1.2. Importance of Investigating the Effect of Large Relative Surface Roughness on Heat Transfer and Pressure Drop

Scaling and corrosion can increase the roughness of a tube over its operating life, which affects the fluid flow characteristics. The friction factor and the heat transfer coefficient are dependent on the surface roughness, among other factors. It is important that engineers account for real operating conditions in the design process. An example is a heat exchanger that handles hard water. Calcium deposit forms upon heat transfer surfaces over time which causes the surface roughness to increase and the tube diameter to decrease. This causes the performance to decline due to the higher pressure drop.

In a recent study, Everts et al. [40] studied the effect of pressure drop and heat transfer on the laminar and transitional flow regimes in the dampening region (low relative surface roughnesses typically less than 0.001). The authors also compiled previous works to study how roughness with heat transfer would affect the occurrence of the transitional flow regime. Everts et al. [40] found that most of the previous studies that focused on the influence of surface roughness in the transitional flow regime can be grouped in the enhancing region (moderate relative surface roughnesses typically less than 0.1 but greater than 0.001). The authors also noted that more studies are required to further our understanding of the influence of surface roughness in the saturating region (large relative surface roughnesses).

1.3. Problem Statement

Several studies investigated transitional flow through smooth tubes. However, studies on transitional flow through rough tubes with large relative roughness are limited. Experimental data for large relative roughness in the transitional and quasi-turbulent flow regimes can equip design engineers to design equipment more accurately with better efficiencies. Furthermore, it can also assist researchers to better understand how rough surfaces affect the pressure drop and heat transfer, particularly in or near the transitional flow regime.

1.4. Purpose of Study

The purpose of this study was to experimentally investigate the effect of large values of relative surface roughness on the heat transfer and pressure drop characteristics in the laminar, transitional, quasi-turbulent, and turbulent flow regimes.

1.5. Objectives

The objectives of the study were to measure flow rates, temperatures, and pressure drops for tubes with different roughnesses to:

- Study the effect of surface roughness on the flow regime boundaries.
- Study Nusselt number and the Colburn j-factors in mixed and forced convection conditions.
- Obtain average friction factors for different heat fluxes as a function of Reynolds numbers for rough tubes.
- Compare the friction factors and Colburn j-factors to study the relationship between the pressure drop and the heat transfer.
- Investigate the effect of heat flux in tubes with large relative surface roughness.

1.6. Scope of Investigation

This research investigated pressure drop and heat transfer in smooth and rough tubes. Experiments were conducted using a horizontal commercially available circular tube with a base inner diameter of 5 mm, a length of 4 m, and a square-edged inlet. The small diameter and length of the tube, allowed for a fully developed flow in the last 1 m at a Reynolds number of 2 000. The constricted diameter was used for the rough tubes. One smooth test section, with negligible roughness, and two rough test sections, with relative roughnesses of 0.04 and 0.11, were tested at different constant heat fluxes between Reynolds numbers of 100 and 8 500. Water was used as the test fluid, and the Prandtl number varied between 3 and 7. The boundary condition was a constant heat flux and the heat fluxes varied between 0.3 and 7 kW/m^2.

1.7. Overview of Dissertation

Chapter 1 presented an introduction in terms of a background to the topic and the objectives. Chapter 2 introduces the reader by explaining fundamental concepts related to the research topic and an overview of the state-of-the-art research on transitional flow. The chapter concludes with studies on the influence of surface roughness that comprises rough micro- and minitubes, rough macrotubes, and enhanced tubes. Chapter 3 outlays the details of the experimental set-up, test section, instrumentation used, data reduction, uncertainty analysis, and experimental procedure. Chapter 4 contains the validation of the friction factors, average Nusselt numbers, and local Nusselt numbers. Chapter 5 presents the results focussing on the flow regime boundaries, pressure drop, and heat transfer characteristics, as well as the relationship between pressure drop and heat transfer. Chapter 6 closes the dissertation with a summary, conclusion, and recommendations. The following appendices are included as well: Appendix A (Calibration of instrumentation), Appendix A (Methods of obtaining surface roughness), and Appendix A (Methods of obtaining the flow regime boundaries).

2. Literature Survey

2.1. Introduction

This chapter gives an overview of the fundamental concepts dealing with this study and thoroughly examines the literature that pertains to the two key topic areas of this study which are the transitional flow regime and rough tubes. The literature is separated into four topic areas for rough tubes: micro- and minitubes friction factor analysis, micro- and minitubes heat transfer analysis, macrotubes friction factor analysis and macrotubes heat transfer analysis.

2.2. Fundamental Concepts

2.2.1. Nondimensionalized parameters

The Reynolds number is a dimensionless number representing the ratio of internal forces to viscous forces acting on the fluid under a forced convection [45]. The Reynolds number can be expressed by:

$$Re = \frac{\rho v D}{\mu} \tag{2.1}$$

For low Reynolds numbers (laminar flow), viscous forces of the fluid manage to suppress random fluctuations which are due to the inertia forces of the fluid. However, at high Reynolds numbers (turbulent flow), the viscous forces of the fluid are no longer able to suppress these large inertia forces of the fluid.

Pressure drop is a function of viscous forces and determines the pumping power requirements [61]:

$$\Delta P = f \frac{L}{D} \frac{\rho V^2}{2} \tag{2.2}$$

The friction factor is named after Henry Darcy and is also known as the Darcy friction factor [61] which describes frictions losses in tubes:

$$f = \frac{8\tau_w}{\rho V^2} \tag{2.3}$$

The Nusselt number is the dimensionless convection heat transfer coefficient [45] which represents the enhancement of heat transfer through the fluid layer because of convection relative to conduction across a fluid layer. For pure conduction, heat transfer across a fluid layer, the Nusselt number is unity [45].

$$Nu = \frac{hD}{k} \tag{2.4}$$

The Prandtl number expresses the relative thickness of velocity and thermal boundary layers [45]:

$$Pr = \frac{v}{\alpha} = \frac{\mu C_p}{k} \quad 2.5$$

The Grashof number represents the ratio of the buoyancy force to the viscous forces acting on fluids and is expressed as:

$$Gr = \frac{g\beta(T_s - T_b)D^3}{v^2} \quad 2.6$$

The Graetz number is the product of the Reynolds number, Prandtl number, and non-dimensional tube length:

$$Gz = RePr\frac{D}{L} \quad 2.7$$

The Graetz number is helpful in determining if the flow is fully developed or not. It is representative of the time for heat to diffuse radially into the liquid by conduction to the time for the liquid to reach an axial distance *x* of the tube length from the tube inlet.

2.2.2. Flow Regimes

The study encounters the four flow regimes which are laminar, transitional, quasi-turbulent, and turbulent. In laminar flow, fluid layers move parallel to each other with zero swirls and eddies. Laminar flow usually occurs at low velocities and free convection effects have significant effects in the laminar flow regime. If the flow is forced convective, fully developed, and steady, then there is no movement of flow particles in the radial direction.

The transitional flow regime is found between the laminar and the turbulent flow regimes and the flow alternates between these flow regimes. Everts and Meyer [62] found that the transitional flow regime can be divided into two separate flow regimes: transitional and quasi-turbulent.

Using dye experiments, Osborne Reynolds visually investigated different flow regimes. Disarranged and random colours were observed indicating high velocity fluctuations within the tube [63]. This rapid mixing of dye with water indicated turbulent flow. Turbulent flow has high pressure drops, high heat transfer coefficients, occurs at high velocities, and is usually dominated by forced convection [28].

2.2.3. Hydrodynamic Entrance Region

The hydrodynamic entry length, which is the region from the tube inlet to where the velocity boundary layer becomes fully developed. This is assumed to correspond to the axial position where the friction factors are within a 2% range of the fully developed friction factor value [45]. The forced convective laminar hydrodynamic entry length can be calculated as [26]:

$$Lh_{FC} = 0.12ReD \quad 2.8$$

The mixed convective hydrodynamic entrance region can be calculated as follows using the bulk fluid properties [26]:

$$Lh_{MC} = 0.12Re_b D(1 + \frac{\mathrm{Pr}_b^{0.11} Gr_b^{0.5}}{Re_b^{0.4}}) \quad 2.9$$

The turbulent hydrodynamic entrance length can be calculated as [61]:

$$Lh = 10D \quad 2.10$$

2.2.4. Thermal Entrance Region

For flow at a uniform temperature entering a tube, depending on the surface conditions, the temperature of fluid will assume the surface temperature. In the entry region, there will be a difference in temperature closer to the surface compared to the centre of the fluid. For a constant heat flux boundary condition there will always be a temperature difference. This temperature difference creates a thermal boundary layer that increases in thickness along the tube length. Everts and Meyer [26] found that the axial position at which the boundary layers merge does not necessarily indicate the point of fully developed flow. The temperature difference also creates convection heat transfer in the tube in the radial direction. After this point, the temperature distribution will be constant in the radial direction. The laminar thermal entrance region for forced convective simultaneously hydrodynamically and thermal developing flow can be calculated as [2]:

$$L_{FC} = 0.12RePrD \quad 2.11$$

The mixed convective thermal entrance region can be calculated as follows [26]:

$$Lt_{MC} = 0.12RePrD(1 - \frac{Gr^{0.1}}{Re^{0.07}\mathrm{Pr}^{0.5}}) \quad 2.12$$

For turbulent flow, the thermal entrance length can be taken as the turbulent hydrodynamic entrance length in Eq. 2.10.

2.2.5. Fully Developed Flow Region

After the hydrodynamic entrance region the flow is said to be hydrodynamically fully developed and the velocity profile remains constant similarly, after the thermal entrance region, the flow is thermally fully developed. The temperature profile can be expressed as:

$$\frac{T_s - T}{T_s - T_m} = constant \quad 2.13$$

Thus, for a fully developed fluid flow, the dimensionless temperature profile is independent of *x*. The temperature profile, however, can still vary along the tube.

2.2.6. Forced and Mixed Convective Flow

Flow can be classified into three convective regimes, namely: Forced convection, free (natural) convection, and mixed convection. Free convection is caused by differences in densities in the fluid. Forced convection occurs under the influence of an external source, for example, a pump

such that buoyancy forces become insignificant. Mixed convection is a combination of the two effects where buoyancy forces remain significant.

Free convection effects have a significant effect on the laminar flow regime due to the low fluid velocities. Free convection in a tube comes about by a difference in temperatures of the fluid inside a tube. The difference in temperature causes a density difference in the fluid inside the tube. Higher temperature fluid (lower density) will rise, while lower temperature fluid (higher density) will settle to the bottom. For a constant heat flux boundary condition, the fluid is heated around the circumference of the tube, and the lower temperature fluid is found in the centre of the tube. The lower density fluid rises/circulates close to the surface of the tube while the lower temperature fluid settles in its place at the centre. A schematic for the effect of free convection flow in tubes by hot or cold surfaces/walls is given in Figure 2.1.

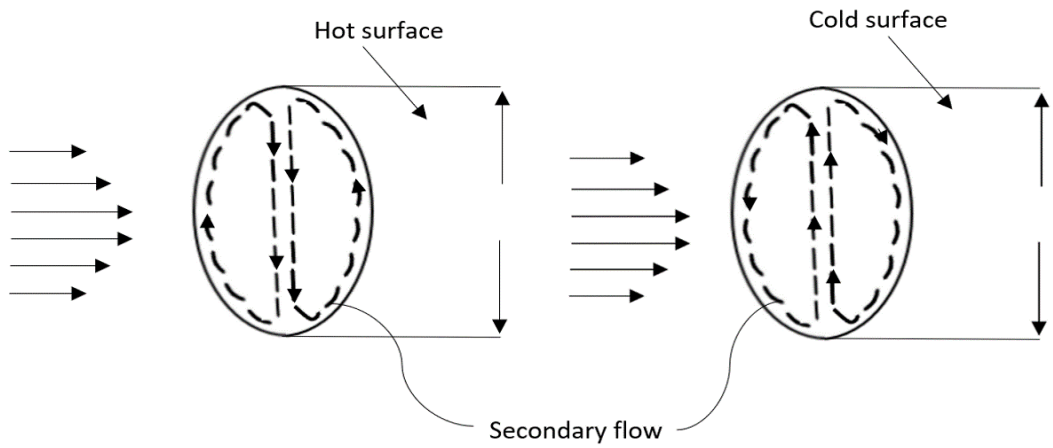

Figure 2.1: Schematic showing secondary/free convection flow (counter-rotating vortices) for hot and cold surfaces. Figure adapted from Ghajar et al. [1]

These buoyancy forces are always present, but it is important to know when these forces are significant or not. Local heat transfer data, such as that used by Ghajar and Tam [7], can be used in order to determine the boundary that is between mixed and forced convection. It was found that free convection effects need a starting length (125 diameters) for them to become dominant. It was also found that forced convection primarily dominated the flow if the Reynolds number is larger than 3 000 for a square-edged inlet geometry. Ghajar and Tam [5] found that forced convection dominated when the local surface heat transfer coefficient ratio (top divided by bottom), $(\frac{h_t}{h_b})$, was above or equal to 0.8 and was assumed to be mixed convection below 0.8.

Everts and Meyer [28] were able to develop original flow regime maps that can be used to determine whether flow is dominated by forced or mixed convection. These flow regime contour maps were created as a function of a temperature difference and heat flux and show contour lines that portray Nusselt number enhancement primarily due to free convection effects.

2.2.7. Roughness Measurements

Roughness has been quantified and expressed in many parameters, which can create confusion. A so-called profile element, as schematically indicated in Figure 2.2, is formed by adjacent peaks and valleys. The arithmetic and quadratic means of deviations of individual profile points from a centre line are used to quantify roughness [66].

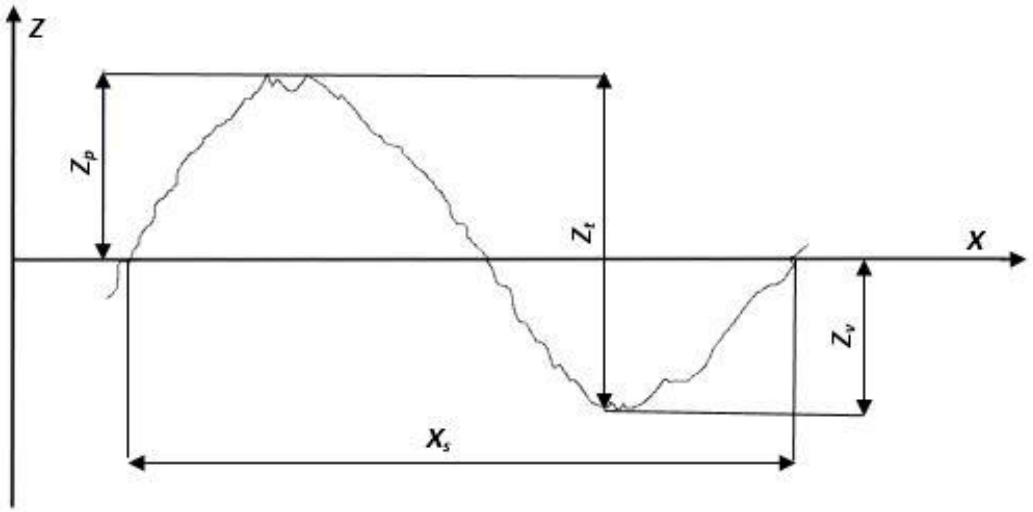

Figure 2.2: An example of a profile element with deviations from its centre line. Figure adapted from Harcarik and Jankovych [67]

The mean roughness height (*Ra*) is the most common one-dimensional roughness parameter. It is the arithmetical mean deviation of the absolute filtered roughness values, which is determined by evaluating profile deviations (*Zt*) about its mean line. *Ra* is defined over the entire evaluation-length and is calculated from:

$$Ra = \frac{1}{n}\sum_{i=1}^{n} |Zt| \qquad 2.14$$

The root mean square (*Rq*) is the arithmetic mean of the squares of deviations (*Yi*) from the mean line to the evaluation profile. *Rq* is defined over the entire evaluation-length and is calculated from:

$$Rq = \left(\frac{1}{n}\sum_{i=1}^{n} (Zt)^2\right)^{\frac{1}{2}} \qquad 2.15$$

The mean roughness depth (*Rz*) is the average distance between the lowest valley and highest peak in a segment which is, thereafter, averaged over several segments of the total evaluation-length. According to Flack and Rose [47], it is the best roughness scale to predict the onset of roughness effects in flow regimes.

The relative surface roughness in this study was characterized by the absolute arithmetical mean roughness, which is most generally used for fluid mechanics applications, quantified using *Ra* for the tube, divided by the inner diameter of the tube (ε/D).

2.3. Transitional Flow: Smooth Tubes

2.3.1. Influence of Inlet Geometries

A significant body of work was conducted to investigate the effect of inlet geometries on transitional flow. The different inlet geometries are square-edged, re-entrant, bellmouth, and hydrodynamically fully developed. Figure 2.3 schematically compares the different inlet geometries where Ghajar and co-workers [6-8,10,12,17] focused on Figure 2.3 (a), (b), and (c), while Meyer and Olivier [20-22] investigated all four. Figure 2.3 (a) and (b) show abrupt changes, while Figure 2.3 (c) and (d) show gradual changes in the inlet geometry.

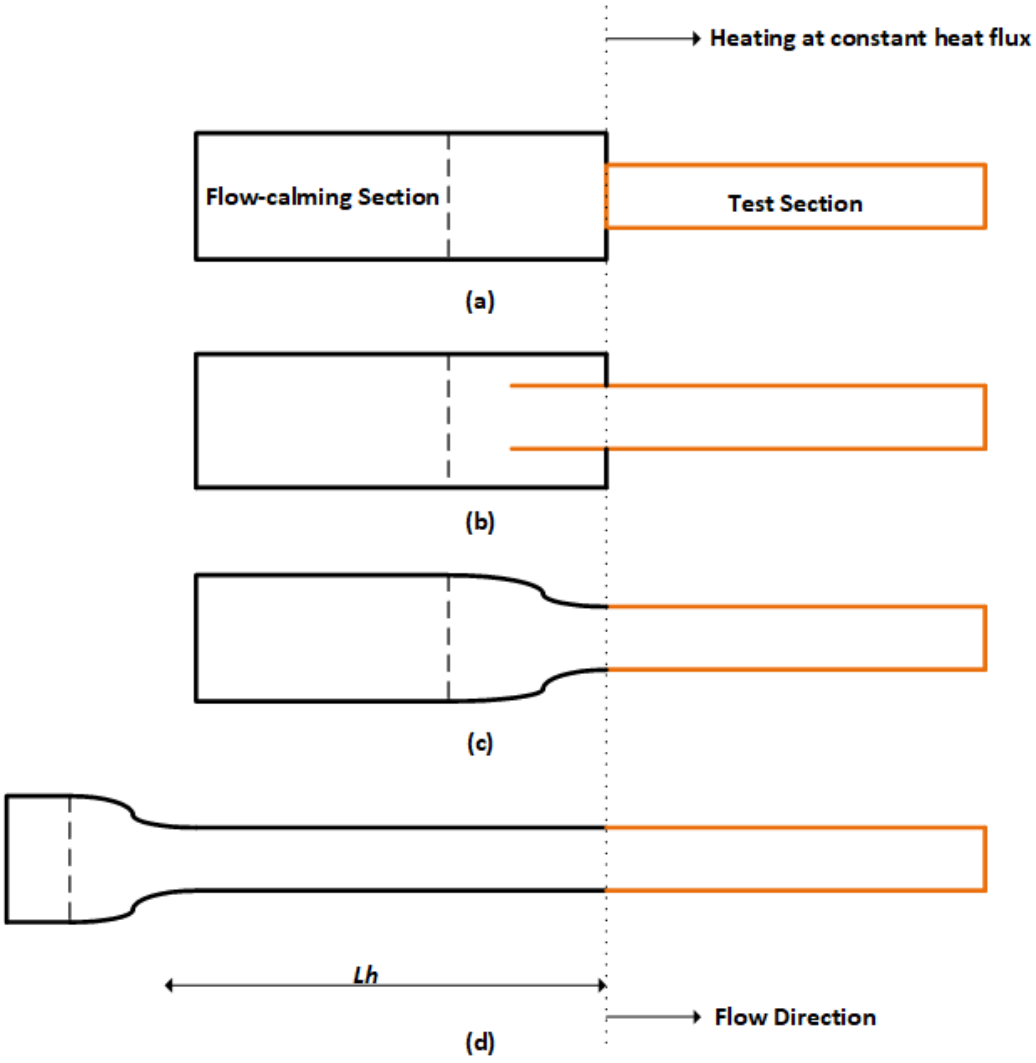

Figure 2.3: Four different inlet geometries of effects on the transitional flow regimes previously studied. Figure adapted from Everts [64].

A series of studies on the effect of inlet geometries on isothermal friction factors were done by Ghajar and co-authors [8,10,15]. In these studies, an abrupt change in the gradient of the

friction factors indicated the onset of the transitional flow regime. The onset and end of the transitional flow regime were found to change for different inlet geometries. It was found that a more abrupt change in inlet geometry influences the transitional regime to occur earlier. Similar findings were also obtained by Olivier and Meyer [20]. Tam et al. [15] also found that due to the greater disturbance caused by an inlet geometry, a longer entrance length was required for the apparent friction factors, which are associated with developing flow, to match the fully developed friction factors.

Tam and Ghajar [10] investigated the effect of inlet geometry on the diabatic friction factors. Similar to the isothermal friction factors, the inlet that produced the least disturbance delayed the onset of the transitional flow regime. Furthermore, an increased heat flux also increased the Reynolds numbers at which the transitional regime onset and ended for all types of inlets tested. However, Olivier and Meyer [20] found that when heating was applied, the transitional regime narrowed, and the diabatic friction factors became independent of the inlet geometries [20]. Similar conclusions were also made in the heat transfer coefficient investigation of Meyer and Olivier [19], where water and 50% v/v water-propylene glycol were mixed and used. Nagendra [68] proposed that inlet disturbances have a negligible effect on transition if the product of diameter-to-length ratio, Rayleigh, and Reynolds numbers exceeds 10^6.

Ghajar and Tam [6,7] investigated the effect of inlet geometry on the heat transfer coefficients and found that the Nusselt number increased throughout the transitional regime with increasing axial position. At the beginning of the tube, the transitional regime had an increase of 3.4%, while at the end, a percentage of 11%. The reason for this was because of the variation of the physical properties. The latter end of the transitional regime increased more than the onset, the cause for this being, that the higher temperature of fluid caused a delay in transition. When focussing specifically on the bellmouth inlet, Tam and Ghajar found that the local heat transfer coefficients decreased to a minimum at x/D = 25. Thereafter, the coefficient increased linearly due to Newton's law of cooling. Surface temperatures as well as fluid temperatures increased linearly for x/D in fully developed flow. The surface-fluid temperature difference should be ~~a~~ constant throughout the rest of the length of the tube for fully developed flow. However, this was found not to be the case since the rate of increase for the fluid's temperature was greater than the rate of the increase of surface temperature. The reason for this occurrence was not fully understood.

2.3.2. Influence of Developing flow

In a recent study by Everts and Meyer [24], the heat transfer characteristics of developing flow were investigated and compared with the fully developed flow in the transitional flow regime for smooth horizontal tubes. Tests were conducted for two tubes with inner diameters of 4 mm and 11.5 mm with maximum length-to-diameter ratios of 1 373 and 872, respectively, in a Reynolds number range between 700 and 10 000 with a boundary condition of constant heat flux. It was noted that not the onset, but the end of transition was dependent on the axial position, which occurred earliest in fully developed flow. Correlations for the transitional regime Reynolds numbers were developed for mixed convection effects with a square-edged inlet [24]. The authors proclaimed that from findings, heat transfer characteristics for developing flow differ from that of fully developed flow for the transitional flow regime. Furthermore, Meyer and Everts [2] found that the flow transitioned quicker with increasing heat fluxes.

2.3.3. Influence Twisted Tape Inserts

Meyer and Abolarin [33] investigated the effects of twisted tape inserts with twist ratios of 3, 4, and 5. The authors used two methods to identify transition points: (1) a standard deviation of temperature measurements and (2) three linear curve fittings on a log-to-log scale. On keeping heat flux constant, it was found that for smaller twist ratios, the onset of transition occurred earlier, the Colburn *j*-factors decreased, and the friction factor increased. On keeping the twist ratio constant, as heat flux was increased it was discovered that the onset of transitional flow got delayed. When the Reynolds number and twist ratio were kept constant, the friction factors decreased.

Abolarin et al. [34,35] further investigated the effects of only clockwise, alternating clockwise, and anti-clockwise as well as peripheral u-cut twisted tape inserts with and without rings on the heat transfer and pressure drop characteristics. It was found that heat transfer was significantly improved, and transition occurred earlier for the alternating clockwise and anti-clockwise twisted tape inserts. The alternating clockwise and anti-clockwise twisted tape inserts had the earliest onset of transition and had the greatest heat transfer enhancement between all the inserts within the transitional flow regime. For the peripheral u-cut twisted tape insert, an increased cut depth ratio and the insertion of rings caused an earlier transition. Heat transfer was enhanced in the transitional flow regime because of increased mixing, recirculation near the tube surface, and tripping of the boundary layer growth on the inner tube surface.

2.3.4. Combined Friction Factor and Heat Transfer Analysis

The friction factor, as well as heat transfer results measured by Tam et al. [15], were plotted on the same graph to study the relationship between the two. It was concluded that the heat transfer data shares a downward trend with the laminar friction factor results. The isothermal friction factors were greater than the diabatic friction factors because of heating. It was found that the onset of the transitional flow regime was inlet dependant and the constant heat flux boundary condition had an influence on the onset of transition for friction factors [18]. Once the Reynolds number reached about 2 300 for a square-edged inlet, the friction factors and heat transfer data started to increase and dissociate from the trend of data of the laminar regime, which notes the onset of the transitional regime [18]. Once the heat transfer results increased to a Reynolds number of 8 000, it started to mimic the fully developed turbulent flow trend by decreasing with increasing Reynolds numbers. However, once the friction factor data reached a Reynolds number of 3 000, the friction factor decreased and began to mimic the fully turbulent flow trends. It was, therefore, concluded from the heat transfer results that transition ended approximately at a Reynolds number of 8 357 for a square-edged inlet. This was significantly later than that of the diabatic friction factor (Reynolds number of 3 941 for a square-edged inlet), implying that the friction factor has a smaller transition range in comparison to heat transfer.

Everts and Meyer [27] found that the flow regime boundaries coincided for both heat transfer and pressure drop. It was found that the boundaries for the smooth tube were the same for the friction factors, Colburn *j*-factors, and *f*/*j*-factors. Thereafter, the conclusion was that this relationship could be used in further studies to differentiate between the flow regimes [27]. The authors explained that Tam et al. [15] had differing boundaries in the transitional flow regime because the quasi-turbulent flow regime was not distinguished separately. The quasi-turbulent flow regime was considered to be part of the transitional flow regime for the Colburn *j*-factors and part of the turbulent flow regime for the friction factors.

2.4. Transitional Flow: Rough Tubes

2.4.1. Background on the Moody Chart

The relative surface roughness (ε/D) is the ratio of the mean height of the surface roughness (ε) inside the tube to the inner tube diameter (D) [44] and has been studied extensively in the past. Unfortunately, theoretical analysis cannot produce a functional form showing the dependence of pressure drop on fluid flow in rough tubes as there are many unknown variables in the analysis. The dependence was rather shown through an experimental analysis where artificially rough surfaces were produced and then tested. As early as 1858, Darcy [45] concluded from experimental pressure drop results that flow in tubes depended on the surface roughness, slope, and tube diameter. This was followed by pioneering work conducted by Nikuradse [44], who conducted experiments by gluing sand grains of different sizes to the inside of tubes, and Colebrook [46], who developed an implicit relation to quantify the effect of relative roughness on the friction factors. The widely used Moody chart, presented in Figure 2.4, is essentially the Colebrook equation plotted over a range of Reynolds numbers and relative surface roughnesses [69].

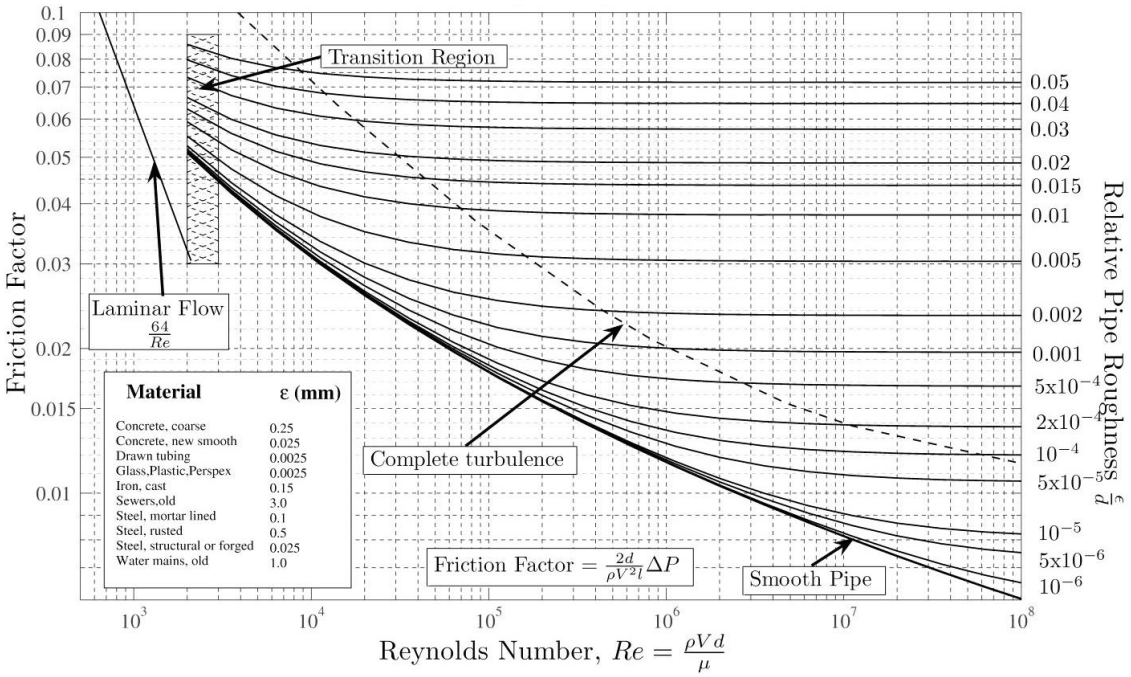

Figure 2.4: The widely used Moody chart [70]

It follows from Figure 2.4 that surface roughness has a significant effect on the friction factors in the turbulent flow regime and a negligible effect on the laminar flow regime. Due to the lack of experimental data on rough tubes in the transitional flow regime, combined with the perceived chaotic behaviour and high uncertainties of transitional flow, the Moody chart provides no specific trends in this flow regime, and the transitional regime is usually greyed out. According to Concha [71], the friction factor is independent of surface roughness for Reynolds numbers between 2 000 and 4 000. However, this is contradictory to the findings of other studies [40,43,72-74] that investigated transitional flow in rough tubes.

The Moody chart led to many other studies that focused on determining accurate correlations for the friction factor of the different flow regimes. Zeghadnia et al. [69] assess thirty-three such equations in terms of accuracy, simplicity (fastest computational time), and coverage of the Moody chart. Avci et al. [75] developed an explicit formula for all the flow regimes for

smooth as well as rough tubes (up to 0.05 relative roughness) that has percentage errors of 2%, 36%, and 10% for laminar, transitional, and turbulent flow regimes, respectively. It should be noted that the percentage deviation is significantly higher for the transitional flow regime than the other flow regimes, which indicates that the influence of surface roughness in this flow regime is not yet fully understood.

Kandlikar [76] reviewed Nikuradse's work [77] and noted that there is still a lot of uncertainty in laminar flow and that the absence of effects of roughness in the laminar regime is questionable. Li et al. [78] also found that for smooth tubes, the product *fRe* was close to 64 in the laminar flow regime, while peak to valley roughnesses of 3-4% led to 15-37% higher friction factors than theory. When Huang and Wan [43] investigated the effects of large surface roughnesses on the friction factors, they found that the product *fRe* was not equal to 64 for laminar flow, but became a quadratic function of relative roughness. However, for relative roughnesses less than 0.03, their results agreed well with Nikuradse in that the laminar friction factor is independent of relative surface roughness.

Kandlikar [76] proposed a constricted flow diameter (Eq. 2.16) to be used to account for the constriction caused by the roughness elements:

$$D_{cf} = D - 2\varepsilon \qquad 2.16$$

For relative roughnesses ranging between 0-5.18%, it was found that surface roughness affected the friction factors in the laminar regime [79], which is contrary to the findings of Nikuradse [77]. However, when using the constricted fluid flow diameter, it was found that the experimental data correlated better with the laminar flow theory. Since micro- and minitubes sometimes violate the threshold of 5% relative roughness set by Taylor et al. [80] and Kandlikar et al. [81], it was suggested to modify the Moody chart to accommodate new experimental data with increased relative roughnesses.

2.4.2. Micro- and Minitubes

Kandlikar [82] classifies microtubes, minitubes and conventional macrotubes as 0.01–0.2 mm, 0.2–3 mm and greater than 3 mm, respectively. When considering the literature on heat transfer and pressure drop in rough tubes, it is found that more research has been conducted using micro- and minitubes than using macrotubes. This is because it is easier to obtain significant relative roughnesses in micro- and minitubes than in macrotubes due to the smaller diameters of the tubes. Meaningful relative surface roughness can be obtained in these tubes using acid etching methods [76,83-85], sanding [79], or by considering the surface finish of the tube itself when the diameters are very small [9]. Smooth microtubes and rough macrotubes may have the same relative surface roughness value.

Many studies concerning the effect of relative surface roughness on the friction factors in the transitional flow regime using micro- and minichannels, as well as micro- and minitubes, have been conducted. Dai and Li [86] compiled an experimental database for friction factors in rough micro- and minichannels. The database consists of 5 569 data points from 33 sources and covers a wide range of Reynolds numbers and relative roughnesses. The authors concluded that for relative roughnesses less than 0.01, surface roughness had no significant influence on the friction factors and critical Reynolds numbers and that the effect of surface roughness only becomes significant when the relative roughness exceeds 0.01 in micro- and minichannels and 0.05 in macrotubes.

A commonality across the studies using micro- and minichannels as well as micro- and minitubes suggests that the critical Reynolds number of the transitional flow regime occurs at lower Reynolds numbers when the surface roughness increases [9,76,78,81,83-85,87]. Tam et al. [85] and Ghajar et al. [9] found that in larger tubes (> 0.84 mm), the transition was not influenced by surface roughness, whereas in smaller tubes (≤ 0.84 mm), the onset of transitional flow regime was advanced for increasing relative surface roughness.

Ghajar et al. [9] noted a considerably larger effective surface roughness (ε_{eff}) than the measured mean roughness (*Ra*); this was due to tolerances and non-uniformity caused by the tube's smaller diameter (microchannels). A smaller diameter partially explains the differences observed between the behaviour of mini- and microchannels of the same relative surface roughness, determined by *Ra*. Furthermore, differences in results in literature with regards to whether diameter and surface roughness affect friction factors at an early transition were observed. It was concluded that these discrepancies could be attributed to inadequate accuracy of instrumentation. Therefore, just as the measurement of inner diameter is important for friction factor results, so is the sensitivity of the instrumentation measuring pressure drop [9].

When investigating both the isothermal and the diabatic friction factors, Tam et al. [85] discovered that heating resulted in a delayed onset of the transitional flow regime but a negligible effect on the end of the transition. Everts and Meyer [24] found similar results when investigating smooth tubes. Tam et al. [85] concluded that the effect of surface roughness on transitional flow was greater at the onset than at the end. Therefore, it also impacted the prominence and width of the transitional flow regime which represents the Reynolds number range in which transition occurs [85].

While several studies investigated the pressure drop characteristics of transitional flow through rough mini- and microtubes, only Kandlikar et al. [83] focused on the heat transfer coefficients. This is mainly due to challenges associated with roughening the inner surfaces of tubes without adding a thermal resistance layer to the inside of the tube or changing the physical properties of the tube [40,41,74]. Kandlikar et al. [83] considered the effects of heat transfer in the stainless-steel minitubes with diameters of 1 067 µm and 620 µm. The internal surfaces of these tubes were acid etched. This resulted in average surface roughnesses measuring between 0.001 and 0.003. In the 1 067 µm tube, it was found that the surface roughness had no effect. In the smaller 620 µm tube, with the same relative surface roughnesses as the larger tube, it was found that there was an increase in Nusselt numbers in the laminar flow regime and the transitional flow regime started earlier.

2.4.3. Macrotubes

Due to the width of the transitional flow regime decreasing for significant surface roughnesses in larger diameter tubes, limited studies investigated the effect of relative surface roughness on the friction factors with a focus on the transitional flow regime using macrotubes. Nikuradse [44] and Huang et al. [43,72] roughened their tubes by gluing sand grains of different sizes to the inside. The results of these studies, focusing solely on isothermal friction factors, concluded an inverse relationship between surface roughness and the critical Reynolds number. Therefore, as surface roughness increased, the critical Reynolds number decreased. Additionally, the width of the transitional flow regime decreased.

Due to the challenges in producing ~~a~~ significant uniform surface roughness in larger diameter tubes without adding thermal resistance layers to the inner surface or changing the physical properties of the tube, very limited studies investigated the effect of relative surface roughness on heat transfer on the transitional flow regime using macrotubes. Dipprey and Sabersky [60]

conducted heat transfer experiments using three tubes with relative roughnesses between 0.0024 and 0.049. The rough tubes were made from electroplating nickel around a few mandrels that were coated in sand grains. Thereafter, the mandrels were dissolved in chemicals that left a nickel tube. This nickel tube was used as the test section and had the appearance of closely packed sand grains. The authors found increases in the heat transfer results by as much as 270% in the turbulent flow regime and even larger increases for the friction factors. However, this observation was not found at high Prandtl numbers in the transitional regime [60]. The authors concluded that different limits exist, depending on the combination of Prandtl number and Reynolds number, that signifies a maximum in which an increase in roughness (friction factor) no longer increases heat transfer. When plotting the heat transfer coefficients as a function of Reynolds number as well as the heat transfer coefficients divided by friction factor as a function of Reynolds number, maxima were observed for these curves. As these maximum values occurred in or near the transitional regime, it indicated heat transfer in rough tubes can be optimized by studying the transitional regime more closely.

Everts et al. [40,73,74] conducted studies that considered the influence of surface roughness on heat transfer in the transitional flow regime. Everts et al. [73,74] focused explicitly on the transitional flow regime by using cyanoacrylate and uniformly sized sand grains to roughen tubes. The study also investigated significant portions of the laminar and turbulent flow regimes. It was found that the surface roughness resulted in increased heat transfer coefficients and advanced the onset of transition. Due to the difficulty characterizing the thermal resistance that the cyanoacrylate adhesive and sand grains imparted on the tube, this study was limited to qualitative heat transfer results.

While most studies either focussed on friction factors or heat transfer coefficients, Everts et al. [40] studied the effects of surface roughness on simultaneous heat transfer and pressure drop measurements of fully developed laminar and transitional flow using macrotubes. Contrary to previous studies, it was found that an increase in surface roughness delayed the onset of the transitional flow regime. Therefore, to quantify the effect of surface roughness on the onset of transitional flow regime, three distinct regions were identified and defined: dampening region (low relative surface roughnesses typically less than 0.001), enhancing region, and saturating region (large relative surface roughnesses typically greater than 0.1). The focus of their study was specifically on the dampening region where the relative surface roughness was less than 0.001 and the authors noted that more research is required in the saturating region.

To the author's best knowledge, only the study of Wu and Little [50], which investigated gas flow through fine channels in the laminar and turbulent flow regimes, considered large relative roughnesses that can be expected to fall in the saturating region [40]. These test sections had unique features such as large asymmetric relative roughness, random roughness, and inequalities in heat flux. Due to the asymmetric and random roughness, the authors could not quantify the relative roughness of the tube. It was found that the Reynolds analogy no longer held in rough channels. Due to these unique features, the general rough tube correlations developed for artificial rough tubes and rough tubes of close-packed sand grains were not suitable for their experimental data.

2.5. Transitional Flow: Enhanced Tubes

In many applications, such as heat exchangers, the surface area of heat transfer is increased by making enhancements to the tube. The enhancements also increase the mixing of the flow and can create more turbulence, thus increasing the heat transfer. This is done by creating an artificial roughness such as corrugation, threads, spirals, wires, dimples, and finned tubes. Garcia and Solano et al. [88] studied the effects of artificial roughness shape on the enhancement of heat transfer coefficients using wire coils, dimpled tubes, and corrugated tubes. The authors found that it is disadvantageous to use artificially roughened tubes below a Reynolds number of 200. This was due to the artificial roughness delaying the establishment of mixed convection. For Reynolds numbers between 200 and 2 000, the wire coil was deemed the best. It is easy and inexpensive to install, has great heat transfer enhancement in the flow regime, and has a predictable behaviour. For Reynolds numbers greater than 2 000, deformed tubes outperformed the wire coil with regard to the heat transfer coefficients [88].

Tam et al. [16] studied the effects of internal microfin tubes on the characteristics of friction factors and heat transfer. It was observed that for tests with no heat flux, the microfinned tubes produced an upward shift in the classical laminar relation in comparison to the smooth tubes. The enhanced tubes transitional flow regime was found to be wider. The cause for these phenomena was due to increased surface roughness. It was found for increasing spiral angle that there was an increase in pressure drop in the turbulent and transitional flow regimes and that the onset of transition took longer. The end of the transitional regime had a quicker onset. The diabatic results demonstrated that the coefficients for heat transfer were greater in the turbulent and the latter end of the transitional flow regimes. This was induced due to the swirling motion of the fluid caused by the profile of the microfins. It was observed that for an increasing spiral angle which causes greater enhanced mixing, the heat transfer coefficients as expected, increased.

Meyer and Olivier [21,22] investigated enhanced tubes with either 25 or 35 fins. For the 15.9 mm diameter tube, the fin height was 0.4 mm, while it was 0.5 mm for the tube diameter of 19.1 mm. From the isothermal friction factors [21], it was concluded that due to the fins causing increased resistance to fluid flow, a transition occurs earlier in comparison to smooth tubes. An interesting observation was made in this study. Namely, a second transition regime was observed between Reynolds numbers of 3 000 to 10 000, which did not occur in prior studies on rough tubes. Although inlet geometries of smooth tubes had a similar effect for friction factors on enhanced tubes in transitional flow, inlet geometries had negligible effects for the second transition. Fins only became effective at rotating fluid at great Reynolds numbers and the increasing helix angle made the end of transition occur earlier. In studying the effect of heating in enhanced tubes [22], both the diabatic friction factors and heat transfer coefficients indicated that transition was independent of inlet geometries. The diabatic friction factors were greater for the isothermal case in the laminar and transitional flow regimes due to free convection effects and the increased mixing caused by the fins. The fins, however, prevented the fluid close to the surface from mixing with the bulk fluid in the centre which was visible from data in laminar flow. This led to greater friction factors because of the greater shear stress and viscosity. It was also found that tubes with a greater helix angle, created a better rotation of the fluid thus increasing heat transfer.

2.6. Conclusions

This chapter gave a brief overview of the fundamental concepts such as the relevant non-dimensional parameters, the different flow regimes, developing and fully developed flow and forced, free, and mixed convective flow. Furthermore, the different parameters that can be used to quantify surface roughness were also explained. Thereafter, the state-of-the-art literature on transitional flow through smooth, rough, and enhanced tubes were reviewed, focussing on both the heat transfer and pressure drop characteristics.

Literature based on the effect of inlet geometries on transitional flow and diabatic friction factors were investigated. In terms of transitional flow, it was found that the onset and end of the transitional flow regime changed for different inlet geometries and a more abrupt change in inlet geometry resulted in the transitional regime occurring earlier. An increased heat flux increased the Reynolds numbers at which the transitional regime onset and ended for all types of inlets. When comparing the heat transfer characteristics of developing flow and fully developed flow, it was found that heat transfer characteristics for developing flow differ from that of fully developed flow for the transitional flow regime. On analysis of the relationship between pressure drop and heat transfer, it was found that the flow regime boundaries for a smooth tube were the same for the friction factors, Colburn j-factors, and f/j-factors when the quasi-turbulent flow regime is considered.

One way of improving the efficiency of the heat exchangers is by making the surface area of heat transfer greater. Enhancements in heat exchangers increase the surface area and mixing, and thus improve its heat transfer and efficiency. Tubes are enhanced using corrugation, threads, spirals, wires, dimples, fins, and deformation. It was found that different enhancements perform better at different Reynolds numbers and can affect the flow regimes considerably. It was generally found that flow transitioned earlier for enhanced tubes.

Due to the challenges in obtaining large relative roughnesses in macrotubes without creating a significant thermal resistance layer, studies that define and investigate the effects of large relative roughness on the heat transfer characteristics of single-phase internal flow are relatively scarce. The purpose of this study was therefore to experimentally investigate the effect of large relative surface roughnesses on the simultaneous heat transfer and pressure drop characteristics of transitional and quasi-turbulent flow.

3. Experimental Set-up and Data Reduction

3.1. Introduction

This chapter provides an overview of the experimental set-up used to conduct heat transfer and pressure drop experiments on smooth and rough tubes. Important components of the experimental set-up such as the flow-calming section, the test section, and the mixers are explained in more detail. The chapter also comprises the experimental procedure used to capture results and the data reduction which is an integral part of the post processing of data.

3.2. Experimental Set-up and Test Sections

The experimental set-up in Figure 3.1 was a closed-loop system in which water was pumped from a thermostat-controlled bath and buffer tank through a filter, flow meter, mixers, flow-calming section, test section, and back to the storage tank. A secondary closed-loop system was connected to the tank to maintain a constant temperature by use of a thermostat-controlled bath with a heating power input of 3.5 kW and a cooling power input of 0.9 kW.

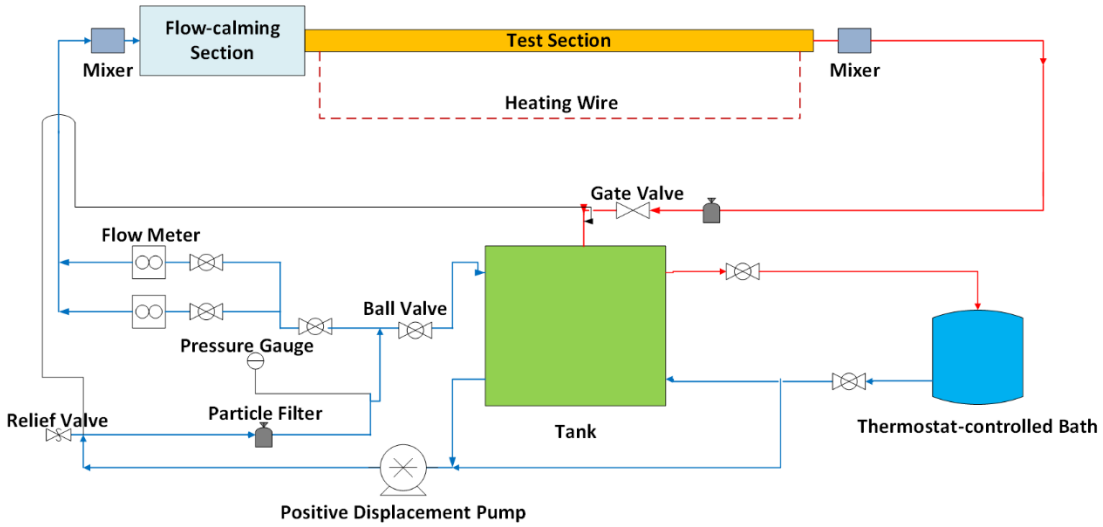

Figure 3.1: Schematic of the experimental set-up that was used to conduct the heat transfer and pressure drop experiments. The test section shown in orange was changed for each relative roughness test.

A 420 ℓ/hr magnetic gear pump was used to circulate the water through the system. The speed of the pump was controlled on the Labview program by changing the voltage signal to it. The pump was connected to the flow loop using a rubber hose to dampen vibrations to the test section. A pressure gauge was attached before the flow meters to monitor the pressure of the system. If the pressure went too high, a pressure relief valve activated, which caused the water to bypass and return to the tank, thus depressurizing the system. To prevent solid particles from being circulated through the system, a 120-micron filter was included. After the filter, a bypass valve was incorporated to increase the backpressure and minimize flow pulsations in the test section to improve the accuracy of the results [89]. The mass flow rate was measured by one of two Coriolis flow meters, CMF 010 or CMF 015, depending on the mass flow rate that was being tested. The two flow meters had a full-scale of 330 ℓ/hr and 108 ℓ/hr, respectively, and accuracies of ±0.05% of the full-scale value.

The same flow-calming section that was used by Bashir et al. [39] was used in this study to ensure a uniform velocity distribution before the flow entered the test section. The flow-

calming section was manufactured from a clear acrylic tube with an outer diameter of 180 mm and length of 616 mm and had a contraction ratio of 33. Mixers were placed before the flow-calming section and after the test section to mix the fluid before measuring uniform inlet and outlet temperatures using Pt100 probes, respectively. The mixer consisted of alternating left and right-hand helical plates [90] that repeatedly sliced the thermal boundary layers to produce a uniform cross-sectional temperature.

Figure 3.2 contains a schematic of the test section, indicating the axial positions of the thermocouple stations (A-U) and the pressure taps (P1 and P2). The inlet of the test section was connected flush to the flow-calming section to obtain a square-edged inlet, while the outlet of the test section was connected to the mixing section. To prevent axial heat conduction from the test section to the flow-calming and mixing sections, the flow-calming section flange and mixing section were manufactured from acetal (which has a low thermal conductivity of 0.31 W/m.K).

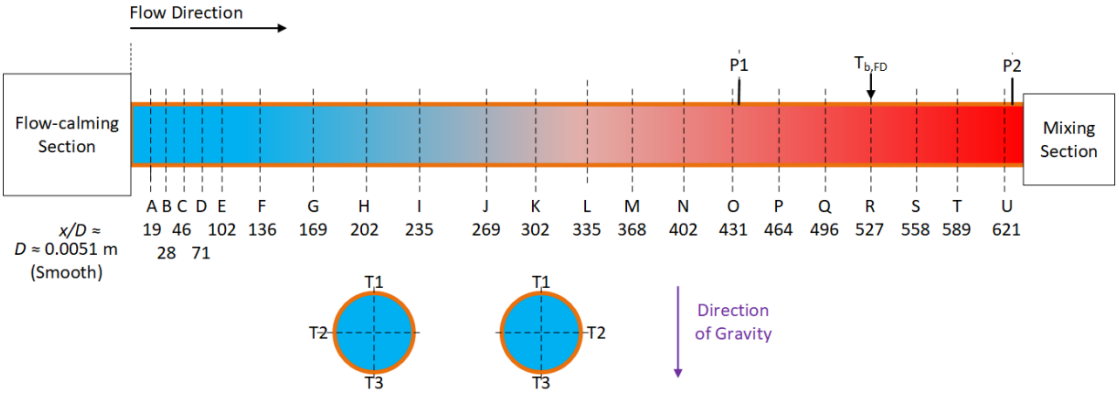

Figure 3.2: Schematic of the test section indicating the axial positions of the thermocouple stations (A-U) and pressure taps (P1 and P2), as well as a cross-sectional view to indicate the alternating thermocouple stations. The placement of the flow-calming section and the mixing section with respect to the test section is also shown.

The test section was manufactured from a hard-drawn copper tube with inner and outer diameters of 5 mm and 6.1 mm, respectively, and a total length of 4 m. The maximum length to diameter ratio, x/D, was 589. A total of 21 thermocouple stations were spaced along the tube length to measure the surface temperatures. As indicated by the cross-sectional view in Figure 3.2, each thermocouple station contained three thermocouples to investigate the circumferential temperature distributions caused by free convection effects. Each thermocouple station contained a thermocouple at the top (T1) and bottom (T3) of the test section, while the third thermocouple, T2, alternated between the left and right of the test section along the tube length. The thermocouples were spaced close to each other near the inlet of the test section to accurately capture the developing temperature profile. Furthermore, a length of 400 mm was left between the last thermocouple station, U, and the mixer to prevent upstream effects from influencing the temperature measurements at the last measuring station. Araldite 2014-2 adhesive with a thermal conductivity of 0.34 W/m.K was used to glue the thermocouples into indentations of approximately 50% of the tube's wall thickness. The Pt100 probes and thermocouples (used to measure the surface temperatures on the test section) were calibrated to accuracies of 0.06°C and 0.1°C, respectively, using a reference temperature thermometer with an accuracy of ±0.03°C. The details of the calibration methods of the Pt100 probes and thermocouples are given in Appendix A.

Pressure taps P1 and P2 in Figure 3.2 were made from a 30 mm long capillary tube, which was silver soldered to the test tube. A 0.4 mm diameter hole was drilled through the capillary and test tubes. This hole was less than 10% of the inner diameter of the test section which prevented the pressure taps from causing obstructions [91]. All burrs were carefully removed from the inside of the tube. A bush tap with a quick-release coupling was installed onto the pressure tap and nylon tubing was used to connect the pressure taps to the pressure transducer which contained interchangeable diaphragms. Three different diaphragms with full-scale values of 2.2 kPa, 14 kPa, and 55 kPa were used. The accuracy of each diaphragm was 0.25% of the full-scale value. The pressure transducers were calibrated using Beta T-140 manometers and the method and details are given in Appendix A.

The pressure taps were placed at the latter part of the test section, 0.97 m apart, where a fully developed flow was expected at certain Reynolds numbers. At a Reynolds number of 1 200, the laminar forced convective [2] and mixed convective [26] thermal entrance lengths were calculated to be 3.8 m and 0.64 m, respectively. The entrance lengths would decrease as the Reynolds number decreases. The average Nusselt numbers and friction factors were calculated in the last 1 m of the test section between the pressure taps (stations O to U in Figure 3.2). Therefore, the average Nusselt numbers and friction factors contained fully developed flow for mixed convection conditions but contained some developing flow (depending on the Reynolds number) for forced convection conditions.

Different methods were investigated to obtain a uniform surface roughness on the inside of the tube and the details are summarised in Appendix A. Ultimately, a unique roughening method was used to achieve a uniform surface roughness over a tube length of 4 m, while minimizing the additional thermal resistance. Because of their high thermal conductivity, copper particles were glued to the inside of the test section. The copper particles were sifted and sorted according to different sizes (75–150 µm and 150–300 µm) to achieve the different surface roughnesses in the tubes. Different types of glues were tested, and the best results were obtained using Soudal Cyanofix 84A because its low viscosity made it easy to spread and cover the tube with a consistent thin glue layer. To achieve a uniform inner surface covering of the glue layer, the glue was first blown through the tube using pressurized air and thereafter, copper particles were blown through the tube from a pressurized container. The particles and glue formed a ripple texture on the tube surface and the heights depended on the size of the particles used. This ripple texture was the primary degree of roughness that disturbed the flow.

The roughness of the smooth tube was measured using a portable roughness tester, Mitutoyo Surftest SJ-210, with a range of -200 µm to 160 µm and a resolution of 0.02 µm. As the surface roughness of the rough tubes exceeded the ranges of the available instrumentation, the surface roughness was obtained using a milling machine and a dial indicator, which had an accuracy of 12 µm. The tube was cut into 12 sample lengths and three readings were taken at different locations on each sample. The readings were then averaged to get a good representation of the average surface roughness along the tube length and the results are summarised in Table 3.1. For rough 1, 67% of the measured data fell within one standard deviation, 93% of the data fell within two standard deviations, and all the data fell within three standard deviations. The uniformity of rough 2 was more uniform as 84% of the measured data fell within one standard deviation and 95% within two standard deviations.

Table 3.1: Summary of the roughness [mm] values and relative roughness for test sections tested.

Tube	Roughness, *Ra* [mm]	Relative roughness, *ε/D*
Smooth	1.917×10^{-3}	3.76×10^{-4}
Rough 1	0.166	0.04
Rough 2	0.443	0.11

To obtain a constant heat flux boundary condition, two 0.38 mm diameter constantan heating wires were tightly wound around the test section and connected in parallel, with opposing polarities, to a direct current (DC) power supply. The accuracy of the 3 kW power supply was 3 W. The opposing currents dampened the electromagnetic interference [89]. Care was taken not to coil the heating wire over the thermocouple junction (where the thermocouple was glued onto the tube) to prevent the surface temperature measurements from being affected. A gap of 1 mm, which was found to be sufficient [89], and was left on either side between the thermocouple junction and the coiled heating wire.

To prevent heat losses from the flow-calming section, test section, and mixers to the surroundings, these components were well-insulated using Armaflex Class O insulation with a thermal conductivity of 0.035 W/m.K. Using one-dimensional heat transfer calculations, a thickness of 80 mm over the test section was found to be sufficient to limit the maximum heat loss to 2%.

A data acquisition system was used to capture the experimental data. This data was then recorded with a National Instruments Labview program. The data acquisition system comprised an SCXI (Signal Conditioning eXtensions for instrumentation), a computer, and National Instruments Labview Software which was used to log the data. The speed of the pump was controlled by changing the voltage input on the Labview program. Mass flow rates, temperatures, and pressure drops were recorded through the Labview program. The data reduction and plots were completed using Matlab software.

3.3. Data Reduction

The mean fluid temperature, T_m, was calculated using a linear distribution over the tube length, L, where x is the distance on the tube to a specific axial position. T_o is the outlet temperature measured by the Pt100 probe in the mixing section, and T_i is the inlet temperature measured by the Pt100 probe in the flow-calming section.

$$T_m = \left(\frac{T_o - T_i}{L}\right) x + T_i \tag{3.1}$$

The bulk fully developed fluid temperature, $T_{b,FD}$, was calculated in the centre of the two pressure taps in Figure 3.2.

$$T_{b,FD} = \left(\frac{T_0 - T_i}{L}\right) 2.7 + T_i \tag{3.2}$$

The thermophysical correlations of water [92] were used to calculate the specific heat capacity, C_p, thermal conductivity, k, Prandtl number, Pr, dynamic viscosity, μ, density, ρ, and the thermal expansion coefficient, β. The fully developed bulk fluid temperature was used to calculate the

bulk fluid properties, while the mean fluid temperatures were used to calculate the local fluid properties.

The Reynolds number, *Re*, is a function of the mass flow rate, $\dot{m}$, dynamic viscosity, μ, and inner diameter, *D*:

$$Re = \frac{4\dot{m}}{\mu D\pi} \tag{3.3}$$

The electrical power input from the power supply was calculated as the product of the voltage and current ($Q_e = VI$) and remained constant. The heat transfer rate to the water ($Q_w = \dot{m}C_p(T_o - T_i)$) should be close to the electrical power input in a well-insulated system, and the energy balance error, *EB,* gives an indication of the heat losses in the system:

$$EB = \left|\frac{VI - \dot{m}C_p(T_o - T_i)}{VI}\right| \times 100 \tag{3.4}$$

To account for minor heat losses to ambient surroundings, the heat transfer rate to the water was used to calculate the heat flux:

$$\dot{q} = \frac{\dot{Q}}{\pi DL} = \frac{\dot{m}C_p(T_o - T_i)}{\pi DL} \tag{3.5}$$

The total thermal resistance across the tube wall, R_{total}, due to the different thermal resistances caused by the glue layers and copper, are summarised in Figure 3.3, and was calculated as:

$$R_{total} = \frac{\ln\left(\frac{D_{o,g}}{D_o}\right)}{2\pi Lk_{o,g}} + \frac{\ln\left(\frac{D_o}{D}\right)}{2\pi Lk_t} + \frac{\ln\left(\frac{D}{D_{i,g}}\right)}{2\pi Lk_{i,g}} + \frac{\ln\left(\frac{D_{i,g}}{D_r}\right)}{2\pi Lk_t} \tag{3.6}$$

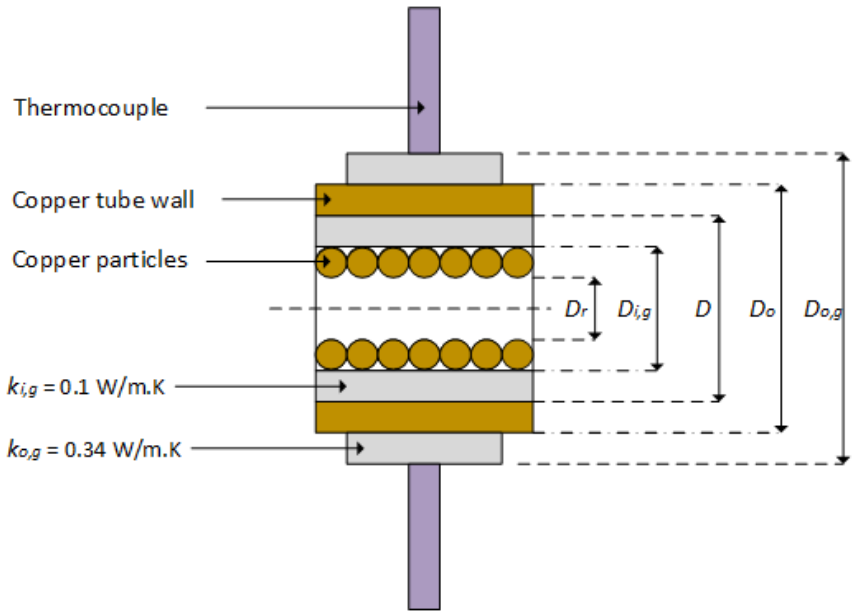

Figure 3.3: Schematic of axial cross-section of a rough tube indicating the different thermal resistances presented in the heat transfer analysis

where $D_{o,g}$ accounts for the thin glue layer between the thermocouple and the surface of the tube, D_o and D are the outer and inner diameters of the tube, $D_{i,g}$ is the inner diameter of the tube with an inner glue layer that fixes the copper particles to the inner tube surface and lastly D_r is the constricted inner diameter of a rough tube. The thermal conductivities of materials with a significant thermal resistance are the thermocouple glue, $k_{o,g}$, and the cyanoacrylate, $k_{i,g}$, that was used to glue the copper particles to the inner surface of the tube, which had thermal conductivities of 0.34 W/m.K and 0.1 W/m.K, respectively. In Eq. 3.6, the diameters remain the same in this instance when analysing rough tubes. The second and last terms of Eq. 3.6, which represented the thermal resistance across the copper tube wall and copper particles, was negligible due to the high thermal conductivity of copper, k_t, being 401 W/m.K.

The temperature difference between the inner surface and the temperature measured by the thermocouple on the test section was thus calculated as the product of the heat input and the total thermal resistance:

$$\Delta T = \dot{Q} R_{total} \tag{3.7}$$

The average outer surface temperature at a thermocouple station, $T_{s,o}$, was taken as the sum of; T_1, T_3 and $2T_2$ (Figure 3.2) thermocouple temperature measurements at the thermocouple station divided by four. This accounted for any temperature differences on the tube's surface from free convection effects. The average inner surface temperature at a thermocouple station was then obtained by subtracting the temperature drop due to the thermal resistance of the glue layers:

$$T_s = T_{s,o} - \Delta T \tag{3.8}$$

The average surface temperature along the tube length was calculated as follows:

$$\overline{T}_s = \frac{1}{L}\int_0^L T_s(x)\,\mathrm{d}x \tag{3.9}$$

The average heat transfer coefficient, h, was calculated from the heat flux, average surface temperature, and bulk fluid temperature:

$$h = \frac{\dot{q}}{(\overline{T}_s - T_b)} \tag{3.10}$$

The average Nusselt numbers, Nu, were calculated from the average heat transfer coefficient as follows:

$$Nu = \frac{hD}{k} \tag{3.11}$$

The local heat transfer coefficient, *h,* was calculated from the heat flux, local surface temperature (Eq. 3.8) and mean fluid temperature (Eq. 3.1), and the local Nusselt numbers, *Nu*, were calculated from the local heat transfer coefficients.

The friction factors, *f*, were calculated using the mass flow rate and pressure drop measurements taken between two pressure taps, distance 0.97 m apart:

$$f = \frac{\Delta P \rho D^5 \pi^2}{(0.97) 8 \dot{m}} \tag{3.12}$$

By replacing *D*, the measured inner diameter of the smooth tube, with D_r, the measured inner diameter of the rough tube (or the constricted flow diameter), the same methodology (Eqs. 3.2-3.5 and Eqs. 3.11-3.13) can be applied for rough tubes.

For validation purposes, the percentage error for a value (*M*) was calculated as follows:

$$\%error = \frac{|M_{exp} - M_{cor}|}{M_{cor}} \tag{3.13}$$

The uncertainties were calculated within a 95% confidence interval using the method of Dunn [93] and examples of the calculations can be found in the work of Everts [64] as well as Everts and Meyer [94]. The bias error was obtained from the inaccuracies of the instrumentation, as summarised in Table 3.2, and the precision error was obtained from the standard deviation of 200 data points.

Table 3.2: Summary of the ranges and inaccuracies of the instrumentation used.

Instrumentation	**Range**	**Inaccuracy**
Thermocouples	<150°C	0.1°C
Pt100s	0.166	0.06°C
Power supply	0–1.5 kW	3 W
Flow meters:		
CMF 010	0–108 ℓ/hr	0.054 ℓ/hr
CMF 015	0–330 ℓ/hr	0.165 ℓ/hr
Pressure transducers:	0–2.2 kPa	5.5 Pa
	0–14 kPa	35 Pa
	0–55 kPa	137.5 Pa

The Reynolds number uncertainties in the smooth tube were less than 1.3% and were found to be insensitive to varying heat fluxes. For the smooth tube, the average Nusselt number uncertainties at a heat flux of 3 kW/m^2 varied between 3.6% and 15% for Reynolds numbers between 1 100 and 5 000. The corresponding friction factor uncertainties varied between 3% and 2%, respectively. As the heat flux was decreased, the Nusselt number uncertainties increased due to the smaller surface-fluid temperature differences, but the friction factor uncertainties did not change significantly. When the surface roughness was increased to rough 2, the Reynolds number uncertainty was not significantly affected and was less than 2%. The average Nusselt number uncertainties varied between 8% and 11% for Reynolds numbers

between 1 100 and 3 000 at a heat flux of 3 kW/m^2 and the corresponding friction factor uncertainties were approximately 3%. The slight increase in the Nusselt number uncertainties with increasing surface roughness was again due to the smaller surface-fluid temperature differences. Table 3.3 summarises uncertainties for heat fluxes 1, 3 and 5 kW/m^2. Table 3.4 summarises the uncertainties for the 3 kW/m^2 heat flux for the different flow regimes, where the boundaries of the flow regimes are confirmed in Chapter 5 and Appendix A.

Table 3.3: Summary of uncertainties [%] for parameters *Re*, *Nu*, *j* and *f* at different roughnesses and heat fluxes.

Tube	**Heat flux [kW/m^2]**	***Re***	***Nu***	***j***	***f***
Smooth	1 kW/m^2	1.1 – 1.2	8.1 – 86	8.2 – 86	2.5 – 3.1
	3 kW/m^2	1.1 – 1.2	3.6 – 17	3.9 – 21	2.5 – 2.9
	5 kW/m^2	1.1 – 1.2	2.8 – 11	3.1 – 12	2.5 – 3.7
Rough 1	1 kW/m^2	1.1 – 1.5	5.2 – 24	5.9 – 24	2.5 – 4.7
	3 kW/m^2	1.1 – 1.6	3.1 – 7.7	3.5 – 7.8	2.5 – 10
	5 kW/m^2	1.1 – 1.4	2.7 – 4.8	3.1 – 5.0	2.5 – 4.4
Rough 2	1 kW/m^2	1.1 – 2.3	7.3 – 88	7.6 – 88	1.4 – 1.7
	3 kW/m^2	1.1 – 2.0	3.9 – 11	4.4 – 11	2.5 – 4.1
	5 kW/m^2	1.1 – 1.4	3.5 – 6.6	3.8 – 6.7	2.5 – 3.3

Table 3.4: Summary of uncertainties [%] for parameters *Re*, *Nu*, *j* and *f* at different roughnesses and flow regimes at a heat flux of 3 kW/m^2.

Tube	**Flow Regime**	***Re***	***Nu***	***j***	***f***
Smooth	Laminar	1.1 – 1.2	3.6 – 4.4	3.9 – 4.6	2.6 – 2.9
	Transition	1.1	4.5 – 5.7	4.8 – 5.9	2.5 – 2.6
	Quasi-turbulent	1.1	5 – 15	5.2 – 15	2.5
	Turbulent	1.1	16 – 21	16 – 21	2.5
Rough 1	Laminar	1.4 – 1.6	3.1 – 3.2	3.5 – 3.6	5 – 10
	Transition	1.3 – 1.4	3.2 – 3.5	3.6 – 3.8	2.8 – 5
	Quasi-turbulent	1.2 – 1.3	3.6 – 4.0	3.9 – 4.3	2.6 – 2.7
	Turbulent	1.1	4.0 – 7.7	4.3 – 7.8	2.5
Rough 2	Laminar	1.5 – 2.0	3.9 – 4.2	4.4 – 4.6	2.7 – 4.1
	Transition	-	-	-	-
	Quasi-turbulent	1.2 – 1.3	4.7 – 6.7	5.0 – 6.9	2.7 – 3.4
	Turbulent	1.2 – 1.1	7.1 – 11	7.2 – 11	2.5 – 2.6

For both Table 3.3 and Table 3.4 the Reynolds number uncertainties were less than 2.3% in all flow regimes with the greatest uncertainties found in the laminar flow regime. The Reynolds number uncertainty decreased at low Reynolds numbers because the accuracy of the flow meters decreased at lower flow rates. To achieve laminar flow in rough tubes, tests were conducted at lower flow rates in comparison to the smooth tube. The effect of heat flux on the Reynolds number uncertainty was negligible. Both the Nusselt number and Colburn *j*-factor uncertainties decreased for a greater heat flux applied, primarily because of the lower

temperature uncertainties attributed to the greater difference between surface and fluid temperature. The laminar flow regime had similar uncertainties across the tubes. However, the uncertainties increased in the transitional flow regime due to temperature fluctuations. The uncertainties, thereafter, increased with increasing Reynolds numbers in the quasi-turbulent and turbulent flow regimes. Rough tubes, however, had lower uncertainties in transition, quasi-turbulent and turbulent flow in comparison to the smooth tube. This is because the flow regimes occurred earlier at lower Reynolds numbers where the surface-fluid temperature difference is greater. The Colburn *j*-factor uncertainties were slightly greater than the Nusselt number uncertainties, except in the turbulent flow regime which was of an equal magnitude. The maximum Nusselt number and Colburn *j*-factor uncertainties (7.8% and 11%) in the turbulent flow regime for rough tubes 1 and 2 respectively, were less than the smooth tube (21%) due to lower Reynolds numbers being tested for. Rough tubes could not be tested to the same high Reynolds numbers as the smooth tube because of the high mean fluid temperature and high pressure drop constraints. The friction factor uncertainties were the greatest in the laminar flow regime due to the low pressure drops found in this regime. The lowest pressure drops were the furthest from the full-scale value of the pressure transducer diaphragm which, therefore, had lower accuracy. The maximum friction factor uncertainty (10%) was found in the laminar flow regime for rough 1. Thereafter, Table 3.4 shows that all other tubes' friction factor uncertainties in the transitional, quasi-turbulent, and turbulent flow regimes were below 5%.

3.4. Experimental Procedure and Test Matrix

Before any readings were taken, steady-state conditions were sought after. Approximately two to three hours were required to reach steady-state conditions after the start-up at the beginning of the day. Steady-state was assumed once there was no significant change in temperature, pressure drop, mass flow rates, and energy balance readings for approximately five minutes. Thereafter, 200 data points were taken at a frequency of 20 Hz, which were then averaged to obtain a single value. Experiments were done by setting the mass flow rate to the maximum Reynolds number and thereafter, reducing the mass flow rate by reducing the pump speed. The bypass and inlet valves were also used to adjust the mass flow rate through the test section and ensure that the pump was operated at high speed to reduce the pulsations created by the magnetic drive gear pump.

The focus of this study was on transitional flow. Therefore, most of the experiments involved testing ranges around the transitional flow regime, while sufficient portions of the laminar and turbulent flow regimes were also covered for the smooth tube. The significant surface roughnesses tested in this study caused the transitional flow regime to occur at significantly lower Reynolds numbers than for a smooth tube. Limiting factors of the experimental set-up determined the tested Reynolds number range which is shown in Table 3.5. The minimum and maximum Reynolds numbers were chosen such that the outlet water temperature was kept below 60°C and the system pressure below 2.5 bar. As summarised in Table 3.5, a total of 557 mass flow rate measurements, 25 560 temperature measurements, and 557 pressure drop measurements were taken.

Table 3.5: The experimental test matrix summarising the number of mass flow rate measurements, pressure drop measurements, temperature measurements and their ranges tested.

Tube	Heat flux [kW/m^2]	Mass flow rate	Pressure drop	Temperature	Reynolds number range
Smooth	0	73	73		500–8 300
	0.3	2	2	130	600–700
	1	36	36	2 340	1 000–8 300
	3	35	35	2 275	1 100–8 300
	5	55	55	3 575	1 200–8 500
	7	54	54	3 510	1 200–8 500
Rough 1	0	31	31		800–6 000
	1	25	25	1 625	200–6 000
	2	22	22	1 430	300–6 000
	3	22	22	1 430	500–6 000
	5	18	18	1 170	800–6 000
	7	17	17	1 105	1 200–6 000
Rough 2	0	49	49		100–4 000
	1	35	35	2 275	200–4 000
	2	29	29	1 185	300–4 000
	3	20	20	1 300	400–4 000
	5	18	18	1 170	800–4 000
	7	16	16	1 040	1 200–3 000
Total		557	557	25 560	

3.5. Conclusions

An overview of the experimental set-up, instrumentation, test section, and roughening method was given. The test section was manufactured from a hard-drawn copper tube with inner and outer diameters of 5 mm and 6.1 mm, respectively and a total length of 4 m. Twenty-one thermocouple stations were placed along the tube to measure surface temperature. Pressure taps were placed at the latter part of the test section, 0.97 m apart, to measure the fully developed pressure drops. A roughening method, which also minimized additional thermal resistance, was used to achieve uniform surface roughness over the tube length. Copper particles were glued to the inside of the test section. Different surface roughnesses were achieved by using different sizes of copper particles in the tubes.

An uncertainty analysis was conducted, and the uncertainties were calculated within a 95% confidence interval. The Reynolds number uncertainties in the smooth tube were less than 1.3% with heat flux found to have a negligible effect. Average Nusselt number uncertainties were found to be between 3.6% and 15% for Reynolds numbers between 1 100 and 5 000. The corresponding friction factor uncertainties varied between 3% and 2%, respectively. For the tube with the greatest roughness (rough 2) the average Nusselt number uncertainties varied between 8% and 11% for Reynolds numbers between 1 100 and 3 000 at a heat flux of 3 kW/m^2 and the corresponding friction factor uncertainties were approximately 3%.

Following the start-up, an estimated time of two to three hours were needed to reach steady-state conditions. A steady state was assumed once there was no significant change in temperature, pressure drop, mass flow rates, and energy balance readings for approximately five minutes. Because this study focused on transitional flow, majority of the experiments involved testing ranges around this. A total of 557 different mass flow rate measurements, 25 560 temperature measurements and 557 pressure drop measurements were taken.

The experimental set-up can be improved by increasing the ranges of its testing. This will enable the testing range to be tested further into the fully rough, turbulent flow regime. Therefore, a bigger dataset can be used to accurately assess the onset of the turbulent flow regime. The limiting factor was the clear acrylic flow-calming section which had a maximum allowable pressure of 3 Bar. Improving the construction of the flow-calming section can improve the maximum pressure that the system can achieve. It is also recommended that improved thermal conductivities for the glues that join the thermocouples to the copper tube section and the copper particles to the inner copper tube section be further researched into and tested. If enhanced, this will reduce the uncertainty of the results obtained.

4. Validation

4.1. Introduction

To show that the results of this study are reliable and repeatable, the laminar and turbulent results obtained using the smooth tube are compared with literature. The validation focuses on the fully developed isothermal friction factors, the average laminar and turbulent Nusselt numbers, as well as the local Nusselt numbers for forced convection and mixed convection conditions.

4.2. Fully Developed Isothermal Friction Factor

A total of 38 data points were taken to validate the fully developed isothermal friction factors between Reynolds numbers 500 and 8 300 in Figure 4.1. Comparing the laminar friction factors to the Poiseuille [95] friction factor in Eq. 4.1 between Reynolds numbers of 500 and 1 900, the friction factors had an average deviation of 2.2%. The deviation increased from 1% at a Reynolds number of 500 to 7.9% at a Reynolds number of 1 900. The transitional flow regime started at a Reynolds number of 2 850 and had a deviation of 18.1% from the Poiseuille equation.

$$f = \frac{64}{Re} \tag{4.1}$$

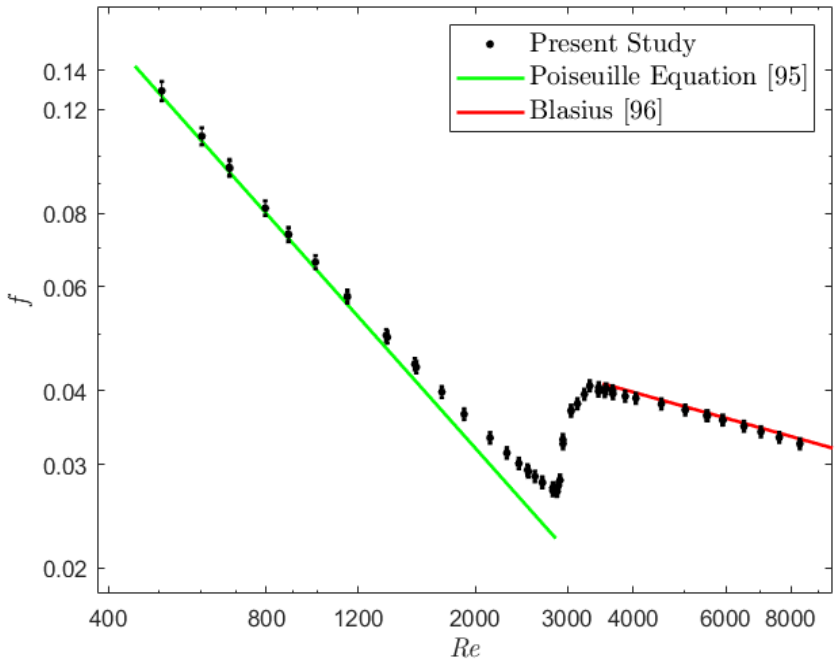

Figure 4.1: Validation of the fully developed isothermal friction factors as a function of Reynolds number with the correlations of Poiseuille [95] and Blasius [96] in the laminar and turbulent flow regimes, respectively.

In the turbulent flow regime, the friction factors were compared to the Blasius [96] correlation in Eq. 4.2 between Reynolds numbers of 3 470 and 8 300. The average deviation was 0.9% with the maximum deviation of 1.8% occurring at a Reynolds number of 3 470.

$$f = 0.316Re^{-0.25} \tag{4.2}$$

4.3. Average Nusselt Numbers

To calculate the average fully developed Nusselt numbers, only the thermocouple stations between the pressure taps (stations O to U in Figure 3.2) were used. A heat flux of 7 kW/m^2 was applied to the test section and measurements were taken between Reynolds numbers of 1 200 to 3 100 in the laminar flow regime and 3 600 to 8 100 in the turbulent flow regime to validate the average Nusselt numbers in Figure 4.2.

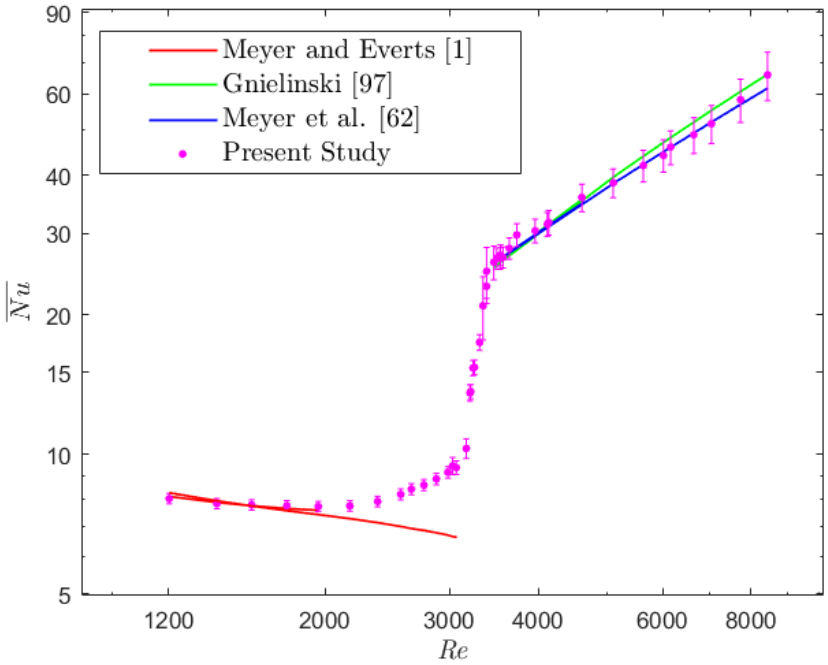

Figure 4.2: Validation of the average Nusselt numbers as a function of Reynolds number at a heat flux of 7 kW/m^2 with the correlation of Meyer and Everts [1] in the laminar flow regime and the correlations of Meyer et al. [62] and Gnielinski [97] in the turbulent flow regime.

The laminar Nusselt numbers were validated using the correlation of Meyer and Everts [2] in Eq. 4.3, which is valid for both developing and fully developed mixed convective laminar flow. The average laminar Nusselt numbers were significantly greater than the theoretical fully developed forced convective Nusselt number of 4.36 for a constant heat flux boundary condition, as free convection effects increased the Nusselt numbers. The average deviation was 1.2% between Reynolds numbers of 1 200 and 2 000 when compared with the correlation of Meyer and Everts [2], while the average deviation between Reynolds numbers of 1 200 and 3 100 was 12.9%. There was an increase in Nusselt numbers between Reynolds numbers of 2 000 to 3 050 because of developing flow. The mixed convection thermal entrance lengths were 2.5 m and 5 m, respectively, for Reynolds numbers of 2 000 and 3 050. Therefore, at a Reynolds number of 2 000 the fully developed section between the pressure taps contained 0% developing flow, however, at a Reynolds number of 3 050 it contained 100% developing flow. As the local heat transfer coefficients are higher for developing flow than fully developed flow, the average Nusselt numbers increased.

$$\overline{\mathrm{Nu}} = 4.36 + \overline{Nu_1} + \overline{Nu_2}$$

$$\overline{Nu_1} = \frac{1}{L}\int_0^{Lt_{MCD}} Nu_1 dL = \frac{1}{L}\left(-0.84 Pr_b^{-0.2} Lt_{MCD} + 0.72 (Re_b D)^{0.54} Pr_b^{0.34} Lt_{MCD}^{0.46}\right)$$

$$\overline{Nu_2} = \frac{1}{L}\int_{Lt_{MCD}}^{L} Nu_2 dL = \frac{1}{L}\left(0.207 Gr_b^{0.305} - 1.19\right) Pr_b^{0.42} (Re_b D)^{-0.08} (L - Lt_{MCD}) \quad 4.3$$

$$Lt_{MCD} = \frac{2.4 Re_b Pr_b^{0.6} D}{Gr_b^{0.57}} \text{ for } L > Lt_{MCD}$$

$$Lt_{MCD} = L \text{ for } L < Lt_{MCD}$$

.

For turbulent flow, the experimental data deviated from the correlation (Eq. 4.4) of Meyer et al. [62] with an average deviation of 1% between Reynolds number 3 600 to 8 400. The maximum deviation of 6.9% was found at a Reynolds number of 8 400. When comparing the experimental data with the correlation of Gnielinski [97] (Eq. 4.5), an average deviation of 2% was obtained between Reynolds numbers of 3 600 and 8 400. The minimum deviation was found to be 0.3% at a Reynolds number 4 100, while the maximum deviation was 5.3% at a Reynolds number of 7 000. The increased deviation at higher Reynolds numbers was due to the increased uncertainties caused by the decreased surface-fluid temperature differences.

$$Nu = \frac{(\xi/8)(Re - 1000)\mathrm{Pr}}{1 + 12.7\sqrt{(\xi/8)}(Pr^{2/3} - 1)}\left[1 + \left(\frac{D}{L}\right)^{2/3}\right]\left(\frac{\mathrm{Pr}}{\mathrm{Pr}_S}\right)^{0.11} \quad 4.4$$

$$\xi = (1.8 \log_{10} Re - 1.5)^{-2}$$

$$Nu = 0.018 Re^{-0.25} (Re - 500)^{1.07} Pr^{0.42} \left(\frac{Pr}{Pr_w}\right)^{0.11} \quad 4.5$$

4.4. Local Laminar Nusselt Numbers: Forced Convection

It is very challenging to experimentally obtain fully developed forced convection conditions in macrotubes [26]. To achieve this, a small heat flux must be applied such that free convection effects caused by heating are negligible. To validate the local forced convective Nusselt numbers in Figure 4.3, a heat flux of only 0.3 kW/m^2 was applied at a bulk Reynolds number of 700 and the data was compared to the correlation of Shah and London [44] (Eq. 4.6) , which is valid for simultaneously hydrodynamically and thermally developing flow. The horizontal black dotted line represents the theoretical Nusselt number of 4.36 for fully developed forced convective flow through tubes heated at a constant heat flux [45]. The data was checked against the flow regime map for developing flow of Everts and Meyer [28] which confirmed that forced convection conditions were to be expected.

$$Nu_{SL} = Nu_1 \times Nu_2 - 1$$

$$Nu_1 = \left[1 + \left(\frac{\pi/(115.2 z^*)}{\{1 + (Pr/0.0207)^{2/3}\}^{1/2}\{1 + (220 z^*/\pi)^{-10/9}\}^{3/5}}\right)^{5/3}\right]^{3/10} \quad 4.6$$

$$Nu_2 = 5.364\left[1 + (220 z^*/\pi)^{-10/9}\right]^{3/10}$$

$$z^* = \frac{\pi}{4Gz}$$

.

The local Nusselt numbers correlated very well with the correlation of Shah and London [44], with an average deviation of 4.4%. The fully developed Nusselt numbers between x/D = 135 and x/D = 590 had an average deviation of 15.2% from 4.36, which was within the uncertainties of the experimental data. The maximum uncertainty of 31.4% was found at the inlet and the average uncertainty was 22.9%. The high uncertainties were due to the very small surface-fluid temperature differences. The surface-fluid temperature difference at the first thermocouple station was 0.33°C and increased along the tube length to 0.46°C at the last thermocouple station, while the difference between the inlet and outlet temperatures was only 1.60°C.

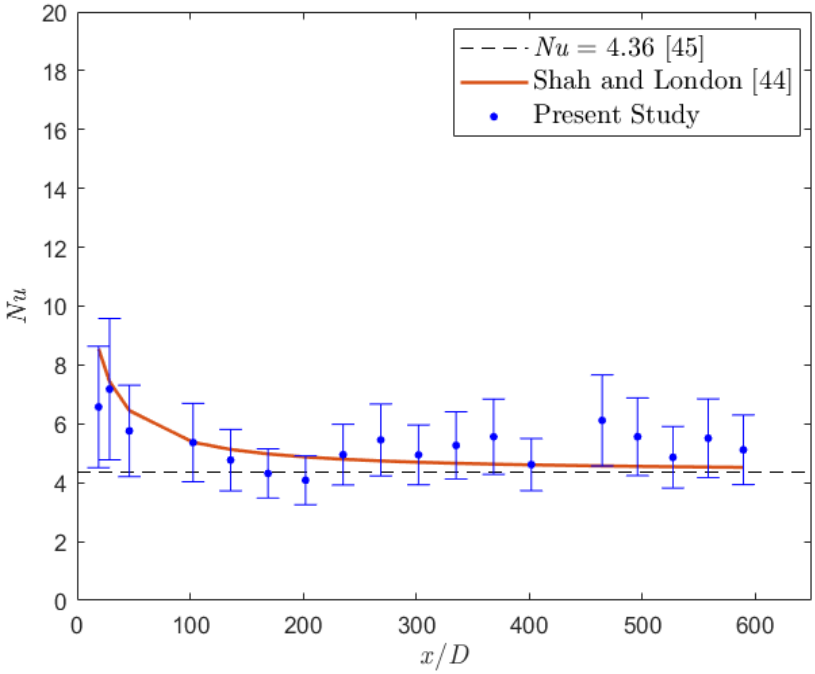

Figure 4.3: Comparison of the local Nusselt numbers as a function of axial position for forced convective laminar flow at Reynolds number of 700 and heat flux of 1 kW/m^2 with the correlation of Shah and London [44] and the theoretical Nusselt number of 4.36 [45].

4.5. Local Laminar Nusselt Numbers: Mixed Convection

The local mixed convective laminar Nusselt numbers were obtained at a heat flux of 7 kW/m^2 and a bulk Reynolds number of 1 200. The flow regime map of Everts and Meyer [28] for developing flow was used to verify that mixed convection conditions were to be expected. Figure 4.4 indicates that the Nusselt numbers were on average 77% greater than the theoretical forced convection Nusselt number of 4.36 due to the heat transfer enhancement caused by free convection effects. The Nusselt numbers correlated very well with the correlation of Meyer and Everts [2], with an average deviation of 0.4%.

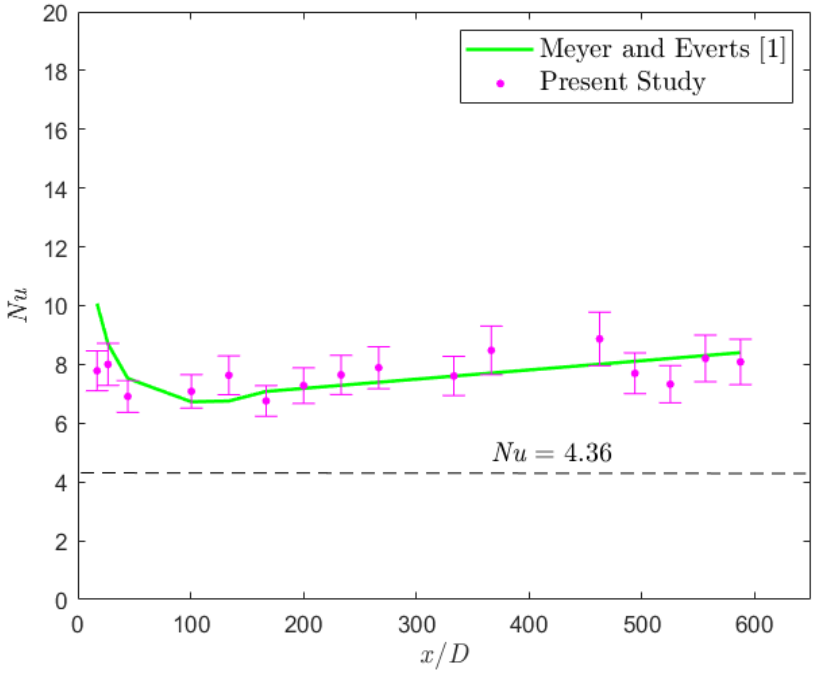

Figure 4.4: Comparison of the local Nusselt numbers as a function of axial position for mixed convection laminar flow at Reynolds number of 1 200 and heat flux of 7 kW/m^2 with the correlation of Meyer and Everts [1]. The dotted line shows a Nusselt number of 4.36.

4.6. Conclusions

The experimental set-up and data reduction method were successfully validated using the smooth tube results. The validation focused on the fully developed isothermal friction factors, average laminar and turbulent Nusselt numbers, and the local Nusselt numbers for both forced and mixed convection conditions. Multiple data points were taken to validate the fully developed isothermal friction factors between Reynolds numbers 500 and 8 300. By comparing the laminar friction factors to correlations between Reynolds numbers of 500 and 1 900, an average deviation of 2.2% was found. A deviation of 18.1% was found where the transitional flow regime started at a Reynolds number of 2 850. Finally, an average deviation of 0.9% was found when comparing friction factors in the turbulent flow regime to correlations. . An empirical correlation that suitably validates a rough tube was not found for the duration of the study. The reason being is that the equations found did not accurately satisfy the type or shape of random ripple roughness found for these tubes.

With regards to average Nusselt numbers, the following average deviations were found from correlations, namely, 1.2% between Reynolds numbers 1 200 and 2 000 for laminar flow, 12.9% between Reynolds numbers of 1 200 and 3 100 for laminar flow due to developing flow and 1% between Reynolds number 3 600 to 8 400 for turbulent flow. In this study, a heat flux of 0.3 kW/m^2 was applied at a bulk Reynolds number of 700 to obtain forced convective conditions. Local Nusselt numbers revealed an average deviation of 4.4% with correlations. Fully developed Nusselt numbers between x/D = 135 and x/D = 590 held an average deviation of 15.2% from 4.36, which was within the uncertainties of the experimental data. Under mixed convection conditions, Nusselt numbers revealed to be 77% greater than theoretical forced convection numbers. This result was due to heat transfer enhancement caused by free convection effects. Nusselt numbers under these conditions revealed an average deviation of 0.4% with the mixed convective correlation.

5. Results

5.1. Introduction

In this chapter, the heat transfer and pressure drop characteristics of smooth and rough tubes are investigated. The specific objective is to investigate the influence of surface roughness and heat flux on friction factors and heat transfer coefficients. The relationship between heat transfer and pressure drop through rough tubes is also investigated.

5.2. Pressure Drop Results

5.2.1. Effect of Surface Roughness

The isothermal (heat flux of 0 kW/m^2 and represented using the black markers) and diabatic (heat flux of 3 kW/m^2 and represented using the red markers) friction factors as a function of Reynolds number are compared in Figure 5.1 for the smooth, rough 1, and rough 2 test sections to investigate the effect of surface roughness on the friction factors in the different flow regimes. In general, there is a clear upward and leftward shift in the friction factors with increasing surface roughness across the different flow regimes. From laminar flow theory, the friction factors for a smooth tube can be given as $f = 64/Re$, which is commonly known as the Poiseuille equation [95] and indicated by the dashed green line. For the smooth tube at a Reynolds number of 1 150, the friction factors correlated very well with the Poiseuille equation [95]. As the Reynolds number was increased further in the laminar flow regime, the friction factors began to deviate slightly from the Poiseuille correlation, and the Reynolds number at which the deviation started was lower for the isothermal ($Re \approx 1\,150$) than the diabatic ($Re \approx 1\,730$) friction factors due to the lower viscosity of the fluid caused from heating.

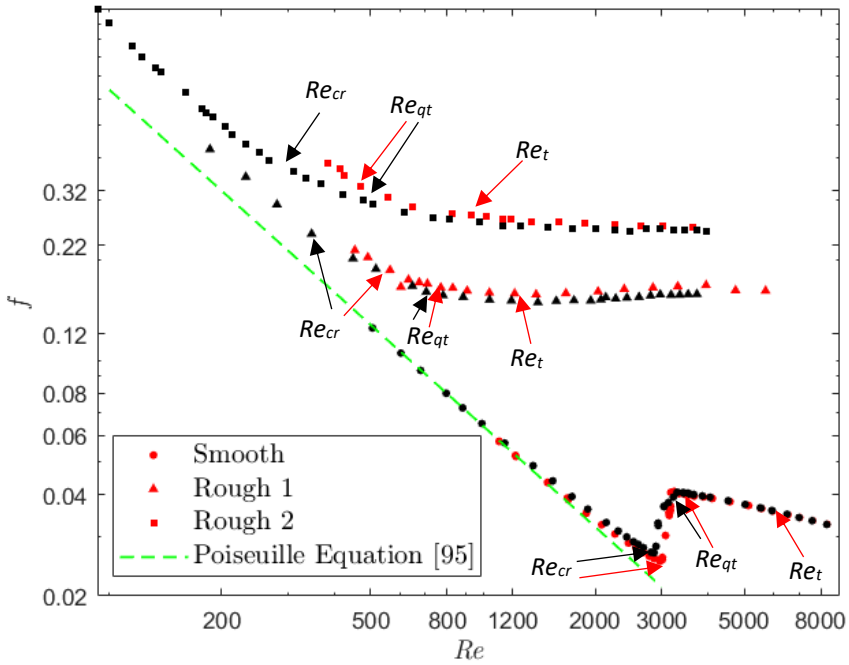

Figure 5.1: Comparison of the isothermal (heat flux of 0 kW/m^2) and diabatic (heat flux of 3 kW/m^2) friction factors for the smooth, rough 1, and rough 2 test sections as a function of Reynolds number, using black and red markers, respectively. Also included are the flow regime boundaries and the Poiseuille equation [95].

Contrary to the trend in the Moody Chart, a significant increase in friction factors with increasing surface roughness was observed in the laminar flow regime. At the minimum Reynolds number of 190, the friction factors increased from the Poiseuille equation with factors of 1.26 and 1.58 for rough 1 and rough 2, respectively. According to Celata et al. [58], the surface roughness breaks up the boundary layers and increases the flow resistance and friction factors, especially in mini- and microtubes. For large values of relative roughness, the flow lines near the roughness elements at the surface would follow the shape of the roughness elements becoming curved lines instead of parallel lines [43]. It was observed by Webb et al. [42] that these flow curves separated from the wall surface and then only reattached a distance six to eight times the height of the roughness elements. This results in a decreased effective flow diameter and thus increased pressure drop and friction factor.

Similar to the findings of previous studies on rough tubes [9,43,72,76,79,81,83,85], an increase in relative surface roughness significantly advanced the onset of the transitional flow regime of both the isothermal and diabatic friction factors due to the increased flow disturbances. However, it follows from Figure 5.1 that the transitional flow regime became less pronounced for rough 1 and even more challenging to identify for rough 2. For the two rough tubes, the critical Reynolds number was considered to be the Reynolds number at which the friction factors began to deviate from the Poiseuille trend (the linear behaviour when plotted on a log-log graph). For isothermal flow, the critical Reynolds numbers corresponded to 350 and 300 for rough 1 and rough 2, respectively. Unfortunately, it was not possible to decrease the Reynolds number below 390 when testing at a heat flux of 3 kW/m^2, because the outlet bulk fluid temperatures became too high. Therefore, it was not possible to conduct experiments in the laminar flow regime and thus to identify the critical Reynolds number.

The roughness elements disturbed the flow boundary layer and increased the size of eddies or swirls to such an extent that the transitional flow behaviour was significantly different from smooth tubes or tubes with lower values of relative surface roughness. The friction factors no longer increased in the transitional flow regime, but continued to decrease with increasing Reynolds number, although the gradient was less than in the laminar flow regime. When comparing the isothermal and diabatic friction factors in rough 1 and rough 2, there were minor differences in the boundaries of the transitional flow regime, which implies that the disturbances caused by the roughness elements completely dominated the heat transfer characteristics inside these two tubes. However, for the smooth tube, the critical Reynolds number was delayed from 2 810 to 2 970 when comparing the isothermal (0 kW/m^2) and diabatic (3 kW/m^2) friction factors, similar to the findings of Everts et al. [40] in the smooth tube. Furthermore, the transition gradients increased, which implies that the flow transitioned faster from the laminar to the quasi-turbulent flow regimes.

In the quasi-turbulent flow regime, the friction factors continued to decrease with increasing Reynolds numbers in both the smooth and rough tubes, however, the gradient was less than in the laminar flow regime, but more than in the fully turbulent flow regime. It follows from Figure 5.1 that increasing the surface roughness also caused the flow to become fully turbulent at lower Reynolds numbers. In the turbulent flow regime, the friction factors became independent of Reynolds number but increased with increasing surface roughness, which corresponded well to the findings of Nikuradse [44]. The negligible difference between the isothermal and diabatic friction factors in the quasi-turbulent and turbulent flow regimes, as well as the boundaries between these flow regimes, were as expected, as any free convection effects were suppressed by the velocity of the fluid.

5.2.2. Effect of Heat Flux

The friction factors as a function of Reynolds number for heat fluxes 1 kW/m^2, 2 kW/m^2, 3 kW/m^2, and 5 kW/m^2 are compared in Figure 5.2 for rough 1 to investigate the effect of heat flux on the friction factors in rough tubes. At low Reynolds numbers in the laminar flow regime, typically below 500, an increase in heat flux also increased the friction factors. This was due to the thermal gradient between the bulk fluid and surface temperature caused by mixed convection, which also affected the velocity profile. Increasing the heat flux increased the shear stresses due to changes in the velocity profile, while the fluid density slightly decreased, causing the friction factors to increase [10]. An increase in the heat flux caused a delay in the onset of the transitional flow regime, which agreed well with the findings of Everts et al. [40].

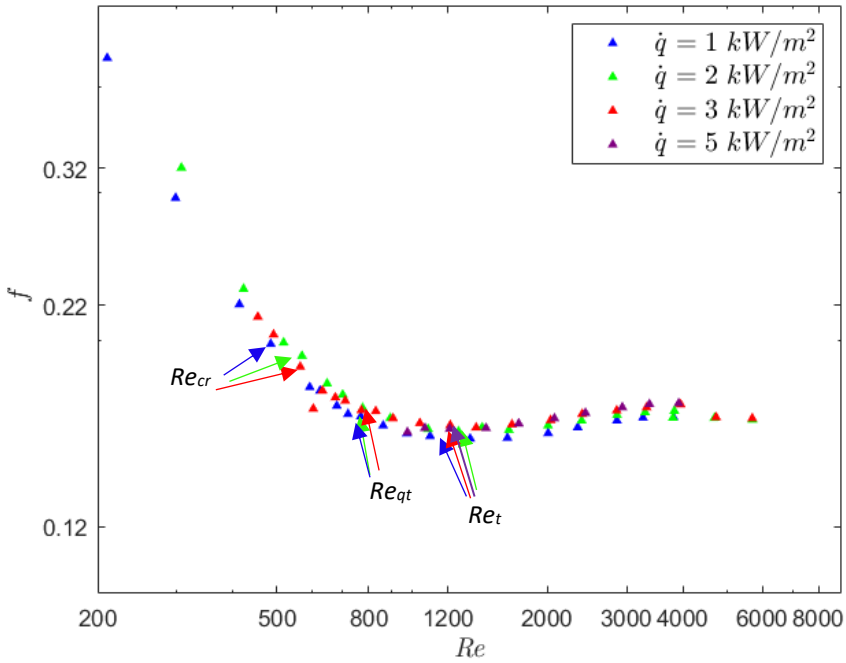

Figure 5.2: Friction factors as a function of Reynolds number for rough 1 at 1 kW/m^2 (blue), 2 kW/m^2 (green), 3 kW/m^2 (red) and 5 kW/m^2 (purple) between pressure taps 1 and 2. The flow regime boundaries for all the heat fluxes are labeled with arrows.

In the transitional flow regime for higher heat fluxes data points were more pronounced. A possible cause for this was due to the increased transition gradient. Furthermore, due to the very narrow width of the transitional flow regime, it was not possible to obtain more data points in the transitional flow regime itself, because it was not possible to conduct experiments at smaller Reynolds number increments. As the roughness inside the tube significantly advanced the onset of all the flow regimes, the majority of the experimental data points fell in the quasi-turbulent and turbulent flow regimes. In these flow regimes, free convection effects were suppressed by the velocity of the fluid, which explains why there is no significant difference between the friction factors when different heat fluxes were applied to the tube.

5.3. Relationship between Pressure Drop and Heat Transfer

Although the boundaries between different flow regimes are often obtained from visual inspection, it followed from Figure 5.1 that it became increasingly difficult when tubes with large values of relative roughness, such as in this study, were used. This became even more challenging when the heat transfer results were investigated in terms of the Nusselt numbers, as will be shown in Figure 5.4. Everts and Meyer [27] found that a direct relationship between pressure drop and heat transfer is valid for all flow regimes in a smooth tube, while Everts et al. [40] confirmed that the boundaries between the different flow regimes are also similar for rough tubes. Therefore, to use the friction factors as a guideline to identify the different flow regimes in the heat transfer results, Figure 5.3 (a), (c), and (e) compare the pressure drop results in terms of the friction factors, and the heat transfer results in terms of the Colburn *j*-factors for smooth, rough 1, and rough 2, respectively. Only heat fluxes of 3 kW/m^2 and 5 kW/m^2 were considered in this analysis due to the high uncertainties in the heat transfer results at the lower heat fluxes.

As expected, the trends of the friction factors and Colburn *j*-factors were similar in all flow regimes for the smooth and rough tubes. Furthermore, as indicated by the red lines, the boundaries between the flow regimes were the same for both the pressure drop and heat transfer results. Heat transfer mechanisms vary the Colburn *j*-factors across the different flow regimes. Interactions between the Reynolds, Prandtl and Nusselt numbers cause these variations. In the laminar flow regime, heat transfer is primarily due to conduction. The Colburn *j*-factors are lower due to limited mixing. In the transitional flow regime, the increase in mixing which leads to a higher convective heat transfer rate which causes the Colburn *j*-factors to increase. Turbulent eddies are enhanced in the quasi-turbulent and turbulent flow regimes which transfer heat more effectively leading to high convective heat transfer rates. Therefore, the Colburn *j*-factors are increased further in these flow regimes.

To gain a better understanding of the overall influence of surface roughness on the heat transfer and pressure drop characteristics, as well as the relationship between pressure drop and heat transfer in rough tubes, the friction factors were divided by the Colburn *j*-factors for the smooth, rough 1 and rough 2 tubes and compared in Figure 5.3 (b), (d), and (f), respectively. This ratio can be used as a guideline to determine the conditions in which an increase in surface roughness would favour an increase in heat transfer rather than an increase in pressure drop, therefore, lower values indicate favourable conditions.

It follows from Figure 5.3 (b) that for a smooth tube, the *f*/*j*-factors decreased significantly in the transitional flow regime, became approximately constant in the quasi-turbulent flow regime and then decreased further in the turbulent flow regime. This confirms that the turbulent flow regime is a favourable flow regime for heat exchangers to operate in and explains why many heat exchangers in practice are designed to operate in this flow regime. For rough 1, Figure 5.3 (d) indicates that when the surface roughness is increased, the *f*/*j*-factors decreased in the laminar and transitional flow regimes, reached a minimum in the quasi-turbulent flow regime, but then increased as the Reynolds number was increased further in the quasi-turbulent and turbulent flow regimes. There was a negligible difference between the results of the two heat fluxes, which indicated that the free convection effects were suppressed by the additional fluid motion caused by the roughness elements. When the surface roughness was increased further to rough 2, Figure 5.3 (f) indicates that the *f*/*j*-factors again decreased in the transitional and quasi-turbulent flow regimes, however, increased significantly in the turbulent flow regime.

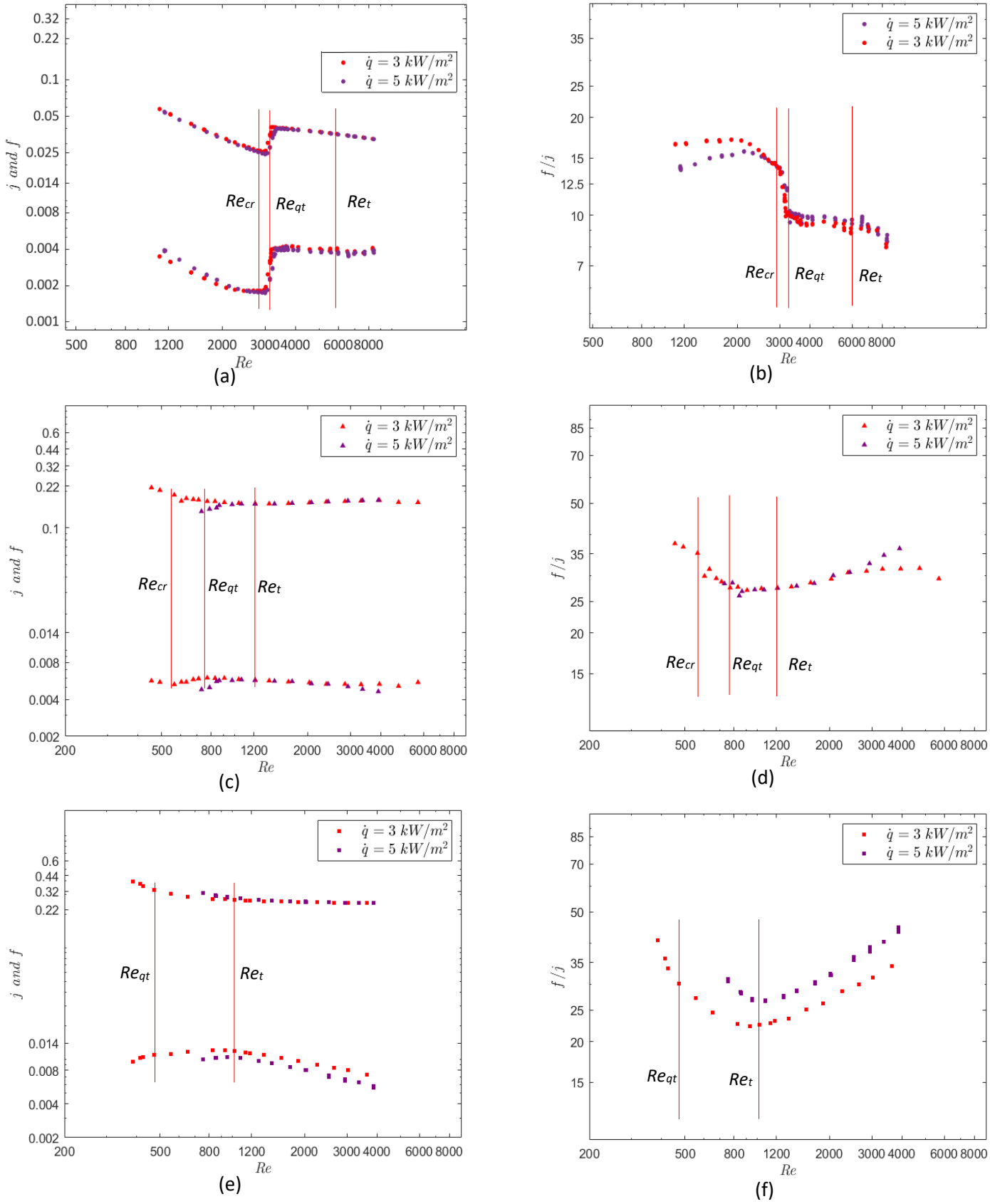

Figure 5.3: Colburn *j*-factors between *x*/*D* = 431 and 621, and friction factors compared on the same axis ((a), (c) and (e)), and friction factors divided by Colburn *j*-factors as a function of Reynolds number ((b), (d) and (f)), for smooth (a, b), rough 1 (c, d), and rough 2 (e, f), respectively.

It can therefore be concluded that although the turbulent flow regime is a favourable flow regime for heat exchangers containing smooth tubes to operate in, this is no longer the case for rough tubes. When the surface roughness inside the tubes become significant, the quasi-turbulent flow regime was found to be a promising flow regime for heat exchangers. This is beneficial, as the flow regime occurred earlier with increasing surface roughness, therefore the heat exchangers can operate at lower mass flow rates which decreases the pressure drop, pumping power and thus operational running costs.

5.4. Heat Transfer Results

5.4.1. Effect of Surface Roughness

To investigate the effect of surface roughness on the heat transfer characteristics in the different flow regimes, the average fully developed Nusselt numbers ($431 < x/D < 621$) at a heat flux of 3 kW/m^2 for smooth, rough 1, and rough 2 are compared in Figure 5.4. A general trend in this figure is that the Nusselt numbers shifted to the left with increasing surface roughness, implying that the boundaries between the different flow regimes occurred at lower Reynolds numbers. For the smooth tube, the average fully developed Nusselt number was 6.6 at a Reynolds number of 1 100 in the laminar flow regime. This was higher than the theoretical Nusselt number of 4.36, and the increase in Nusselt number can primarily be attributed to the enhanced heat transfer caused by free convection effects. Using the flow regime map of Everts and Meyer [28], it was confirmed that mixed convection conditions existed. Between Reynolds numbers of 2 000 to 3 000, the Nusselt numbers increased further (as seen in Figure 5.4). However, this increase was not due to mixed convection, but rather due to developing flow, because the thermal entrance length extended into the fully developed region.

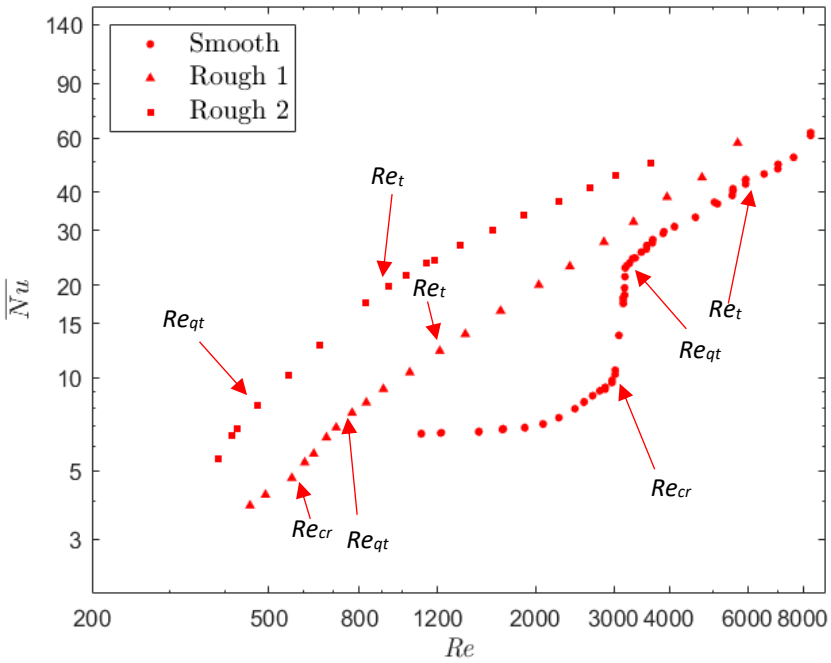

Figure 5.4: Average fully developed Nusselt numbers for smooth, rough 1 and rough 2 tubes at a heat flux of 3 kW/m^2 as a function of Reynolds number. The flow regime boundaries are labeled and indicated using red arrows.

For rough 1, the laminar Nusselt numbers increased significantly with increasing Reynolds number, which suggests that an increase in surface roughness increases the thermal entrance

length. Unfortunately, it was not possible to decrease the Reynolds number further and therefore, it was not possible to obtain fully developed laminar flow in rough 1 or any laminar flow in rough 2. Furthermore, due to the significant shift in the flow regime boundaries between smooth and rough 1, it was not possible to have comparable results at a fixed Reynolds number in the laminar flow regime. Therefore, to gain a better understanding of the effect of surface roughness on thermal entrance length in the laminar flow regime, it is suggested to conduct experiments using tubes with lower values of relative surface roughness and longer tube lengths.

Another interesting observation from Figure 5.4 was that for rough 1 and rough 2, the laminar Nusselt numbers decreased significantly with decreasing Reynolds number and did not approach the theoretical Nusselt number of 4.36 for fully developed laminar flow through a tube heated at a constant heat flux. Instead, it can be postulated from this graph that the Nusselt numbers would approach unity when the Reynolds number tends to zero. This was similar to the results obtained by Everts et al. [38] who investigated opposing and assisting flow in vertical tubes. At a Reynolds number of zero, the heat transfer is by conduction only and therefore the Nusselt number is expected to be unity. As the Reynolds number is increased, convection effects become significant, which increases the Nusselt numbers. Due to the very low flow rates that are associated with laminar flow through these rough tubes, the convection heat transfer component began to decrease which led to decreased Nusselt numbers.

Other authors such as Li et al. [55] and Liu et al. [56] found similar trends when using water as the testing fluid in rough microtubes. At low Reynolds numbers, the Nusselt numbers did not correlate with classical laminar theory and were lower than expected. Li et al. [55] concluded that this was due to the variation in the thermophysical properties which caused the Nusselt number to be less than that of Shah and London [44]. Liu et al. [56] found that their experimental data deviated from conventional theory when the relative roughness was greater than 1.5% and the discrepancies seemed to increase at low Reynolds numbers and larger relative tube wall thickness. They concluded that such discrepancies were because of the tube wall axial heat conduction occurring at low Reynolds numbers. Maranzana et al. [59], Gamrat et al. [57], Herwig et al. [98], and Li et al. [99] also indicated that at low Reynolds numbers, conduction along tube walls becomes significant and competes with internal forced convection.

It follows from Figure 5.4 that the transitional flow regime began at a Reynolds number of 3 020 in the smooth tube and ended at a Reynolds number of 3 180. For rough 1, the transitional flow regime occurred at a Reynolds number of 560 and ended at a Reynolds number of 760. As with the friction factor results in Figure 5.1, the width of the transitional flow regime decreased significantly and became less pronounced with increasing surface roughness. This was because roughness elements were sufficient to cause fluctuations in the flow, breaking up the laminar sublayers and also disturbing the general transitional flow fluctuating behaviour that is typically found in smooth tubes [73,74]. The heat transfer characteristics throughout the different flow regimes therefore had some elements of turbulent flow behaviour, which also explains why the Nusselt numbers tend to gradually increase with increasing Reynolds number.

The onset of the quasi-turbulent flow regime and turbulent flow regimes for the smooth tube occurred at Reynolds numbers of 3 180 and 6 000, respectively. As the surface roughness was increased, the onset of the quasi-turbulent and turbulent flow regimes for rough 1 occurred at Reynolds numbers of 760 and 1 200, respectively, while it advanced in rough 2 to Reynolds numbers of 490 and 930, respectively. In both the quasi-turbulent and turbulent flow regimes, an increase in surface roughness increased the Nusselt numbers due to the enhanced mixing caused by the roughness elements.

5.4.2. Effect of Heat Flux

To investigate the effects of heat flux on the heat transfer characteristics in rough tubes, Figure 5.5 compares the average Nusselt numbers obtained in smooth and rough 1 at different heat fluxes. For the smooth tube, the critical Reynolds numbers were 2 920, 3 020, and 3 072 for the 1 kW/m^2, 3 kW/m^2, and 5 kW/m^2, respectively. A higher heat flux caused a later transition, and this was due to the lower viscosity of the fluid caused by the heating. For rough 1, in the laminar flow regime, the velocity of the fluid was not sufficient to fully suppress free convection effects and the surface-fluid temperature differences were higher which led to decreased Nusselt number uncertainties. It is interesting to note that the Nusselt numbers still seem to decrease with increasing heat flux, which is contrary to the usual trend of laminar flow through horizontal tubes. This is in good agreement with the findings of Everts et al. [38] who investigated opposing and assisting flow through vertical tubes. The same trend was found for opposing flow in vertical tubes which confirms that the roughness elements inside the tube obstruct the free convection effects inside the tube.

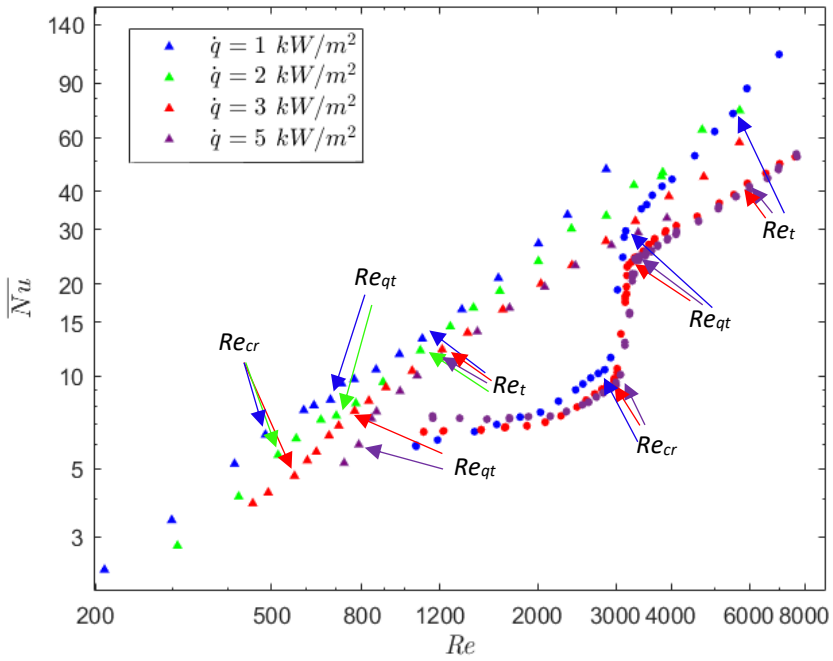

Figure 5.5: Average Nusselt number as a function of Reynolds number for smooth (circles) and rough 1 (triangles) at 1 kW/m^2 (blue), 2 kW/m^2 (green) – rough 1 only, 3 kW/m^2 (red) and 5 kW/m^2 (purple) between x/D = 431 and x/D = 621. The flow regime boundaries for all the heat fluxes are labeled with arrows.

Similar, to previous studies [10,33,89], an increase in heat flux delayed the onset of the transitional flow regime. Furthermore, the quasi-turbulent flow regime was also delayed for increasing heat fluxes. The effect of heat flux on the onset of transitional and the quasi-turbulent flow regime was slight and negligible, respectively. The relative surface roughness of rough 1 is expected to fall into the saturating region, as defined by Everts et al. [40]. In this region the influence of heat flux and thus the Grashof number is expected to have negligible effects on the critical Reynolds number, as flow fluctuations inside the rough tube suppresses it. Furthermore, the shape of the roughness elements [40], may have a greater influence on the Reynolds number of transition more so than the roughness height, as the roughness particle sizes are significant in comparison to the tube's diameter.

As the Reynolds number was increased, free convection effects decreased, and heat flux was expected to have a negligible influence on the turbulent flow regime. This explains why the differences between the Nusselt numbers at heat fluxes of 3 kW/m^2 and 5 kW/m^2 were negligible. However, at heat fluxes of 1 kW/m^2 (smooth and rough 1) and 2 kW/m^2 (rough 1), the turbulent Nusselt numbers diverged from the higher heat fluxes. This was not due to enhanced heat transfer, but rather due to the increased uncertainties caused by the small surface-fluid temperature differences at these heat fluxes. This could be attributed to greater heat losses to the environment.

5.5. Conclusions

In this chapter, the effect of surface roughness on the flow regime boundaries, friction factors, and Nusselt numbers was investigated. Additionally, the relationship between heat transfer and pressure drop through rough tubes was investigated.

The most important findings were found in the relationship between heat transfer and pressure drop. Firstly, trends of the friction factors and Colburn *j*-factors were similar in all the flow regimes for the smooth and rough tubes and the boundaries between the flow regimes were the same for both the pressure drop and heat transfer results. Secondly, on comparing heat fluxes of 3 kW/m^2 and 5 kW/m^2, there was a negligible difference between the results of the two heat fluxes, which indicated that the free convection effects were suppressed by the additional fluid motion caused by the roughness elements. Finally, the turbulent flow regime is the favourable flow regime for heat exchangers containing smooth tubes to operate in, however, this is no longer the case for rough tubes. In tubes with significant surface roughness, the quasi-turbulent flow regime was found to be the most appealing flow regime for heat exchangers to operate in. This was found through the ratio of *f*/*j*-factors being the lowest in the quasi-turbulent flow regime. In addition, the flow regimes occurred earlier with increasing surface roughness, therefore, heat exchangers can operate at lower mass flow rates which decreases the pressure drop, pumping power, and thus operational running costs.

A significant increase in friction factors with increasing surface roughness was observed in the laminar flow regime which was contrary to the trend in the Moody Chart. This was attributed to the decreased effective flow diameter and thus increased pressure drops and friction factors. An increased heat flux caused a slight increase in the friction factors at Reynolds numbers below 500 due to mixed convection. However, generally when the isothermal and diabatic friction factors were compared, there were minor differences in the boundaries of the transitional flow regime, which implied that the disturbances caused by the roughness elements completely suppressed the free convection effects inside the tubes. Additionally, the increase in relative surface roughness significantly advanced the onset of the transitional, quasi-turbulent, and turbulent flow regimes of both the isothermal and diabatic friction factors due to the increased flow disturbances. Furthermore, the significant size of roughness elements disturbed the flow boundary layer and increased the size of eddies or swirls to such an extent that the transitional flow behaviour was significantly different from smooth tubes or tubes with low values of relative surface roughness. Additionally, an increased heat flux increased the transition gradient of the transitional flow regime.

The Nusselt numbers increased significantly with increasing Reynolds number, which suggested that an increase in surface roughness increased the thermal entrance length for rough tube 1. To obtain a deeper understanding of the effect of surface roughness on thermal entrance length in the laminar flow regime, it is suggested to conduct experiments using tubes with lower values of relative surface roughness and longer tubes for further studies. The laminar Nusselt numbers in the rough tubes decreased significantly with decreasing Reynolds number and did

not approach the theoretical Nusselt number of 4.36 for fully developed laminar flow through a tube heated at a constant heat flux. Instead, it was postulated that it would decrease to unity as the Reynolds number tends to zero which signifies heat transfer by conduction only. The low flow rates associated with laminar flow through these rough tubes, decreased convection heat transfer component which led to decreased Nusselt numbers. Additionally, the relative roughness of both rough tubes falls in the saturating region where the influence of heat flux and thus the Grashof number is expected to have negligible effects on the critical Reynolds number. Like the friction factors, the width of the transitional flow regime decreased significantly and became less pronounced with increasing surface roughness. This was because roughness elements were sufficient to cause fluctuations in the flow, breaking up the laminar sublayers and disturbed the general transitional flow fluctuating behaviour that is typically found in smooth tubes. An increase in heat flux slightly delayed the onset of the transitional flow regime and had negligible effect on the quasi turbulent flow regime. An increase in surface roughness increased the Nusselt numbers due to the enhanced mixing caused by the roughness elements. However, free convection effects had a minor influence on the quasi-turbulent and turbulent flow regimes due to the high velocity of the fluid.

6. Conclusions and Recommendations

6.1. Summary

Many studies investigated on the effect of heat transfer and pressure drop on the transitional flow regime for smooth or enhanced tubes. Few studies investigated the effect of heat transfer and pressure drop in rough tubes; however, the majority of these studies belong to micro- and minitubes or investigated low relative roughness in macrotubes. Therefore, the study experimentally investigated the effects that large relative roughness has on heat transfer and pressure drop characteristics of flow through horizontal macrotubes heated at a constant heat flux. Experiments were conducted using three horizontal circular tubes with a base inner diameter of 5 mm, a length of 4 m, and a square-edged inlet. The constricted diameter was used for the rough tubes. Two rough tubes with relative roughnesses of 0.04 and 0.11, which fall within the saturating region were used. A total of 25 560 and 557 temperature and pressure drop measurements were taken, respectively. Overall, the heat fluxes were tested at 0, 1, 2, 3, 5, and 7 kW/m^2, and Reynolds number were tested in the range between 100–8 500.

6.2. Conclusions

It was found that for rough tubes with a relative roughness of 0.04 and 0.11 at a constant heat flux of 3 kW/m^2, the quasi-turbulent flow regime occurred at a Reynolds number of 760 and 490, respectively. Transition for the tube with a relative roughness of 0.04 occurred at a Reynolds number of 560 while for the tube with larger roughness, the critical Reynolds number was below 390. It was found that transition, the quasi-turbulent, and the turbulent flow regimes would commence early for an increase in relative roughness.

The heat transfer and more so, the pressure drop, increased with an increase in relative roughness. Tubes with large relative roughness showed non-linear behaviour for the friction factors and did not correlate with classical laminar theory even at low Reynolds numbers. This was mainly attributed to the constricted flow diameter and flow obstructions by the roughness elements. Trends of the friction factors and Colburn *j*-factors were similar in all the flow regimes for the smooth and rough tubes and the boundaries between the flow regimes were the same for both the pressure drop and heat transfer results. There was a negligible difference between the two heat fluxes, which indicated that the free convection effects were suppressed by the additional fluid motion caused by the roughness elements. The effect of roughness on this flow regime was an earlier occurrence and shortening of the width of the transitional flow regime.

The turbulent flow regime is the favourable flow regime for heat exchangers containing smooth tubes to operate in, however, this is no longer the case for rough tubes. In tubes with significant surface roughness, the quasi-turbulent flow regime was found to be the most appealing flow regime for heat exchangers to operate in. This was found through the *f*/*j*-factors being the lowest in the quasi-turbulent flow regime. Additionally, the flow regimes occurred earlier with increasing surface roughness, therefore, heat exchangers can operate at lower mass flow rates which decreases the pressure drop, pumping power and thus operational running costs. The quasi-turbulent is also less unpredictable and chaotic than the transitional flow regime. Practical challenges in designing large roughness in tubes are that tubes are more susceptible to blockages and great fluctuations in pressure drops that can cause damage to equipment. Engineers can optimize their design by working within the quasi-turbulent flow regime for significantly rough tubes to minimize pressure drop with the best heat transfer results.

6.3. Recommendations

The recommendations can be summarised into the following:

- Further investigations should be done to study the effects of developing flow in the laminar flow regime for rough tubes and low Reynolds numbers.
- Investigation into how the shape and size of the ripple roughness elements affect the heat transfer and pressure drop will also be valuable.
- Further investigation of scientific methods to quantify the location of the flow regime boundaries for rough and enhanced tubes would be useful.
- A modified flow-calming section can be used to test at higher pressure drops into the turbulent flow regime for rough tubes – this will enable testing at Reynolds numbers 10 000 and above which are commonly used in cooling circuits and heat exchangers generally operating in the turbulent flow regime.
- Tests can be conducted with other fluids of different Prandtl numbers to see how it compares to water.
- Tests can be done on the influence of the flow attack angle. The elements on the inner tube are formed in a certain shape and size, therefore, changing the flow attack angle (switching the tube around) might give differing results.
- More testing is required at different surface roughnesses to build a complete map of the friction factor and Nusselt number against the Reynolds number. Thereafter, one could develop correlations to determine the friction factor and Nusselt number with the relative roughness as an independent variable.
- Tests can be conducted with a larger diameter tube. Eddies caused by the no slip condition in a rough tube are bigger at the bottom of the tube than at the top due to gravity. Therefore, greater mixing will be prevalent at the bottom of the tube than at the top causing a lower surface temperature at the bottom than at the top of the tube. Although, it is difficult to measure for a tube with a 5 mm diameter, it will be easier to measure the difference in heat transfer coefficients between the top and bottom of the tube for a rough tube with a larger diameter.
- Tests can be conducted with lower values of relative surface roughness to obtain a deeper understanding of the effect of surface roughness on thermal entrance length in the laminar flow regime.
- Tests can be conducted with longer tubes to reach fully developed flow at all Reynolds numbers

7. References

[1] O. Levenspiel, Engineering flow and heat exchange, Springer, 2014.
[2] J.P. Meyer, M. Everts, Single-phase mixed convection of developing and fully developed flow in smooth horizontal circular tubes in the laminar and transitional flow regimes, International Journal of Heat and Mass Transfer, 117 (2018) 1251-1273.
[3] J.P. Meyer, Heat transfer in tubes in the transitional flow regime, in: International Heat Transfer Conference Digital Library, Begel House Inc., 2014.
[4] O. Reynolds, XXIX. An experimental investigation of the circumstances which determine whether the motion of water shall be direct or sinuous, and of the law of resistance in parallel channels, Philos. Trans. R. Soc. London, (174) (1883) 935-982.
[5] A.J. Ghajar, L.-M. Tam, Flow regime map for a horizontal pipe with uniform wall heat flux and three inlet configurations, Experimental Thermal and Fluid Science, 10(3) (1995) 287-297.
[6] A.J. Ghajar, L.-M. Tam, Heat transfer measurements and correlations in the transition region for a circular tube with three different inlet configurations, Experimental thermal and fluid science, 8(1) (1994) 79-90.
[7] A. Ghajar, L. Tam, Laminar-transition-turbulent forced and mixed convective heat transfer correlations for pipe flows with different inlet configurations, American Society of Mechanical Engineers, Heat Transfer Division,(Publication) HTD., 181 (1991) 15-23.
[8] A.J. Ghajar, K.F. Madon, Pressure drop measurements in the transition region for a circular tube with three different inlet configurations, Experimental thermal and fluid science, 5(1) (1992) 129-135.
[9] A.J. Ghajar, C.C. Tang, W.L. Cook, Experimental investigation of friction factor in the transition region for water flow in minitubes and microtubes, Heat Transfer Engineering, 31(8) (2010) 646-657.
[10] L.M. Tam, A.J. Ghajar, Effect of inlet geometry and heating on the fully developed friction factor in the transition region of a horizontal tube, Experimental thermal and fluid science, 15(1) (1997) 52-64.
[11] L.M. Tam, A.J. Ghajar, Transitional heat transfer in plain horizontal tubes, Heat Transfer Engineering, 27(5) (2006) 23-38.
[12] L.M. Tam, A.J. Ghajar, The unusual behavior of local heat transfer coefficient in a circular tube with a bell-mouth inlet, Experimental Thermal and Fluid Science, 16(3) (1998) 187-194.
[13] L. Tam, A. Ghajar, H. Tam, S. Tam, Development of a flow regime map for a horizontal pipe with the multi-classification Support Vector Machines, in: ASME 2008 Heat Transfer Summer Conference collocated with the Fluids Engineering, Energy Sustainability, and 3rd Energy Nanotechnology Conferences, American Society of Mechanical Engineers, 2008, pp. 537-547.
[14] H. Tam, L. Tam, A. Ghajar, C. Cheong, Development of a unified flow regime map for a horizontal pipe with the support vector machines, in: AIP Conf. Proc., AIP, 2010, pp. 608-613.
[15] H.K. Tam, L.M. Tam, A.J. Ghajar, Effect of inlet geometries and heating on the entrance and fully-developed friction factors in the laminar and transition regions of a horizontal tube, Experimental thermal and fluid science, 44 (2013) 680-696.
[16] H.K. Tam, L.M. Tam, A.J. Ghajar, S.C. Tam, T. Zhang, Experimental investigation of heat transfer, friction factor, and optimal fin geometries for the internally microfin tubes in the transition and turbulent regions, Journal of enhanced heat transfer, 19(5) (2012).
[17] H.K. Tam, L.M. Tam, A.J. Ghajar, Q. Wang, Experimental Investigation of The Heat Transfer ia a Horizontal Mini-Tube with Three Different Inlet Configurations, in: ASTFE Digital Library, Begel House Inc., 2017.
[18] J.G. Afshin, Transitional Flow in Tubes: Recommended Correlations for Calculation of Pressure Drop and Heat Transfer, in, Knovel.

[19] J.P. Meyer, J.A. Olivier, Heat transfer and pressure drop characteristics of smooth horizontal tubes in the transitional flow regime, Heat Transfer Engineering, 35(14-15) (2014) 1246-1253.
[20] J. Olivier, J.P. Meyer, Single-phase heat transfer and pressure drop of the cooling of water inside smooth tubes for transitional flow with different inlet geometries (RP-1280), HVAC&R Research, 16(4) (2010) 471-496.
[21] J.P. Meyer, J. Olivier, Transitional flow inside enhanced tubes for fully developed and developing flow with different types of inlet disturbances: Part I–Adiabatic pressure drops, International Journal of Heat and Mass Transfer, 54(7-8) (2011) 1587-1597.
[22] J.P. Meyer, J. Olivier, Transitional flow inside enhanced tubes for fully developed and developing flow with different types of inlet disturbances: Part II–heat transfer, International Journal of Heat and Mass Transfer, 54(7-8) (2011) 1598-1607.
[23] J.P. Meyer, A.I. Bashir, M. Everts, Single-phase mixed convective heat transfer and pressure drop in the laminar and transitional flow regimes in smooth inclined tubes heated at a constant heat flux, Experimental Thermal and Fluid Science, 109 (2019) 109890.
[24] M. Everts, J.P. Meyer, Heat transfer of developing and fully developed flow in smooth horizontal tubes in the transitional flow regime, International Journal of Heat and Mass Transfer, 117 (2018) 1331-1351.
[25] M. Everts, J.P. Meyer, Heat transfer of developing flow in the transitional flow regime, in: ASTFE Digital Library, Begel House Inc., 2015.
[26] M. Everts, J.P. Meyer, Laminar hydrodynamic and thermal entrance lengths for simultaneously hydrodynamically and thermally developing forced and mixed convective flows in horizontal tubes, Experimental Thermal and Fluid Science, 118 (2020) 110153.
[27] M. Everts, J. Meyer, Relationship between pressure drop and heat transfer of developing and fully developed flow in smooth horizontal circular tubes in the laminar, transitional, quasi-turbulent and turbulent flow regimes, International Journal of Heat and Mass Transfer, 117 (2017).
[28] M. Everts, J.P. Meyer, Flow regime maps for smooth horizontal tubes at a constant heat flux, International Journal of Heat and Mass Transfer, 117 (2018) 1274-1290.
[29] A.H. Pordanjani, S. Aghakhani, M. Afrand, M. Sharifpur, J.P. Meyer, H. Xu, H.M. Ali, N. Karimi, G. Cheraghian, Nanofluids: Physical phenomena, applications in thermal systems and the environment effects-a critical review, Journal of Cleaner Production, 320 (2021) 128573.
[30] J.P. Meyer, S.A. Adio, M. Sharifpur, P.N. Nwosu, The viscosity of nanofluids: a review of the theoretical, empirical, and numerical models, Heat Transfer Engineering, 37(5) (2016) 387-421.
[31] H.Ş. Aybar, M. Sharifpur, M.R. Azizian, M. Mehrabi, J.P. Meyer, A review of thermal conductivity models for nanofluids, Heat Transfer Engineering, 36(13) (2015) 1085-1110.
[32] J.P. Meyer, M. Everts, A.T. Hall, F.A. Mulock-Houwer, M. Joubert, L.M. Pallent, E.S. Vause, Inlet tube spacing and protrusion inlet effects on multiple circular tubes in the laminar, transitional and turbulent flow regimes, International Journal of Heat and Mass Transfer, 118 (2018) 257-274.
[33] J.P. Meyer, S. Abolarin, Heat transfer and pressure drop in the transitional flow regime for a smooth circular tube with twisted tape inserts and a square-edged inlet, International Journal of Heat and Mass Transfer, 117 (2018) 11-29.
[34] S. Abolarin, M. Everts, J.P. Meyer, Heat transfer and pressure drop characteristics of alternating clockwise and counter clockwise twisted tape inserts in the transitional flow regime, International Journal of Heat and Mass Transfer, 133 (2019) 203-217.
[35] S. Abolarin, M. Everts, J.P. Meyer, The influence of peripheral u-cut twisted tapes and ring inserts on the heat transfer and pressure drop characteristics in the transitional flow regime, International Journal of Heat and Mass Transfer, 132 (2019) 970-984.

[36] D.D. Ndenguma, J. Dirker, J.P. Meyer, Transitional flow regime heat transfer and pressure drop in an annulus with non-uniform wall temperatures, International Journal of Heat and Mass Transfer, 108 (2017) 2239-2252.
[37] J. Dirker, J.P. Meyer, Convective heat transfer coefficients in concentric annuli, Heat Transfer Engineering, 26(2) (2005) 38-44.
[38] M. Everts, S. Bhattacharyya, A.I. Bashir, J.P. Meyer, Heat transfer characteristics of assisting and opposing laminar flow through a vertical circular tube at low Reynolds numbers, Applied Thermal Engineering, 179 (2020) 115696.
[39] A.I. Bashir, M. Everts, R. Bennacer, J.P. Meyer, Single-phase forced convection heat transfer and pressure drop in circular tubes in the laminar and transitional flow regimes, Experimental Thermal and Fluid Science, 109 (2019) 109891.
[40] M. Everts, P. Robbertse, B. Spitholt, The effects of surface roughness on fully developed laminar and transitional flow friction factors and heat transfer coefficients in horizontal circular tubes, Experimental Thermal and Fluid Science, (2022).
[41] M. Everts, S.R. Ayres, F.A.M. Houwer, C.P. Vanderwagen, N.M. Kotze, J.P. Meyer, The influence of surface roughness on heat transfer in the transitional flow regime, in: International Heat Transfer Conference Digital Library, Begel House Inc., 2014.
[42] R. Webb, E. Eckert, R. Goldstein, Heat transfer and friction in tubes with repeated-rib roughness, International journal of heat and mass transfer, 14(4) (1971) 601-617.
[43] K. Huang, J. Wan, C. Chen, Y. Li, D. Mao, M. Zhang, Experimental investigation on friction factor in pipes with large roughness, Experimental thermal and fluid science, 50 (2013) 147-153.
[44] J. Nikuradse, Laws of flow in rough pipes, National Advisory Committee for Aeronautics Washington, 1950.
[45] Y.A. Cengel, and Ghajar, A.J., Heat and Mass Transfer Fundamentals & Applications, 5th Edition ed., Grawhil Education, Stillwater, 2015.
[46] C. Colebrook, C. White, Experiments with fluid friction in roughened pipes, Proc. R. Soc. Lond. A, 161(906) (1937) 367-381.
[47] K.A. Flack, M.P. Schultz, W.B. Rose, The onset of roughness effects in the transitionally rough regime, International Journal of Heat and Fluid Flow, 35 (2012) 160-167.
[48] Y. Zhao, Z. Liu, Experimental studies on flow visualization and heat transfer characteristics in microtubes, in: International Heat Transfer Conference 13, Begel House Inc., 2006.
[49] C.Y. Yang, T.Y. Lin, Heat transfer characteristics of water flow in microtubes, Experimental Thermal and Fluid Science, 32(2) (2007) 432-439.
[50] P. Wu, W. Little, Measurement of the heat transfer characteristics of gas flow in fine channel heat exchangers used for microminiature refrigerators, Cryogenics, 24(8) (1984) 415-420.
[51] L.M. Tam, H.K. Tam, A.J. Ghajar, W. San Ng, I.W. Wong, K.F. Leong, C.K. Wu, The effect of inner surface roughness and heating on friction factor in horizontal micro-tubes, in: ASME-JSME-KSME 2011 Joint Fluids Engineering Conference, American Society of Mechanical Engineers, 2011, pp. 2971-2978.
[52] H.K. Tam, L.M. Tam, A.J. Ghajar, Experimental analysis of the single-phase heat transfer and friction factor inside the horizontal internally micro-fin tube, in: ASME/JSME Thermal Engineering Joint Conference, 2011, pp. T10106.
[53] H. Tam, H.K. Tam, A.J. Ghajar, W. Ng, I.W. Wong, K.F. Leong, C.K. Wu, The effect of inner surface roughness and heating on friction factor in horizontal micro-tubes, ASME Paper No. AJK2011-16027, (2011).
[54] G. Morini, M. Lorenzini, S. Salvigni, G. Celata, Experimental analysis of microconvective heat transfer in the laminar and transitional regions, Experimental heat transfer, 23(1) (2009) 73-93.

[55] Z. Liu, C. Zhang, Y. Huo, X. Zhao, Flow and heat transfer in rough micro steel tubes, Experimental heat transfer, 20(4) (2007) 289-306.
[56] Z. Li, Y.-L. He, G.-H. Tang, W.-Q. Tao, Experimental and numerical studies of liquid flow and heat transfer in microtubes, International journal of heat and mass transfer, 50(17-18) (2007) 3447-3460.
[57] G. Gamrat, M. Favre-Marinet, D. Asendrych, Conduction and entrance effects on laminar liquid flow and heat transfer in rectangular microchannels, International Journal of Heat and Mass Transfer, 48(14) (2005) 2943-2954.
[58] G.P. Celata, M. Cumo, M. Guglielmi, G. Zummo, Experimental investigation of hydraulic and single-phase heat transfer in 0.130-mm capillary tube, Microscale Thermophysical Engineering, 6(2) (2002) 85-97.
[59] G. Maranzana, I. Perry, D. Maillet, Mini-and micro-channels: influence of axial conduction in the walls, International journal of heat and mass transfer, 47(17-18) (2004) 3993-4004.
[60] D.F. Dipprey, R.H. Sabersky, Heat and momentum transfer in smooth and rough tubes at various Prandtl numbers, International Journal of Heat and Mass Transfer, 6(5) (1963) 329-353.
[61] Y. Cengel, J. Cimbala, Fundamentals and Application. 2006, in, McGraw-Hill, USA.
[62] J.P. Meyer, Everts, M., Coetzee, N., Grote, K. and Steyn, M., Heat transfer characteristics of quasi-turbulent and turbulent flow in smooth circular tubes., International Communications in Heat and Mass Transfer, 105 (2019) 84-106.
[63] F.M. White, I. Corfield, Viscous fluid flow, McGraw-Hill New York, 2006.
[64] M. Everts, Single-phase mixed convection of developing and fully developed flow in smooth horizontal tubes in the laminar, transitional, quasi-turbulent and turbulent flow regimes, University of Pretoria, 2018.
[65] L. Tam, A. Ghajar, H. Tam, S. Tam, Development of a flow regime map for a horizontal pipe with the multi-classification Support Vector Machines, in: ASME 2008 Heat Transfer Summer Conference collocated with the Fluids Engineering, Energy Sustainability, and 3rd Energy Nanotechnology Conferences, American Society of Mechanical Engineers Digital Collection, 2009, pp. 537-547.
[66] E. ISO, 4287–Geometrical Product Specifications (GPS)–Surface Texture: Profile Method–Terms, Definitions and Surface Texture Parameters, International Organization for Standardization: Geneva, Switzerland, (1997).
[67] M. Harcarik, R. Jankovych, Relationship between values of profile and areal surface texture parameters, MM Sci. J, 5 (2016) 1659-1662.
[68] H. Nagendra, Interaction of free and forced convection in horizontal tubes in the transition regime, J. Fluid Mech., 57(2) (1973) 269-288.
[69] L. Zeghadnia, J.L. Robert, B. Achour, Explicit solutions for turbulent flow friction factor: A review, assessment and approaches classification, Ain Shams Engineering Journal, 10(1) (2019) 243-252.
[70] S. Beck, R. Collins, in, University of Sheffield, 2008.
[71] F. Concha, Settling velocities of particulate systems 15: Velocities in turbulent Newtonian flows, International Journal of Mineral Processing, 88(3-4) (2008) 89-93.
[72] K. Huang, J. Wan, C. Chen, D. Mao, Y. Li, Experiments investigation of the effects of surface roughness on laminar flow in macro tubes, Experimental thermal and fluid science, 45 (2013) 243-248.
[73] S.R.A. M. Everts, F.A.M. Houwer, C.P. Vanderwagen, N.M. Kotze, J.P. Meyer, The influence of surface roughness on heat transfer in the transitional flow regime of a parabolic trough, in.
[74] M. Everts, S.R. Ayres, F.A. Mulock Houwer, C.P. Vanderwagen, N.M. Kotze, J.P. Meyer, The influence of surface roughness on heat transfer in the transitional flow regime, in: Proceedings of the 15th International Heat Transfer Conference, IHTC 2014, 2014.

[75] A. Avci, I. Karagoz, A new explicit friction factor formula for laminar, transition and turbulent flows in smooth and rough pipes, European Journal of Mechanics - B/Fluids, 78 (2019) 182-187.
[76] S. Kandlikar, Roughness effects at microscale–reassessing Nikuradse's experiments on liquid flow in rough tubes, Bulletin of the Polish Academy of Sciences: Technical Sciences, (2005).
[77] J. Nikuradse, Stromungsgesetz in rauhren rohren, vDI Forschungshefte 361 (English translation: Laws of flow in rough pipes), Tech. Rep. NACA Technical Memorandum 1292. National Advisory Commission for Aeronautics, 1950.
[78] Z.-X. Li, Experimental study on flow characteristics of liquid in circular microtubes, Microscale Thermophysical Engineering, 7(3) (2003) 253-265.
[79] T.P. Brackbill, S.G. Kandlikar, Effects of low uniform relative roughness on single-phase friction factors in microchannels and minichannels, in: ASME 2007 5th International Conference on Nanochannels, Microchannels, and Minichannels, American Society of Mechanical Engineers, 2007, pp. 509-518.
[80] J.B. Taylor, A.L. Carrano, S.G. Kandlikar, Characterization of the effect of surface roughness and texture on fluid flow—past, present, and future, International journal of thermal sciences, 45(10) (2006) 962-968.
[81] S.G. Kandlikar, D. Schmitt, A.L. Carrano, J.B. Taylor, Characterization of surface roughness effects on pressure drop in single-phase flow in minichannels, Phys. Fluids, 17(10) (2005) 100606.
[82] S.G. Kandlikar, A roadmap for implementing minichannels in refrigeration and air-conditioning systems—Current status and future directions, Heat Transfer Engineering, 28(12) (2007) 973-985.
[83] S.G. Kandlikar, S. Joshi, S. Tian, Effect of surface roughness on heat transfer and fluid flow characteristics at low Reynolds numbers in small diameter tubes, Heat Transfer Engineering, 24(3) (2003) 4-16.
[84] T.P. Brackbill, S.G. Kandlikar, Application of lubrication theory and study of roughness pitch during laminar, transition, and low Reynolds number turbulent flow at microscale, Heat transfer engineering, 31(8) (2010) 635-645.
[85] L.M. Tam, H.K. Tam, A.J. Ghajar, W. San Ng, C.K. Wu, The effect of inner surface roughness and heating on friction factor in horizontal mini-tubes, in: International Heat Transfer Conference Digital Library, Begel House Inc., 2014.
[86] B. Dai, M. Li, Y. Ma, Effect of surface roughness on liquid friction and transition characteristics in micro- and mini-channels, Applied Thermal Engineering, 67(1) (2014) 283-293.
[87] G.M. Mala, D. Li, Flow characteristics of water in microtubes, International journal of heat and fluid flow, 20(2) (1999) 142-148.
[88] A. García, J. Solano, P. Vicente, A. Viedma, The influence of artificial roughness shape on heat transfer enhancement: Corrugated tubes, dimpled tubes and wire coils, Applied Thermal Engineering, 35 (2012) 196-201.
[89] M. Everts, Heat transfer and pressure drop of developing flow in smooth tubes in the transitional flow regime, University of Pretoria, 2015.
[90] A. Bakker, R.D. LaRoche, E.M. Marshall, Laminar flow in static mixers with helical elements, The online CFM book, 546 (2000).
[91] R. Rayle, Influence of orifice geometry on static pressure measurements, American Society of Mechanical Engineers, 1959.
[92] C. Popiel, J. Wojtkowiak, Simple formulas for thermophysical properties of liquid water for heat transfer calculations (from 0 C to 150 C), Heat transfer engineering, 19(3) (1998) 87-101.
[93] P.F. Dunn, M.P. Davis, Measurement and data analysis for engineering and science, CRC press, 2017.

[94] J. Meyer, M. De Paepe, The Art of Measuring in the Thermal Sciences, CRC Press, 2020.
[95] J.L.M. Poiseulle, Recherches expérimentelles sur le mouvement des liquids dans le tubes de trés petits diamétres, Comptes Rendu 11, 961-967 (1840) 1041-1048.
[96] H.D. Blasius, Ähnlichkeitsgesetz bei Reibungsvorgängen in Flüssigkeiten, Forsch. Arb. Ing.-Wes, (1913) 131-137, .
[97] V. Gnielinski, New equations for heat and mass transfer in turbulent pipe and channel flow, Int. Chem. Eng., 16(2) (1976) 359-368.
[98] H. Herwig, O. Hausner, Critical view on “new results in micro-fluid mechanics”: an example, International Journal of Heat and Mass Transfer, 46(5) (2003) 935-937.
[99] J. Li, G. Peterson, P. Cheng, Three-dimensional analysis of heat transfer in a micro-heat sink with single phase flow, International Journal of Heat and Mass Transfer, 47(19-20) (2004) 4215-4231.
[100] S.G. Kandlikar, S. Joshi, S. Tian, Effect of channel roughness on heat transfer and fluid flow characteristics at low Reynolds numbers in small diameter tubes, Atmosphere, 4(6) (2001) 7.
[101] S.R. Ayres, The influence of surface roughness on the transitional flow regime University of Pretoria, Pretoria, 2013.

Appendix A. Calibration of Instrumentation

A.1. Introduction

The accuracy of electronic instruments drifts with temperature and time. This can affect the accuracy of measuring instrumentation over time. It is important to adjust for this inaccuracy. Calibration means verifying the accuracy of a measuring instrument and adjusting for any such measurement error to verify the performance of an instrument and compare it to its factory specifications. Appendix A describes the calibration process for measuring instrumentation, such as Pt100s, thermocouples and pressure transducers. Linear regression sample figures are also included from the calibration that was done.

A.2. Pt100 calibration

The Pt100 probes were calibrated against a digital thermometer (DigiCal DCS2) which has an accuracy of 0.03°C. The Pt100 probes, as well as the digital thermometer, were placed in a thermostat-controlled bath (LAUDA PROLINE RP1845C). The Pt100s were calibrated in the range of 15°C to 65°C in 2.5°C intervals. An upward and downward run was completed to show that a linear curve was obtained and to observe the differences due to hysteresis.

After the set temperature remained steady in the thermostat-controlled bath, 200 measuring points were taken. Linear curve fits of the average of the 200 measuring points are plotted against the reading taken on the digital thermometer. The linear curve fits obtained for the two Pt100 probes are shown in Figure A.1 and Figure A.2. Readings taken for the upward run are identified by red markers and readings for the downward run by green markers in both Figure A.1 and Figure A.2. The markers (green) of the downward temperature run, overlap the markers (red) of the upward temperature run. The differences due to hysteresis are negligible in temperature readings for the inlet and outlet Pt100 probes.

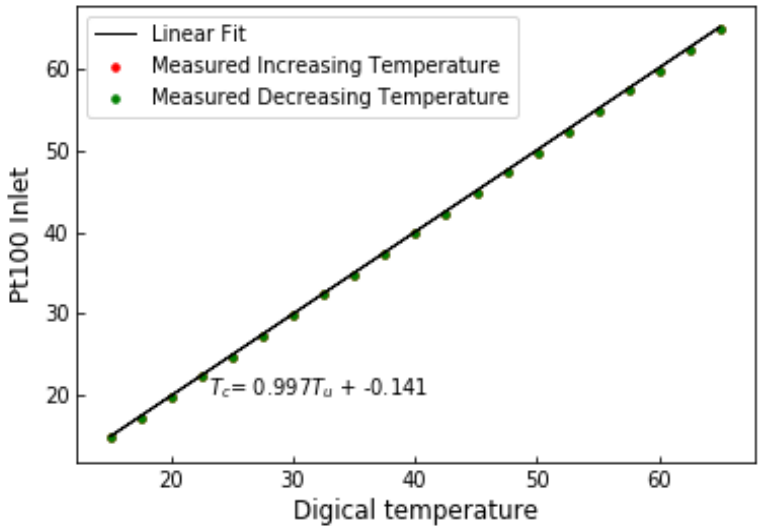

Figure A.1: Pt100 inlet probe calibration linear curve fit.

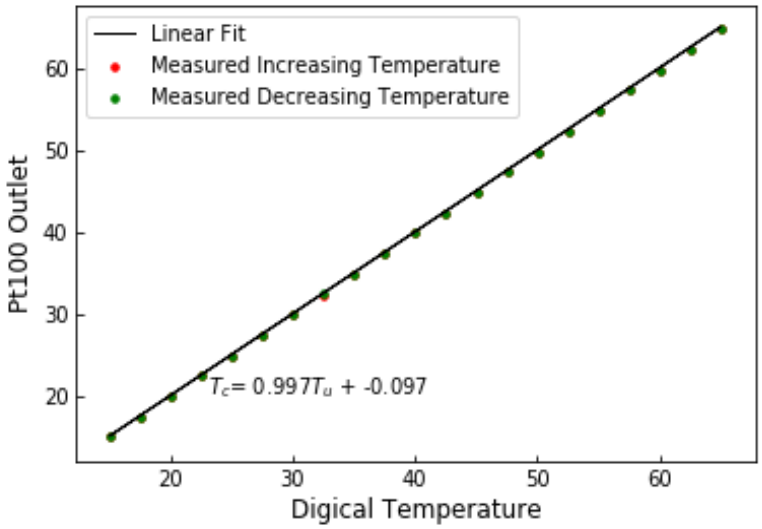

Figure A.2: Pt100 outlet probe calibration linear curve fit.

A linear curve fit was done through the average recorded data using both the upward and downward runs. Using the calibration factors obtained from the linear curve fits in Figure A.1 and Figure A.2 the calibrated temperatures are obtained by:

$$T_{calibrated} = \frac{T_{uncalibrated} - c}{m} \quad \text{A.1}$$

To observe the error between the uncalibrated and calibrated temperatures from the digital thermometer, Figure A.3 and Figure A.4 are shown.

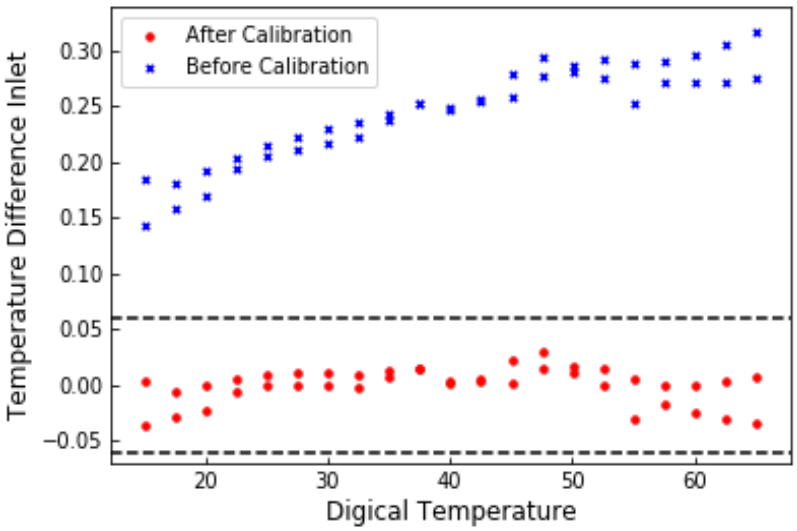

Figure A.3: Temperature difference of the uncalibrated and calibrated Pt100 inlet probe temperatures with the digital thermometer readings.

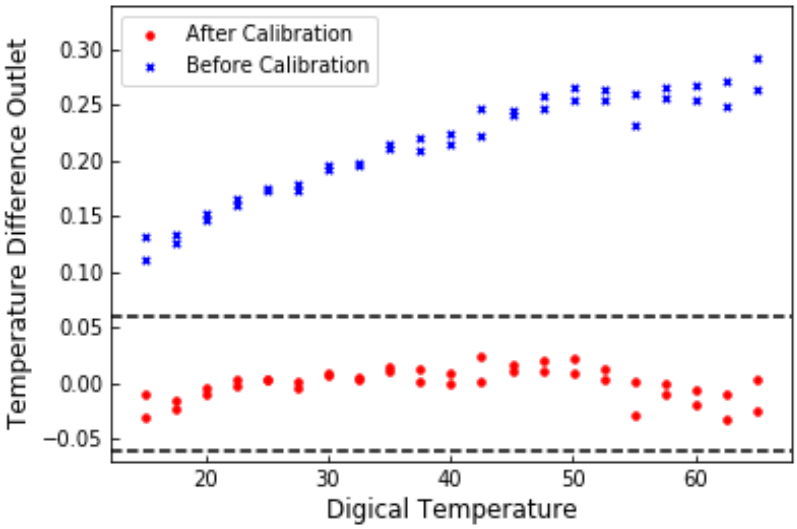

Figure A.4: Temperature difference of the uncalibrated and calibrated Pt100 outlet probe temperatures with the digital thermometer readings.

In Figure A.3 and Figure A.4 the difference between the uncalibrated temperatures and temperatures of the digital thermometer are demarcated by blue and the difference between the calibrated temperatures and temperatures of the digital thermometer are demarcated by red. The uncertainty of the Pt100 probes given by the manufacturer is 0.06°C which is demarcated by the black dotted lines in Figure A.3 and Figure A.4. The uncertainty of the calibrated values is less than this, however, 0.06°C specified by the manufacturer is used in the uncertainty analysis to be conservative. The maximum difference between the Pt100 inlet probe and digital thermometer reading before calibration in Figure A.3 is 0.316°C and after calibration is 0.030°C. The maximum difference between the Pt100 outlet probe and digital thermometer reading before calibration in Figure A.4 is 0.292°C and after calibration is 0.025°C. The difference between the calibrated Pt100 values and the digital thermometer falls within the 0.06°C band, thus concluding the calibration of the Pt100 probes successful. Four cycles such as this were completed, and the average calibration factors of the cycles were used in the data analysis.

A.3. Thermocouple calibration

In situ calibration was used to calibrate the thermocouples. Using this method, thermocouples are already attached when calibration is done which accounts for the change of properties to the thermocouple junction during the attachment process. Thus, the thermocouple calibration process is trusted to be more reliable. A thermostat-controlled bath (LAUDA PROLINE RP1845C) was used to set and pump water with the desired temperature through the test section.

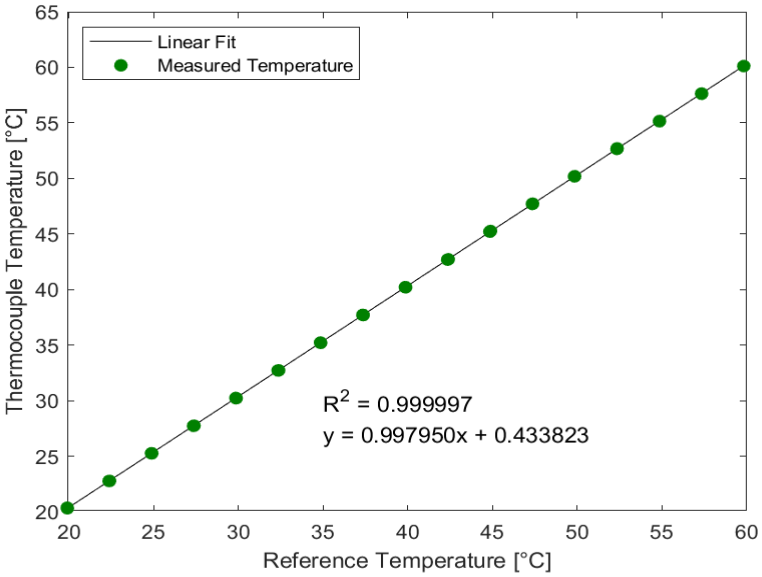

Figure A.5: Example linear curve fit for increasing 20–60 °C and decreasing 60–20 °C for thermocouple 1A.

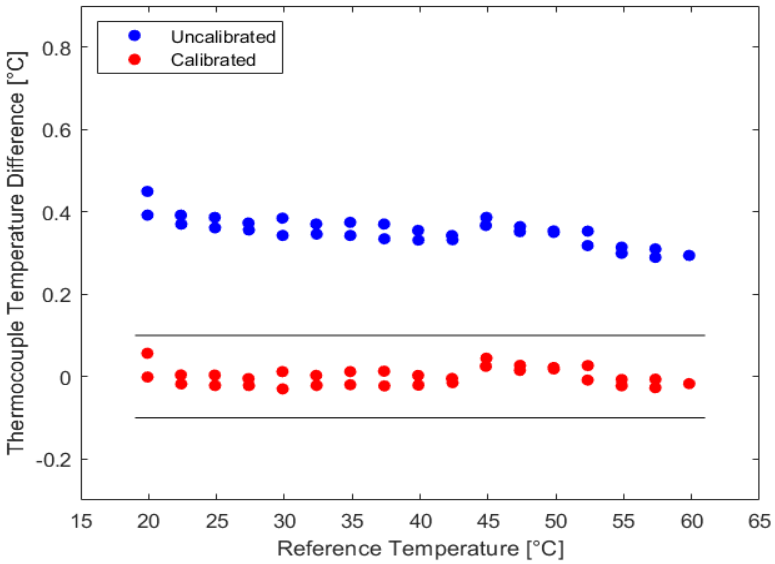

Figure A.6: Example temperature difference between the thermometer and the thermocouple 1A, before (blue markers) and after (red markers) calibration. The black lines represent the uncertainty bands of the thermocouple.

The thermostat-controlled bath was connected to a mixer thereafter the test section and another mixer before water was returned to the thermostat-controlled bath. Pt100 probes that were calibrated before were placed after the mixers to accurately measure the inlet and outlet bulk temperatures. The mixer at the inlet was placed in an insulated acetal manifold which also housed the inlet Pt100 probe thereafter. Another acetal manifold housed a mixer and thereafter, the outlet Pt100 probe. The mixers, pipes, and test section were insulated which prevented heat loss between the inlet and outlet Pt100 probes thus making the temperature difference between the Pt100 probes very small. The average of the Pt100 probes was used as the reference. The thermocouples were calibrated between a temperature range of 20°C to 60°C in 2.5°C increments to an accuracy of 0.1°C. Examples of the linear curve fits for some of the thermocouples can be found displayed in Figure A.5. The difference between the

uncalibrated temperatures and temperatures of the mean Pt100 probes (reference temperature) are demarcated by blue and the difference between the calibrated temperatures and temperatures of the reference temperature is demarcated by red in Figure A.6.

A.4. Pressure Diaphragm Calibration

The pressure drop across the test section was measured with a Validyne DP15 pressure transducer. The inaccuracy of the pressure transducer diaphragm was 0.25% of its full-scale. The difference in pressure from the displacement of the diaphragm was converted to a voltage by the pressure transducer. This is done by measuring the change in electrical capacitance from the displacement of the diaphragm. The Validyne CD280 carrier demodulator was used to amplify and convert to a current signal which is displayed through the National Instruments data acquisition system. The current signal is a range between 4-20 mA which represented ~~the~~ 0-100% of the full-scale value. One set of diaphragms was used for low Reynolds numbers (less than 4 000) and another set for Reynolds numbers greater than 2 000. The diaphragms were calibrated using a Beta T-140 manometer. The calibration of the pressure transducer diaphragm is shown in Figure A.7 and Figure A.8.

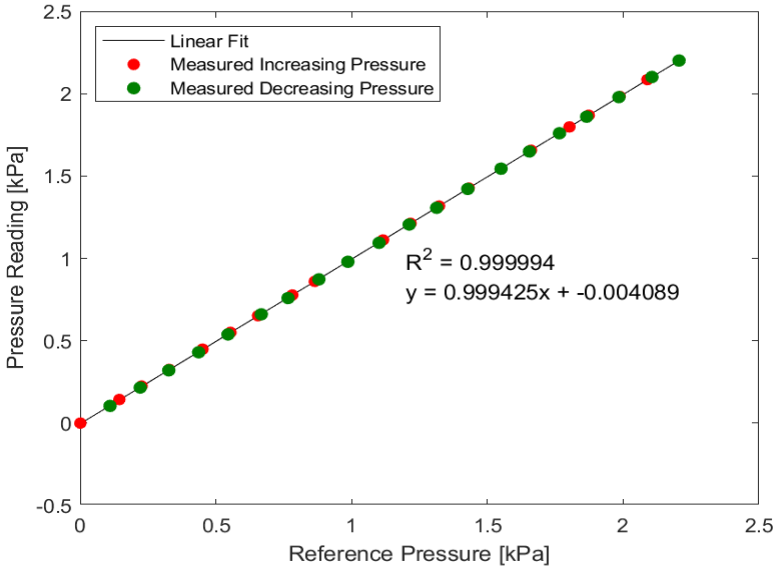

Figure A.7: Linear Curve fit for increasing [0–2.2 kPa] and decreasing [2.2–0 kPa] pressure readings as a function of a pressure reference (manometer readings).

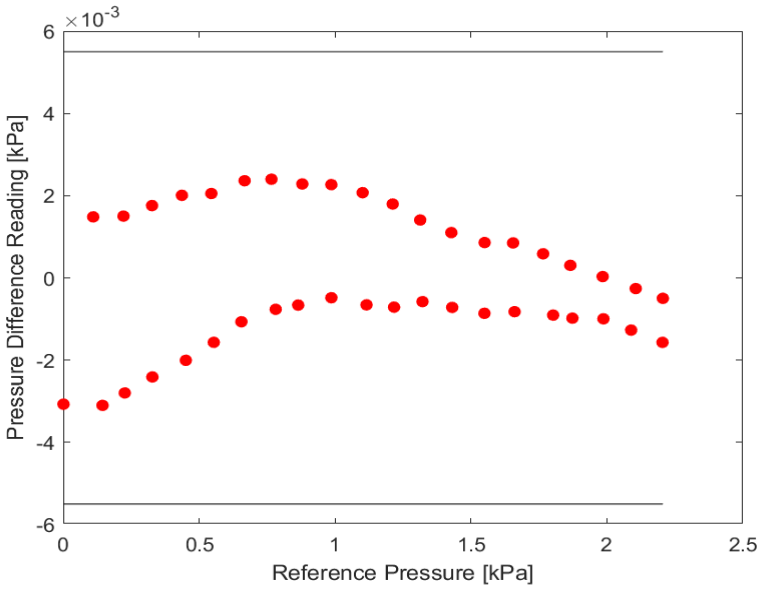

Figure A.8: Linear Curve fit for increasing [0–2.2 kPa] and decreasing [2.2–0 kPa] pressure readings as a function of a pressure reference (manometer readings).

A.5. Conclusions

Testing only began after verification of the calibration results were complete. Recalibration was also done after 6 months. This was to prevent measurement errors in the results. The calibration process for measuring instrumentation in this experimental study, such as: Pt100s, thermocouples, and pressure transducers were described, where the instrumentation was calibrated to accuracies of 0.06°C, 0.1°C and 0.25% full-scale value of pressure transducer diaphragm, respectively.

Appendix B. Methods of Obtaining Higher Surface Roughness

B.1. Introduction

Different methods were investigated to achieve a uniform substantial inner surface roughness for copper tubes. The tubes were required to have a natural random uniform roughness which differs from the artificial profiles of studies of enhanced tubes. The tubes were also required to maintain their surface roughness to provide consistency throughout the experimental testing. Therefore, a method such as electroplating which can accomplish a suitable substantial surface roughness, falls short in that deposits get degraded at high Reynolds numbers in the turbulent flow regime.

Conventional rough tubes (sand particles glued to the inner surface) such as those by Nikuradse [44] have been investigated for friction factors. However, studies on heat transfer coefficients are limited and the reason for this is that heat loss occurs through the glue and sand-particle layer, or air gaps trapped in between the sand particles. Studies on heat transfer through rough tubes with a sand-particle glue layer are found to have contradictory findings, for example, Nusselt numbers in rough tubes compared to smooth tubes in the turbulent flow regime increased for Everts [72] but decreased for Ayres [101]. This study investigated unique methods such as - chemical etching (HCl and FeCl), sand blasting, a combination of sandblasting and chemical etching, and copper particles glued to the inner surface to find the most suitable construction of rough tube for heat transfer and pressure drop testing.

B.2. Chemical Etching

Numerous studies used chemical etching which takes a commercial micro- or minitube and smoothens it with chemicals, namely, hydrochloric acid. This provided different grades of roughness for analysis. Kandlikar [100] found that tubes first smoothen out with chemical etching. However, after some time spent in the agent it begins to increase in roughness again. This was experimented with for a rough microtube, and the results are shown below in Table B.1.

Table B.1: Roughness results of tubes that were chemically etched and first sandblasted and then chemically etched.

Rz [µm]			Average Rz		ε/D
24.149	23.293	-	23.721	HCl smooth 24 hours	0.004476
21.088	33.319	30.516	28.30767	HCl and sandblasted 24hours	0.005341
21.104	27.239	24.036	24.12633	HCl and sandblasted 48 hours	0.004552
4.011	4.011	2.889	3.637	HCl and sandblasted 72hours	0.000686
33.127	33.309	36.532	34.32267	FeCl and sandblasted 45min	0.006476
17.541	17.441	17.963	17.64833	FeCl and smooth 45min	0.00333
25.878	25.81	30.432	27.37333	HCl and sandblasted 17 hours	0.005165
25.373	25.193	20.482	23.68267	HCl and sandblasted 10 hours	0.004468
23.912	19.372	19.153	20.81233	FeCl and sandblasted 15min	0.003927
8.482	19.23	12.552	13.42133	Smooth only	0.002532
7.103	6.406	6.703	6.737333	HCl smooth 14 hours	0.001271
28.736	31.503	27.251	29.16333	HCl and sandblasted 14 hours	0.005503
22.802	19.249	25.417	22.48933	HCl and sandblasted 1 week	0.004243
26.769	34.113	30.248	30.37667	Sandblasted only	0.005731
7.068	6.901	3.644	5.871	HCl smooth 10 hours	0.001108

It is seen that etching the tube makes it smoother. Some test sections were first sandblasted and then chemically etched to see if higher roughnesses could be achieved. For smooth tubes only with chemical etching the relative roughness first decreased and then increased to a relative roughness larger than its original at 24 hours. A combination of sandblasting and etching with ferrous chloride gave the largest relative roughness of 0.0065 but had great discoloration and corrosion. Comparing tubes where sandblasting and HCl was used, to see the effect on roughness against time spent in chemical, this is shown in Figure B.1.

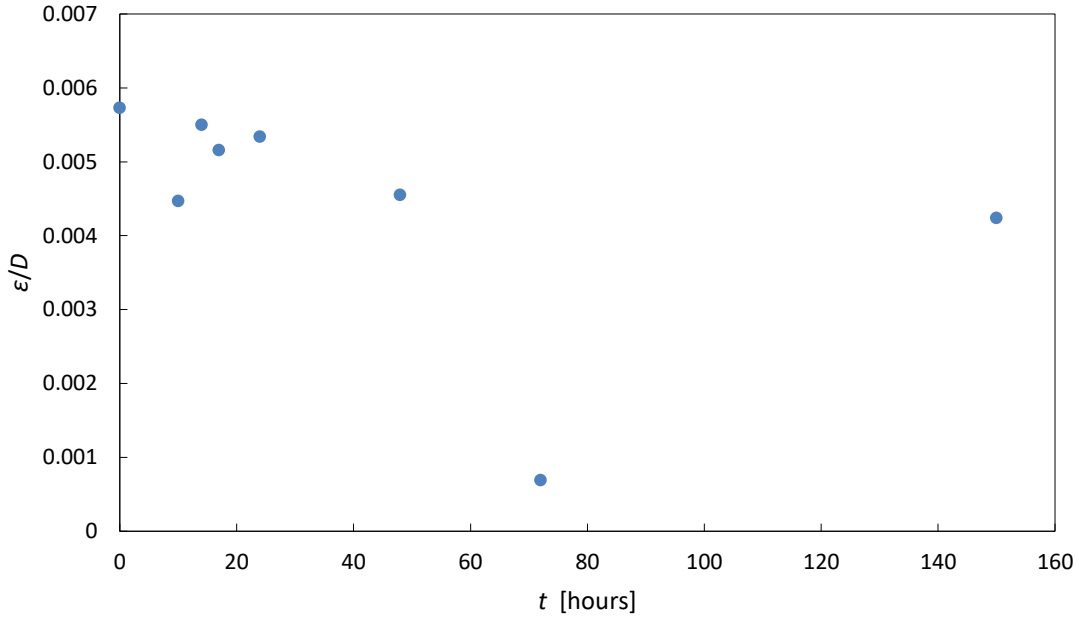

Figure B.1: Roughness of sandblasted tube against time [hours] spent in HCl.

The point at 10 hours, 0.00447 = ε/*D* could be an error in measuring since it does not follow the trend of the other points. After 70 hours the tube becomes very smooth. Although the roughness did increase at 150 hours, the tube was inadequate to use due to its high corrosion which depleted the thickness and strength of the tube.

B.3. Gluing Copper Particles

Since glue and sand particles affect the heat transfer characteristics they cannot be used in the study. Therefore, using a specialized method to glue copper particles uniformly was investigated and used. The copper particles were sifted and sorted according to different sizes to achieve the different surface roughnesses in the tubes. Different types of glues were tested, and the best results were obtained using Soudal Cyanofix 84A, because its low viscosity made it easy to spread and cover the tube with a consistent thin glue layer. To achieve a great uniform inner surface covering of the glue layer, the glue was first blown through the tube using pressurized air and thereafter, copper particles were blown through the tube from a pressurized container. The particles and glue formed a varying ripple shape on the tube surface and the heights depended on the size of the particles that were used. The tube was thereafter, cut longitudinally and an equal number of random samples over the tube length were taken for measuring the surface roughness. An example of measurements from one sample is shown in Table B.2. The roughness values measured for that sample gave a relative roughness of 0.04.

Table B.2: Roughness values collected over a sample and calculation of the relative roughness over that sample.

Zi [mm]	*Zi - Zmean*	Absolute		*Ra* [mm]	*Dr* [mm]	*ε /Dr*
1.00	-0.24	0.24		0.17	4.26	0.04
1.30	0.05	0.05				
1.49	0.24	0.24				
1.12	-0.13	0.13				
1.12	-0.13	0.13				
1.11	-0.13	0.13				
1.06	-0.19	0.19				
1.44	0.19	0.19				
1.47	0.22	0.22				

B.4. Conclusions

Methods were investigated to increase the surface roughness of the tube. It was difficult to achieve a uniform roughness on tubes greater than 2 m in length. Sandblasting had promising results in terms of uniformity; however, a large relative roughness could not be achieved with this method. Gluing copper particles using a specialized application method, was thus found to be the most suitable method for the experimental study.

Appendix C. Evaluation of Criteria of Flow Regime Boundaries

C.1. Introduction

The transitional flow regime diminishes as tubes become rougher and can altogether vanish if the tube is rough enough. It becomes increasingly difficult to identify and develop correlations for tubes of large roughness. Thus, a deeper understanding of data needs to be analysed, to sufficiently identify the flow regimes. Appendix A focuses specifically on the flow regime boundaries. It investigates methods for determining the boundaries of the transitional flow regime as well as factors influencing the width and occurrence of the transitional flow regime in smooth and rough tubes. The Appendix also investigates the outcomes of how the methods correlate to each other and which is the easiest and most reliable method to identify the transitional flow regime in rough tubes.

Methods, namely, the standard deviation as done by Meyer and Abolarin [33], numerical change in gradients and linear line method as investigated by Everts [64] and existing correlations as done by Mala and Li [87] were used for identifying the different flow regimes.

C.2. Available Criteria on Smooth Tubes

Everts and Meyer [27] recently developed a set of correlations to quantitively define the boundaries between the different flow regimes for smooth tubes, as well as the transitional flow characteristics. These equations and methods used in prior studies will be applied to rough tubes to find their suitability thereof. The critical Reynolds number was defined as:

$$Re = Re_{cr} \text{ when : } \left(\frac{dj}{dRe}\right)_{i-2:i} = 0 \qquad \text{C.1}$$

The Reynolds number at the end of the transitional flow regime or the onset of the quasi-turbulent flow regime, Re_{qt}, was calculated from:

$$Re = Re_{qt} \text{ when : } \left(\frac{d^2Nu}{dRe^2}\right)_{i:i+2} \geq -0.00015 \qquad \text{C.2}$$

The onset of the turbulent flow regime, Re_t, was located at the intersection of the Nusselt number gradients in the quasi-turbulent and turbulent flow regimes:

$$Re = Re_t \text{ when : } \left(\frac{dNu}{dRe}\right)_{qt} = \left(\frac{dNu}{dRe}\right)_{t} \qquad \text{C.3}$$

The width of the transitional flow regime was obtained from the Reynolds numbers at the onset and end of the transitional flow regime:

$$\Delta Re = Re_{qt} - Re_{qt} \quad \text{C.4}$$

C.3. Available Criteria Applied to Rough Tubes

A recent study [40] found that even a small increase in surface roughness affects the boundaries and width of the transitional flow regime. Rather than obtaining the flow regime boundaries from visual inspection, different methods that make use of the standard deviation [33], numerical change in the gradients [27], and existing correlations [87] have been developed to obtain the flow regime boundaries for smooth tubes. These methods were employed for the rough tube results of this study and compared to evaluate their suitability for rough tubes.

Meyer and Abolarin [33] used the standard deviation method to obtain the flow regime boundaries. The standard deviation was approximately 0.2°C in the transitional flow regime and 0.1°C in the laminar and turbulent flow regimes for a smooth tube. However, on using a tube with a twisted tape insert, the standard deviation decreased to 0.12°C in the transitional flow regime, while it remained approximately 0.1°C in the laminar and turbulent flow regimes.

Figure C.1 (a) and (b) compare the standard deviation of the average surface temperature of all measuring thermocouples for the two rough tubes. It is clearly shown that standard deviation right of the purple dotted line is greater. This indicates that all elements of laminar flow have ended, thereby, indicating an approximate onset of the quasi-turbulent flow regime. The standard deviation (left of the purple dotted line) of the surface temperatures varied from 0.0417°C to 0.0430°C in Figure C.1(a) and from 0.0404°C to 0.0420°C in Figure C.1 (b). Both rough tubes had similar standard deviation ranges in their temperatures. The laminar flow regimes standard deviations were slightly lower in both tubes, and this is shown left of purple dotted line in Figure C.1. From Figure C.1, it is seen that there are some high standard deviation data throughout all the flow regimes. This shows that the heat transfer characteristics throughout the different flow regimes, therefore, had some elements of turbulent flow behaviour. This could be caused due to the roughness of elements extending past the boundary layer and producing eddies in the flow. The onset of the transitional flow regime (Re_{cr}) for rough 1 occurred when the standard deviations per heat flux increased in Figure C.1 (a). However, it is difficult to fully disclose the boundaries of the flow regimes from standard deviation data alone as the difference in the range of the standard deviation data for rough tubes are below the uncertainty of the measuring instruments of 0.1°C. The standard deviation method of Meyer and Abolarin [33] found a smaller difference in the standard deviation between the flow regimes with the addition of a twisted tape insert. Similarly, in tubes with large roughness, the standard deviation varies minutely when mixing is present. The average standard deviation of surface temperatures increases (right of the purple dotted line) in Figure C.1 (a) and (b).

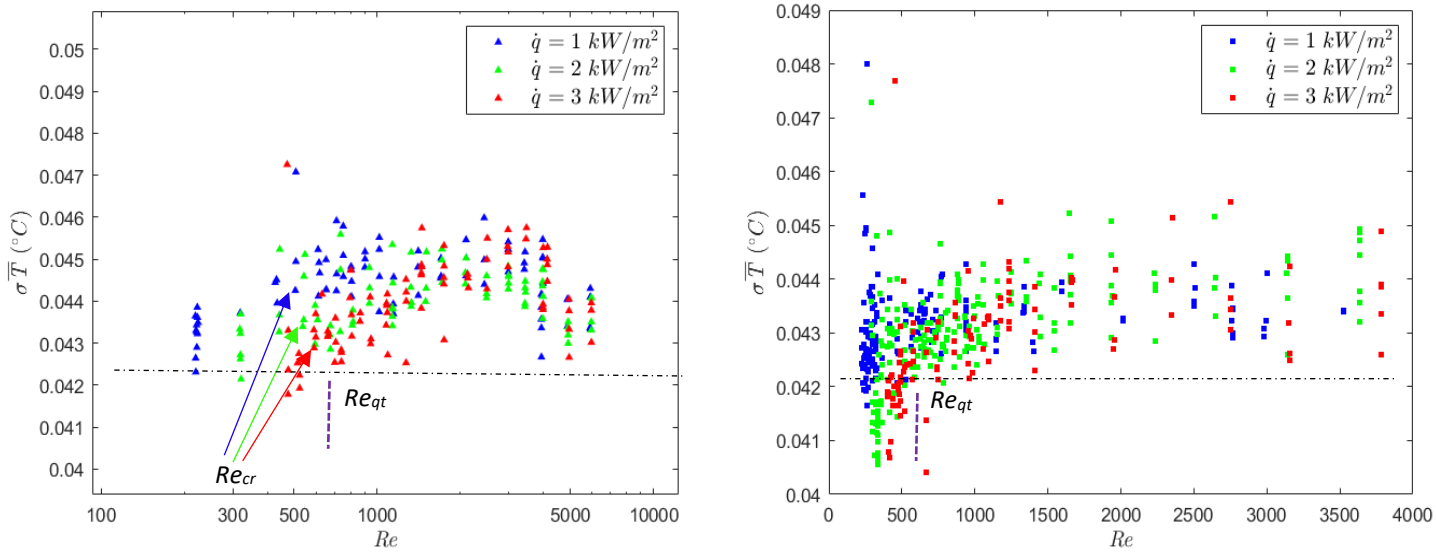

Figure C.1: Standard Deviations for average surface temperatures (a) and (b), at heat fluxes of 1, 2, and 3 kW/m^2 for rough tubes 1 (a) and 2 (b). Rough tube 1 (a) is plotted on a log x-axis for clarity on the Re_{cr} positions. The black dotted lines indicate that to the left of the purple dotted line there is low standard deviation data while to the right there is higher standard deviation data.

Meyer and Abolarin [33] could not identify the flow regimes by only using the standard deviation method. A complimentary linear-line method was therefore used. This method used three linear curve fits to express the flow regimes. However, because the transitional flow regime differs in tubes with large roughness and the transition from laminar to quasi-turbulent happens in a curved or quadratic form, this method cannot be used.

Ghajar et al. [9] and Tam et al. [85], on the other hand, found that the onset of the transitional flow regime corresponds to the Reynolds number at which the friction factors started to deviate by more than 5% from the Poiseuille equation ($f = 64/Re$). The laminar flow regime was found to be affected by roughness in Everts et al. [40] by tubes with low relative roughness. On using tubes with large relative roughness, the friction factors increased considerably in the laminar flow regime. In Figure C.2(a) and (b) the shifted Poiseuille equation was plotted together with the isothermal friction factor data for rough 1 and rough 2, respectively. The Poiseuille equation was shifted to the data point at the lowest Reynolds number. To prevent changes in viscosity (due to heating) from affecting the results, the isothermal friction factors were used to obtain the transitional Reynolds numbers. Although an increase in surface roughness was expected to have a negligible influence on the laminar friction factors [45], it follows from Figure C.2 (a) and (b) that an increase in surface roughness increased the laminar friction factors. For Reynolds numbers between 200 and 2 000, the average deviation from the shifted Poiseuille equation for rough 1 in Figure C.2 (a) was 8%, while the average deviation from the shifted Poiseuille equation for rough 2 in Figure C.2 (b) was 21%. For both Figure C.2 (a) and (b), it was difficult to differentiate between laminar and transition as few points only, followed the shifted linear line of Poiseuille. The data departs from the Poiseuille equation and shows non-linearity, more so in rough 2, which has a greater relative roughness. Therefore, for this reason, at low Reynolds numbers in rough tubes, the method of obtaining the transitional Reynolds number using a 5% departure criteria as Ghajar et al. [9] and Tam et al. [85] from the Poiseuille equation was not usable since the criteria would incorrectly predict the transitional Reynolds number. On shifting the Poiseuille equation to the lowest Reynolds number data point, it is shown in Figure C.2 (a) and (b) that only 1–2 data points fall onto the shifted Poiseuille equation.

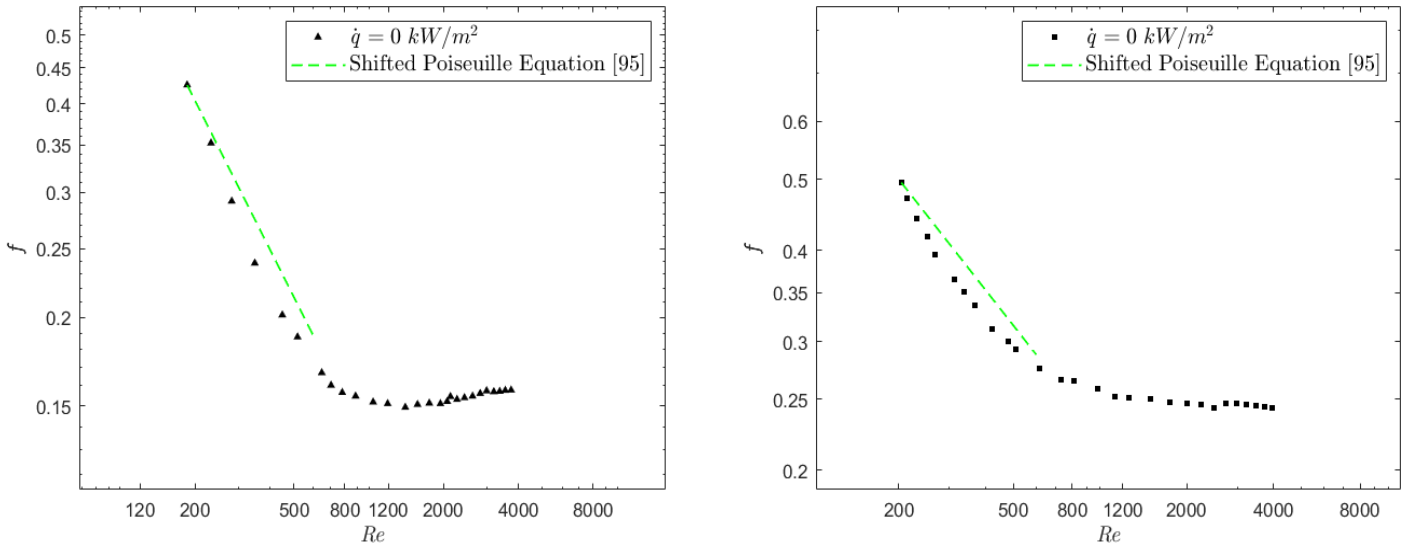

(a) (b)

Figure C.2: Comparison of the parallel shift of the shifted Poiseuille equation in broken green with the friction factor of rough tubes as a function of Reynolds number for 0 kW/m^2 on a log-log scale for tubes rough 1 (a) and rough 2 (b).

The method of numerical changes in the gradients as done by Everts and Meyer [27] was applied and tested for its suitability as well as in identifying the flow regime boundaries in rough tubes for transition using Eqs. C.1, C.2 and C.3. The critical Reynolds number was taken by Everts and Meyer [27] for a smooth tube when the first derivative of the Colburn *j*-factors with respect to the Reynolds number was equal to 0. For rough 1 in Figure C.3 (a) the Colburn *j*-factors with respect to the Reynolds number at a heat flux of 3 kW/m^2 was approximately 0 (1.6×10^{-7}) at a Reynolds number close to 600.

It was difficult to obtain the flow regime boundaries with criteria used by Everts and Meyer [27] for tubes with high surface roughness. The properties of the transitional flow regime are suppressed in comparison to a smooth tube. For a tube with large roughness, the width of the transitional flow regime becomes negligible whereby it is difficult to identify between the critical Reynolds number Re_{cr} and the onset of the quasi-turbulent flow regime Re_{qt}.

According to Eq. C.2, the quasi-turbulent Reynolds number that was taken by Everts and Meyer [27] for a smooth tube was when the second derivative of the Nusselt number with respect to the Reynolds number is greater than or equal to -0.00015. However, in rough tubes this method becomes unsuitable and cannot be used as criteria. This is shown in Figure C.3 (c) and (d) as majority of the data for the second derivative of the Nusselt numbers are above the broken line of -0.00015.

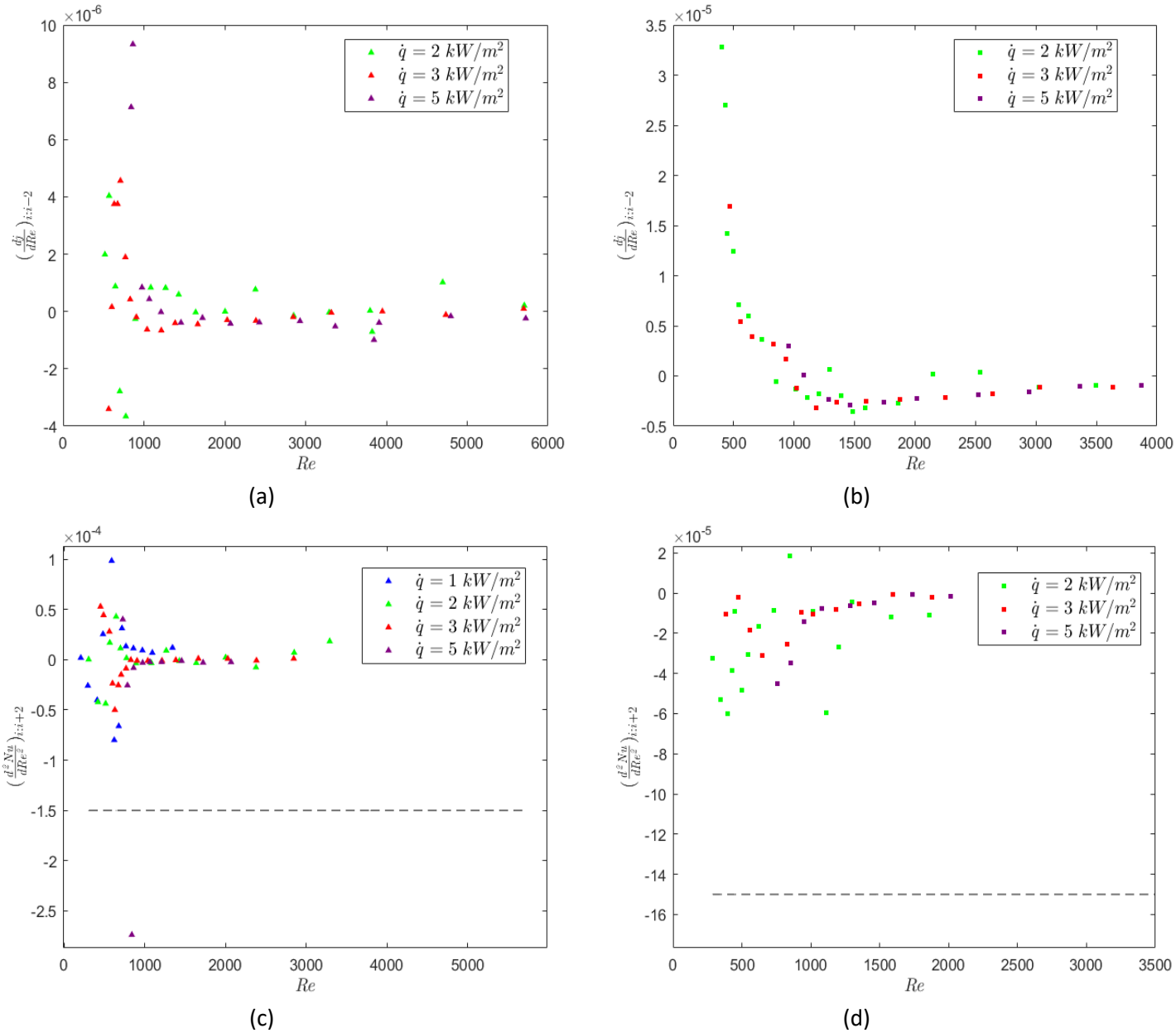

Figure C.3: First derivative for numerical gradient change for Colburn *j*-factors for rough tubes 1 (a) and 2 (b) and second derivative for numerical gradient change for the Nusselt numbers rough tubes 1 (c) and 2 (d) at heat fluxes of 2, 3, and 5 kW/m^2. The broken lines equal to -0.00015 (c) and (d) are plotted as well for reference.

Everts and Meyer [27] used a power curve fit on the derivative of Nusselt numbers and compared it with the derivative of the Colburn equation [45] with a 10% uncertainty to obtain the turbulent Reynolds number. Higher uncertainties generally exist in the turbulent flow regime due to the small surface-fluid temperature differences. The onset of the turbulent flow regime was therefore obtained using the friction factors and shifted Blasius equation [96] rather than the Nusselt numbers, due to the lower uncertainties associated with the friction factors.

To obtain the onset of the turbulent flow regime, previous studies that investigated microfin [16,52] and rough tubes [87] compared the friction factors with the Blasius [45] correlation. The flow was turbulent once the friction factors fell onto or made a parallel shift from the

correlation. Tam et al. [52], in studying microfin tubes, considered the first point that was not parallel to the shifted Blasius equation to be turbulent and the same method was applied here.

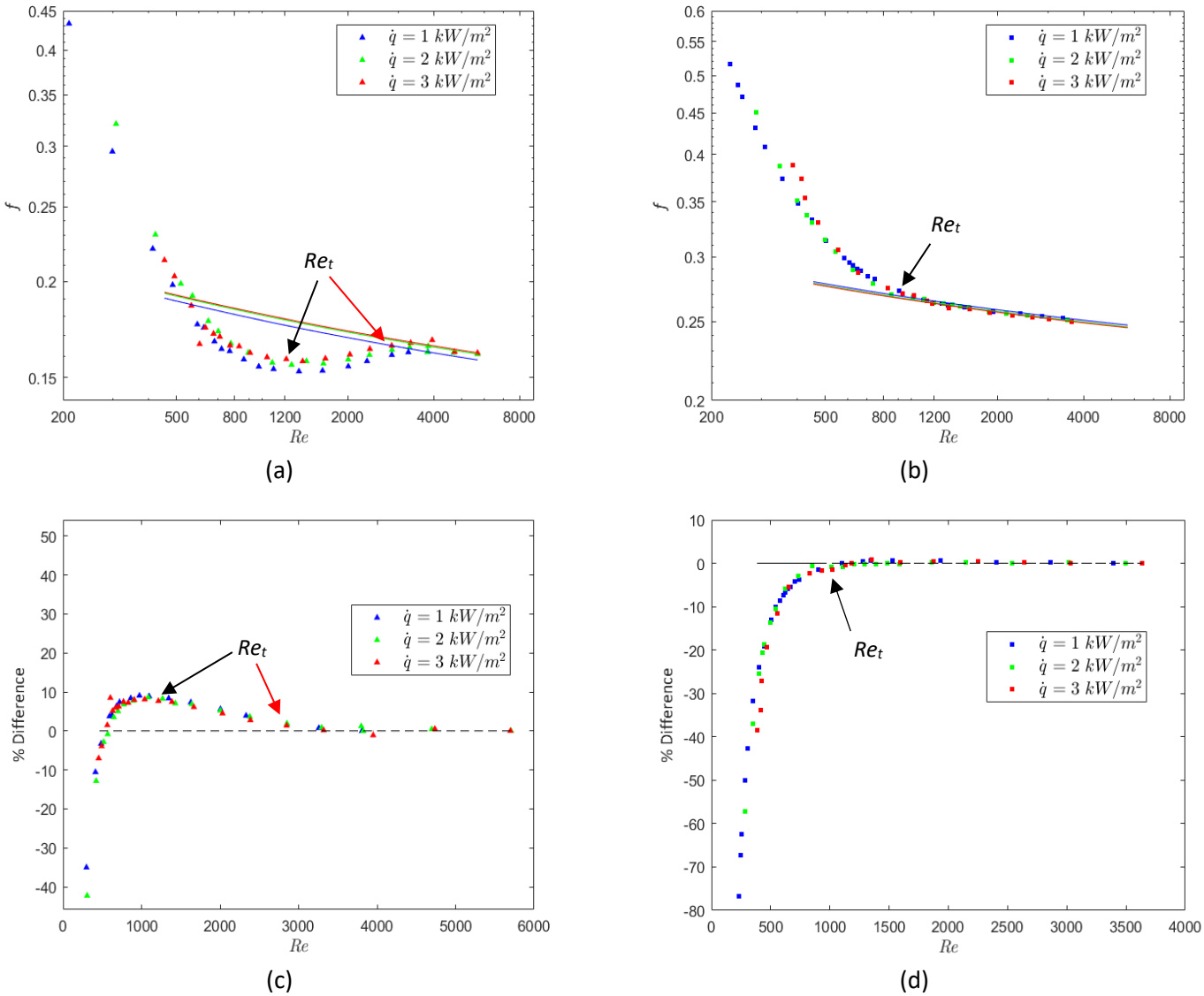

Figure C.4: Comparison of the parallel shift of the Blasius equation in solid colour lines with the friction factor of rough tubes as a function of Reynolds number for heat fluxes of 1, 2, and 3 kW/m^2 on a log-log scale rough 1 (a) and rough 2 (b) and, the difference in percentage given between the friction factors and the shifted Blasius equation for rough tubes 1 (c) and 2 (d). Re_t is shown with black arrows.

In Figure C.4 (a) and (b), the friction factors as a function of Reynolds numbers were plotted on a log-log scale and a shifted Blasius correlation was done for each heat flux. Figure C.4 (a) indicates with a red arrow that the friction factors departed from the shifted Blasius correlation at a Reynolds number of approximately 2 850. Figure C.4 (c) confirms this by showing the deviance from the correlation in percentages. This Reynolds number corresponded to a percentage difference of 2%. However, rough 1 has sufficient variance of data in the turbulent flow regime such that an 8% uncertainty band can be used on the data to obtain the turbulent Reynolds number. Using this approach, a conservative Reynolds number of 1 215 is obtained and selected as shown with black arrows in Figure C.4 (a) and (b). As the surface roughness increased, it follows from Figure C.4 (b) that the friction factors began to depart from the

shifted Blasius correlation around Reynolds numbers of 930. Therefore, the onset of the turbulent flow regime advances for increasing surface roughness.

C.4. Investigated Criteria for Rough Tubes

Methods (standard deviation [33], numerical changes in the gradients [27], and existing correlations [87] that can apply well to smooth tubes, do not necessarily perform well when applied to tubes with large roughnesses. This section investigates possible new criteria that can be applied to tubes with large relative roughness. Using a similar approach as Everts and Meyer [27], the change in gradient (of three data points) of the Colburn *j*-factors, friction factors and Nusselt numbers as a function of Reynolds numbers were plotted in Figure C.5. Due to the high uncertainties associated with the heat transfer data at a heat flux of 1 kW/m^2, this heat flux was omitted in Figure C.5 (b) and (d).

The numerical changes in the Colburn *j*-factor gradient for rough 1 and 2 are compared at different heat fluxes in Figure C.5 (a) and (b), respectively. For the Colburn *j*-factor first derivative, a peak in the gradient was identified as the inflection point Re' [27]. For rough 1, Figure C.5 (a) the data points before the peaks or inflection points in the 1, 2, 3 and 5 kW/m^2 heat flux results correspond to the end of the laminar flow regime for the standard deviation in surface temperatures. The inflection points in Figure C.5 (a) corresponded to $\left(\frac{dj}{dRe}\right)_{i:i+2} \approx 4.2 \times 10^{-6}$. This was found very close to the transition point (Re_{cr}), which further emphasizes the decrease of width of the transitional flow regime. For rough 2, it is not clear where the inflection point is located as the numerical change of the Colburn *j*-factors continues to increase into the laminar flow regime. This could be a result of non-linear curve flow at low Reynolds numbers with large roughness. Therefore, the inflection points Re' cannot be identified for rough 2.

The numerical change of the second derivative of the Nusselt number showed satisfactory criteria to identify the quasi-turbulent flow regime. The quasi-turbulent Reynolds numbers corresponded with those identified using the standard deviation in surface temperatures Figure C.1 (a) and the numerical gradient change for the second derivative of Nusselt numbers Figure C.5 (c). The quasi-turbulent Reynolds numbers were chosen when the second derivate of the Nusselt number was approximately equal to 0 (Eq. C.5) after the laminar flow regime for both rough 1 and 2. No other consistent criteria can be identified in using the second derivative of the Nusselt number for rough tubes in finding flow regime criteria.

$$Re = Re_{qt} \text{ when: } \left(\frac{d^2Nu}{dRe^2}\right)_{i:i+2} \approx 0 \qquad \text{C.5}$$

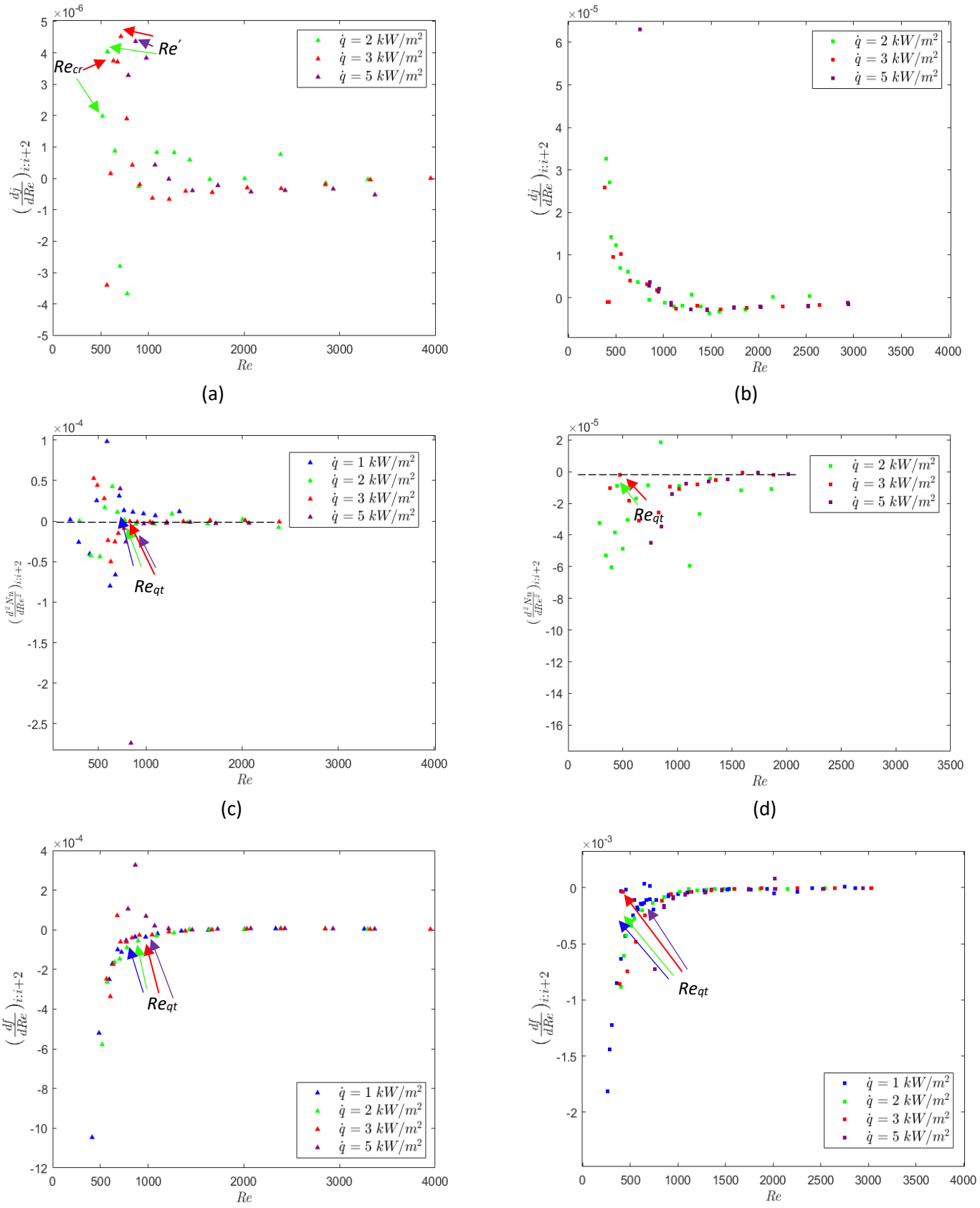

Figure C.5: Numerical gradient changes for Colburn *j*-factors for rough tubes 1 (a) and 2 (b), the second derivate of Nusselt numbers rough tubes 1 (c) and 2 (d) and the first derivative of friction factors rough tube 1 (e) and 2 (f) at heat fluxes of 1, 2, 3, and 5 kW/m^2.

The numerical change in the friction factor gradient as a function of Reynolds number is presented for different heat fluxes in Figure C.5 (e) and (f) for rough 1 and 2. From the friction factor data it is apparent how the data approached and thereafter settled in the turbulent flow regime with increasing Reynolds number. Figure C.5 (e) and (f) present the numerical change in friction factor with regard to the Reynolds number. The variations in data that do not conform to the general trend because at large roughness the particles create great resistance to flow. At low flow rates, an accumulation of pressure is required to overcome the resistance of the roughness. This will create pulses and slight variations in data such as the Reynolds numbers, friction factors and Nusselt numbers (mass flow rate, pressure, and temperature readings).

The quasi-turbulent Reynolds numbers chosen for $\left(\frac{df}{dRe}\right)_{i:i+2}$ in Figure C.5 (e) and (f) for rough 1 and 2 were at the end of the gradient changing in the numerical gradient data for $\left(\frac{df}{dRe}\right)_{i:i+2}$. The quasi-turbulent data in Figure C.5 (e) and (f) corresponded with the Reynolds number at which the quasi-turbulent flow regime begins in the standard deviation criteria and the previous numerical change criteria. A general expression can be given to obtaining the quasi-turbulent Reynolds number using the change in friction factors with respect to the Reynolds number. Once the trend approaches a zero gradient, the onset of the quasi-turbulent flow regime is identified. For rough 1, the quasi-turbulent Reynolds numbers were found when $\left(\frac{df}{dRe}\right)_{i:i+2} \geq -2 \times 10^{-5}$ and for rough 2 when $\left(\frac{df}{dRe}\right)_{i:i+2} \geq -5.7 \times 10^{-5}$.

C.5. Summary of Flow Regime Boundaries

Table C.1 summarises the flow regime boundaries (using the different methods) for rough tubes 1 and 2, respectively. Table C.1 was used as a guideline in selecting the flow regime boundaries. The Reynolds numbers summarised in Table C.1 approximately correlate with boundaries in Chapter 5. The log-log plots of friction factors and Colburn *j*-factors as a function of Reynolds number in combination with Table C.1 was ultimately used as selection criteria.

The standard deviation data of the temperatures showed that after a certain Reynolds number, the fluid is in a quasi-turbulent flow regime. However, it is difficult to point out the quasi-turbulent Reynolds number for each heat flux using the standard deviation of the temperatures. The reason for this is that at large roughness, heat flux was found to have a very small effect on the change in Reynolds number of the boundaries. The critical Reynolds number was also approximately obtained using the standard deviation in temperature data. However, this could only be done for rough 1.

The numerical change in gradient method can be used to obtain the change in gradient and to get a more accurate prediction of the occurrence of the onset of the quasi-turbulent flow regime. Using the shifted Blasius equation [96] the turbulent Reynolds number was located with ease. It was found that using some smooth tube criteria for obtaining the flow regime boundaries does not necessarily work for rough tubes and new criteria was therefore, investigated, adapted, and selected.

Table C.1: Evaluation of the transition, quasi-turbulent and turbulent flow regime boundaries summarising boundary Reynolds number criteria for rough 1 and rough 2 at 1, 2, and 3 kW/m^2

	Rough 1									**Rough 2**					
	1 kW/m^2			**2 kW/m^2**			**3 kW/m^2**			**1 kW/m^2**		**2 kW/m^2**		**3 kW/m^2**	
	Re_{cr}	Re_{qt}	Re_t	Re_{cr}	Re_{qt}	Re_t	Re_{cr}	Re_{qt}	Re_t	Re_{qt}	Re_t	Re_{qt}	Re_t	Re_{qt}	Re_t
Standard Deviation															
T	≈490	≈700		≈540	≈700		≈560	≈760		≈494		≈494		≈494	
Numerical Change															
j				520	701		600	710				481		489	
f		680			701			710		472		481		489	
Nu^2					701			710				481		489	
Deviation from Existing Correlation															
Relocated Blasius			1 215			1 215			1 215		930		930		930

C.6. Conclusions

Available methods used in prior studies were used to identify the different flow regimes for rough tubes. It was found that methods used for smooth tubes were not necessarily suitable for rough tubes. Methods for identifying the different flow regimes as a function of roughness and its shape should be investigated further in studies. Appendix A was useful in finding indicators for the occurrence of the different flow regimes. Ultimately, both Appendix A and the visual selection of results were used as tools to select the flow regime boundaries.